Emissions and Atmospheric Chemistry of Furanoids from Biomass Burning: Insights from Laboratory to Atmospheric Observations

Manolis Romanias, Matthew Coggon, Fatima Al Ali, James Burkholder, Philippe Dagaut, Zachary Decker, Carsten Warneke, Chelsea Stockwell, James Roberts, Alexandre Tomas, et al.

ACS EARTH AND SPACE CHEMISTRY

http://pubs.acs.org/journal/aesccq
Review

Emissions and Atmospheric Chemistry of Furanoids from Biomass Burning: Insights from Laboratory to Atmospheric Observations

Manolis N. Romanias,* Matthew M. Coggon,* Fatima Al Ali, James B. Burkholder, Philippe Dagaut, Zachary Decker, Carsten Warneke, Chelsea E. Stockwell, James M. Roberts, Alexandre Tomas, Nicolas Houzel, Cecile Coeur, and Steven S. Brown

Cite This: https://doi.org/10.1021/acsearthspacechem.3c00226

Read Online

ACCESS | Metrics & More | Article Recommendations | Supporting Information

ABSTRACT: Furanoids are a class of reactive volatile organic compounds that are major products from the pyrolysis and combustion of biomass polymers, including cellulose, hemicellulose, and lignin. Biomass burning is an atmospheric source of furanoids that is increasing in frequency and intensity throughout regions of the world. Once emitted to the atmosphere, furanoids may react with the major atmospheric oxidants to form secondary pollutants that are hazardous to human health, including ozone (O_3) and secondary organic aerosol (SOA). This review is a comprehensive assessment of the literature between 1977 and the present describing the emissions and atmospheric fate of furanoids emitted from wild, prescribed, and domestic fires. The review is organized by presenting the physical properties of key furanoids first, followed by a summary of the biopolymer pyrolysis and combustion reactions that lead to furanoid formation. Next, furanoid emissions factors are compiled across the typical fuels consumed by biomass burning to highlight the key species emitted in smoke. We next review the available kinetic and atmospheric degradation mechanism data that characterize the reaction rates, gas-phase products, and SOA formed as a result of furanoid reactions with OH, NO_3, O_3, and Cl radicals. We then describe studies that have focused on evaluating furanoid atmospheric chemistry and their impacts on air quality using a combination of field observations and model simulations. We conclude with a perspective that identifies future research directions that would address key data gaps and improve the understanding of furanoid atmospheric processes.

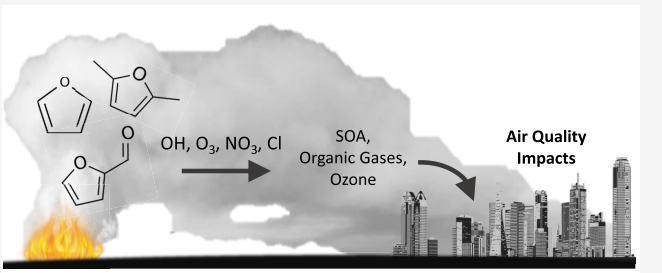

KEYWORDS: *wildfires, smoke, air pollution, atmospheric oxidants, volatile organic compounds*

1. INTRODUCTION

Furanoids are a class of heterocyclic organic molecules that are trace species present in the atmosphere. Furanoids are broadly defined as an organic molecule containing a five-membered ring with four carbons and one oxygen. A furanoid can be aromatic (Figure 1A), partially saturated, or fully saturated (Figure 1B). The replacement of hydrogen atoms by functional groups, including hydroxy (−OH), aldehyde (−(H)C═O), ketone (−(R)C═O), methyl ($-CH_3$), and aromatic ($-C_6H_6$) moieties leads to a range of furanoid compounds with different chemical and physical properties. The functionality of a furanoid determines its overall photochemistry and reactivity with atmospheric oxidants. The atmospheric chemistry of furanoids has implications for the oxidation capacity of the atmosphere and the formation of atmospheric pollutants such as ozone (O_3) and secondary organic aerosol (SOA).

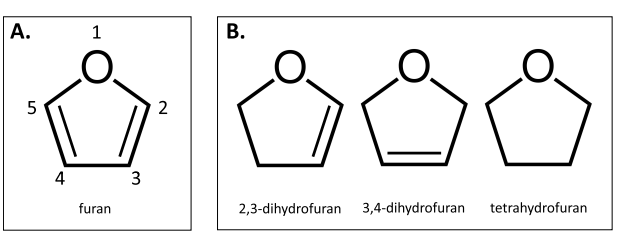

Figure 1. Basic structures of (A) aromatic furanoids and (B) partially and fully saturated heterocyclic furanoids.

Furanoids are emitted to the atmosphere from natural sources such as biomass burning[1,2] and anthropogenic consumption of chemical products,[3] flavorings and food,[4−6] and biofuels.[7,8] Future anthropogenic sources of furanoids may include the use of methylated furanoids as fuel additives.[8−10] Select furanoids, such as 3-methylfuran, have also been observed to form as

Received: July 28, 2023
Revised: March 6, 2024
Accepted: March 6, 2024

products from the atmospheric chemistry of isoprene in the presence of high mixing ratios of nitrogen oxides.[11] Furanoids are observed in outdoor and indoor air[12,13] and are prevalent in remote and urban regions in part due to the ubiquity of biomass combustion worldwide.[1,2,14−16] Furanoids emitted from biomass burning are derived from the pyrolysis of biopolymers and combustion of pyrolysis products.[1,2,17,18]

Efforts have been conducted over the past decade to quantify biomass burning emissions and better understand the atmospheric fate of important biomass burning constituents, including furanoids. Broadly, biomass burning is a major source of carbon to the Earth's atmosphere that results from land clearing and land-use change, naturally induced fires, and domestic heating and cooking.[1] Biomass burning emissions are increasing in northern latitudes due to higher wildfire frequency.[19] It is estimated that the annual burned area in the Western U.S. has increased by more than 50% from 1979 to 2019.[19] These higher emissions have increased the regional atmospheric abundance of highly reactive organic molecules, including furanoids.

The atmospheric chemistry of biomass burning emissions contributes to the formation of global tropospheric ozone and recent field measurements show that remote air masses impacted by biomass burning contain equivalent or higher ozone mixing ratios than those impacted by anthropogenic emissions.[20] Furanoids have been identified as abundant volatile organic compounds (VOCs) in biomass burning plumes (BBVOCs), and measurements of smoke from temperate forests show that furanoids comprise 10 ± 5% of the mass emitted as nonmethane organic gases.[1,2,21−24] Biomass burning emissions have been previously reviewed,[1,2] but there has not been a clear focus on critically reviewing furanoid emissions, their flux to the atmosphere from biomass burning, and present research gaps.

Once emitted, furanoids are expected to react in the atmosphere to produce O_3, SOA, and other secondary products that degrade air quality and alter the oxidative capacity of the atmosphere. Unlike other important atmospheric constituents, such as nonheterocyclic aromatics,[25] oxygenates,[26,27] and biogenic VOCs,[28,29] the atmospheric chemistry of furanoids has not been thoroughly reviewed and reactions describing their degradation have not been widely incorporated into mechanisms used for 3D chemical transport models (e.g., GEOS-Chem, the Regional Atmospheric Chemical Mechanism, RACM).

Literature studies on furanoids span five decades and include small- or large-scale field campaigns, laboratory experiments in photochemical reactors, and chemical modeling to simulate biomass burning plume impacts on air quality and climate. Recent studies suggest that furanoids are responsible for ∼10−25% of the OH and NO_3 radical reactivity[30] in biomass burning plumes and 10−20% of the ozone formed in early plume oxidation.[31,32] The accuracy of air quality simulations and the interpretation of field or laboratory observations rely on the knowledge of furanoid kinetics, photochemistry, and the degradation mechanisms by the major atmospheric oxidants.

This work is a review of literature between 1977 and 2023 describing the emissions and chemical fate of furanoids. The goals of this review include the following.

- Review field and laboratory literature describing the emissions of furanoids from the pyrolysis and combustion of biomass polymers.
- Review literature describing the atmospheric degradation of furanoids by the major atmospheric oxidants (i.e., OH, NO_3, O_3, and Cl) and UV−vis photolysis. The atmospheric lifetimes of furanoids will also be discussed with the aim to identify their atmospheric fate and potential to form secondary pollutants.
- Review the literature describing the reaction mechanisms and gas-phase products formed by the reaction of furanoids with the principal oxidants of the atmosphere. The available SOA yields from furanoid oxidation are summarized.
- Review literature describing field observations and modeling studies of furanoid degradation, products, and atmospheric chemistry. We note that the number of studies that have employed furanoid chemistry in models is limited, however, the available studies highlight the importance of furanoids in the atmospheric chemistry of biomass burning plumes.

2. PHYSICAL PROPERTIES OF FURANOIDS EMITTED FROM BIOMASS BURNING

An understanding of the impact of furanoids on the environment and human health requires knowledge of the chemical and physical properties of these compounds and their atmospheric degradation products. Table 1 summarizes the physical properties of a series of furanoids that have been identified as atmospheric pollutants in biomass burning smoke, have been studied in laboratory kinetic experiments, or have been evaluated to determine atmospheric degradation mechanisms. Although these compounds have a similar base structure (a heterocyclic ring), the addition of various substituents and presence or absence of aromaticity differentiates their physical and chemical properties. Note that acronyms for select species are presented in this table and these abbreviations are used throughout the text.

3. FURANOID EMISSIONS FROM BIOMASS BURNING

Biomass burning releases a wide spectrum of VOCs, and the amount and composition of these emissions depend on fuel type (e.g., boreal, temperate forest, savanna, etc.), fuel composition (e.g., nitrogen, cellulose, and lignin content), and combustion conditions (e.g., flaming vs smoldering).[17,18,33−36] This section summarizes research that has characterized furanoid emissions. Section 3.1 reviews the fundamental pyrolysis and combustion reactions of biomass polymers that release furanoids to the atmosphere. Section 3.2 connects these reactions to observations of furanoid emissions from various forms of biomass burning, such as wildfires and residential wood burning. Finally, Section 3.3 utilizes furanoid emission factors to estimate the global flux of furanoids to the atmosphere

3.1. Biopolymer Pyrolysis and Combustion Reactions Contributing to Furanoid Emissions. VOC emissions from biomass burning primarily result from smoldering combustion, which is a flameless type of burning that emits particulate matter and gases. Smoldering can transition to flaming combustion with additional oxygen supply and heat from spontaneous ignition of pyrolysis gases or secondary char oxidation.[37,38] During smoldering, the pyrolysis temperatures alter the mechanism of biomass decomposition, resulting in changes to the VOC emission profile.[17,18,35,39,40] At low to medium temperatures (300−500 °C), cellulose, hemicellulose, and lignin (Figure 2)

https://doi.org/10.1021/acsearthspacechem.3c00226
ACS Earth Space Chem. XXXX, XXX, XXX−XXX

Table 1. Physical Properties of Furanoids Considered within the Framework of This Review

Compound	Molecular formula	Canonical SMILES	CAS Number	Phase (298 K)	Molecular weight (g mol^{-1})	Density (g cm^{-3})	Vapor pressure (Torr, 298 ± 5 K)	Flash point (°C)	Freezing/melting point (°C)	Boiling point (°C)
Tetrahydrofuran (THF)[a]	C_4H_8O	C1CCOC1	109-99-9	Liquid	72.11	0.89	127.5	−17	−108.5	65
[2-methyltetrahydrofuran][a,b]	$C_5H_{10}O$	CC1CCCO1	96-47-9	Liquid	86.13	0.86	No available data	−11	−137	78
[2,5-dimethyltetrahydrofuran][a,b]	$C_6H_{12}O$	CC1CCC(O1)C	1003-38-9	Liquid	100.16	0.83	2.3[c]	26	−45	90
2,3-dihydrofuran[a]	C_4H_6O	C1COC=C1	1191-99-7	Liquid	70.09	0.93	258[c]	−24	−24	54
2,5-dihydrofuran[a]	C_4H_6O	C1C=CCO1	1708-29-8	Liquid	70.09	1.0	145.4[c]	−16	−83.55[c]	66
Furan[a]	C_4H_4O	C1=COC=C1	110-00-9	Liquid	68.08	0.93	596[c]	−35	−85.6	31.3
2-methylfuran (2-MF)[a]	C_5H_6O	CC1=CC=CO1	534-22-5	Liquid	82.10	0.91	104.2	−26	−88.7	63
3-methylfuran (3-MF)[a]	C_5H_6O	CC1=COC=C1	930-27-8	Liquid	82.10	0.92	161[c]	−22	−67.86[c]	65
2,3-dimethylfuran (2,3-DMF)[a]	C_6H_8O	CC1=C(OC=C1)C	14920-89	Liquid	96.12	0.91	41.3[c]	−1	−48.91[c]	42
2,4-dimethylfuran (2,4-DMF)[a]	C_6H_8O	CC1=CC(=CO1)C	3710-43-8	No available data	96.12	0.91	52.4[c]	0.8 ± 5.6[c]	−48.91[c]	95.2
2,5-dimethylfuran (2,5-DMF)[a]	C_6H_8O	CC1=CC=C(O1)C	625-86-5	Liquid	96.13	0.9	57.1[c]	−1	−62	92.0
2,3,5-trimethyl furan[a]	$C_7H_{10}O$	CC1=CC(=C(O1)C)C	10504-04-8	Liquid	110.15	0.89	14.4[c]	20	−30.23[c]	121
[Tetramethyl-furan][a,b]	$C_8H_{12}O$	CC1=C(OC(=C1C)C)C	10599-58-3	No available data	124.18	0.9	3.08	42.3	−11.81[c]	160.6
2-ethylfuran[a]	C_6H_8O	CCC1=CC=CO1	3208-16-0	Liquid	96.13	0.91	53.9[c]	−2.2	−55.17[c]	92
3-ethylfuran[c]	C_6H_8O	CCC1=COC=C1	67363-95-5	Liquid	96.13	0.91	65.1	−5.7	−55.17	89.8
2-propylfuran[a]	$C_7H_{10}O$	CCCC1=CC=CO1	4229-91-8	Liquid	110.15	0.91	17.7[c]	24	No available data	121.3[c]
2-ethyl-5-methyl furan[c]	$C_7H_{10}O$	CCC1=CC=C(O1)C	1703-52-2	Liquid	110.154	0.9	19.3	15.1	−36.49	119.1
Aldehydes										
2-furanaldehyde (2-furfural)[a]	$C_5H_4O_2$	C1=COC(=C1)C=O	98-01-1	Liquid	96.09	1.16	2.2[c]	60[c]	−36	162
3-furanaldehyde (3-furfural)[a]	$C_5H_4O_2$	C1=COC=C1C=O	498-60-2	Liquid	96	1.11	4.9[c]	48	No available data	144
5-methyl-2-furfural[a]	$C_6H_6O_2$	CC1=CC=C(O1)C=O	620-02-0	Liquid	110.11	1.10	0.6[c]	72.8[c]	26	187
5-hydroxy-2-furfural[c]	$C_5H_4O_3$	C1=C(OC(=C1)O)C=O	107997-80-8	Solid	112.08	1.4	0.0	106.3	No available data	252.2
5-hydroxymethyl-2-furfural[a]	$C_6H_6O_3$	C1=C(OC(=C1)C=O)CO	67-47-0	Solid	126.11	1.29	0.0[c]	79	32	114 (1 mmHg)
Ketones										
2(3H)-furanone[c]	$C_4H_4O_2$	C1C=COC1=O	20825-71-2	Liquid	84.07[b]	1.2 ± 0.1[b]	0.98[c]	105.2[c]	−40.90[c]	179.67[c]
2(5H)-furanone[c]	$C_4H_4O_2$	C1C=CC(=O)O1	497-23-4	Liquid	84.07	1.2	0.3	101.1	−40.90	203
[5-methyl-2(3H)-furanone][a,c]	$C_5H_6O_2$	CC1=CCC(=O)O1	591-12-8	No available data	98.1	1.1[c]	0.0[c]	78.9±16.1[c]	−33.14[c]	210.0[c]
Maleic anhydride[a]	$C_4H_2O_3$	C1=CC(=O)OC1=O	108-31-6	Solid	98.06	1.48	0.3[c]	−51.57	53	200
[5-methyl-5-vinyltetrahydrofuran-2-ol][a,b]	$C_7H_{12}O_2$	CC1(CCC(O1)O)C=C	40478-73-7	No available data	128.16	No available data	No available data	No available data	No available data	No available data
Alcohols /acids										
2-furanmethanol[a]	$C_5H_6O_2$	C1=COC(=C1)CO	98-00-0	Liquid	98.10	1.13	1.0[c]	75	−31	170
2-furoic acid[a]	$C_5H_4O_3$	C1=COC(=C1)C(=O)O	88-14-2	Solid	112.08	0.659	0.0[c]	139.3	130	232.1
Furanoids with aromatic ring substitutions										
2,3-dihydrobenzofuran[a]	C_8H_8O	C1COC2=CC=CC=C21	496-16-2	Liquid	120.15	1.06	0.836[c]	66	−21	188
2,3-benzofuran[a]	C_8H_6O	C1=CC=C2C(=C1)C=CO2	271-89-6	Liquid	118.13	1.07	0.43	50	−18	173
2-methylbenzofuran[a]	C_9H_8O	CC1=CC2=CC=CC=C2O1	4265-25-2	Liquid	132.15	1.057	0.6[c]	67	No available data	197
3-methylbenzofuran[a]	C_9H_8O	CC1=COC2=CC=CC=C12	21535-97-7	Liquid	132.16	132.16 1.046	0.5[c]	73.2[c]	16.26[c]	198.5[c]

https://doi.org/10.1021/acsearthspacechem.3c00226
ACS Earth Space Chem. XXXX, XXX, XXX−XXX

Table 1. continued

[a]Information taken from Safety Data Sheet (SDS) or Material Safety Data Sheet (MSDS). [b]Compounds in brackets have not been identified in biomass burning plumes but have been studied for their reactivity toward atmospheric oxidants. Acronyms for select species are given in parentheses. [c]Information taken from Chemspider, https://www.chemspider.com/, either using estimated algorithms to predict the physicochemical molecular properties of compounds from Advanced Chemistry Development (ACD) Inc. or using the EPI suite of the Environmental Protection Agency.

undergo depolymerization and fragmentation, resulting in emissions rich with functionalized molecules.

At high temperatures (>500 °C), these processes lead to a greater degree of aromatization, resulting in the formation of char (solid), tar, and volatile aromatics (e.g., polycyclic aromatic hydrocarbons). In addition to the burning phase, furanoid emissions may also vary by the extent to which biomass is composed of different polymers. Furan derivatives, such as furanaldehydes, are major products of cellulose and hemicellulose, whereas phenolic compounds are the major products from lignin.[17]

Due to its polymeric structure, cellulose pyrolysis is complex and far from being well-characterized, although it has been the topic of many studies over almost 70 years. Experimental works utilize many techniques, e.g., thermogravimetric analysis coupled to Fourier transform infrared spectroscopy (TGA-FTIR), fast pyrolysis, pyrolysis gas chromatography−mass spectrometry (Py-GC/MS), fixed-bed pyrolysis system, gas chromatography−mass spectrometry (GC-MS), elemental analysis, and FTIR spectroscopy.

Kinetics and reaction pathways for cellulose pyrolysis have been proposed by Lin et al.[40] based on measurements performed with a Pyroprobe reactor and a thermogravimetric gas analyzer coupled to mass spectrometry (Figure 3). The authors considered depolymerization of solid cellulose to yield levoglucosan (LGA), which can undergo dehydration and isomerization reactions to form levoglucosenone (LGO), 1,4:3,6-dianhydro-β-D-glucopyranose (DGP), and 1,6-anhydro-β-D-glucofuranose (AGF). Further reactions of anhydrosugars can form furanoids, e.g., 2-furanaldehyde (2-furfural) and 5-hydroxymethyl-2-furfural, by dehydration or hydroxyacetone, glycolaldehyde, and glyceraldehyde by decomposition and retroaldol reaction.

The pyrolysis of hemicellulose has been described in the literature,[41−43] though this polymer is less studied than other biomass components. Both experimental and computational (density function theory) studies have been published. A range of experimental techniques has been used to study these reactions, including TGA−FTIR, fast pyrolysis, Py-GC/MS, fixed-bed pyrolysis system, GC-MS, CHNS/O elementary analysis, and surface FTIR spectroscopy. 2-methylfuran is a prominent furanoid that has been detected among the products of hemicellulose pyrolysis.[42]

The pyrolysis of lignin has been investigated experimentally[44−47] and has recently been reviewed.[48,49] Besides the formation of light gases (H_2, CO, CO_2, CH_4, C_2, and $>C_2$), aromatics have been observed to be a large fraction of the products observed in liquid extracts.[47,49] These aromatics include furan and furanoids functionalized with aromatic rings (e.g., 2,3-dihydrobenzofuran and benzofuran)[47]

The pyrolysis of cellulose/hemicellulose/lignin mixtures[17,50] has also been investigated in order to simulate lignocellulosic biomass. It has been reported that an additive law based on the individual conversion of cellulose, hemicellulose, and lignin could not predict yields of products from the pyrolysis of "real" lignocellulosic biomass.[48,51−53] Also, interactions between lignocellulosic biomass constituents and minerals naturally present in biomass (e.g., sodium, potassium, calcium, magnesium, iron, phosphorus, and aluminum) can influence the yields of pyrolysis products.[48,54] The pyrolysis of lignocellulosic biomass is a complex chemical process which can result in a wider range of furanoid compounds than the pyrolysis of individual biopolymers, as shown in a relatively

https://doi.org/10.1021/acsearthspacechem.3c00226
ACS Earth Space Chem. XXXX, XXX, XXX−XXX

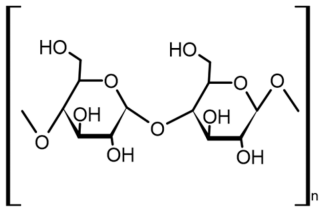

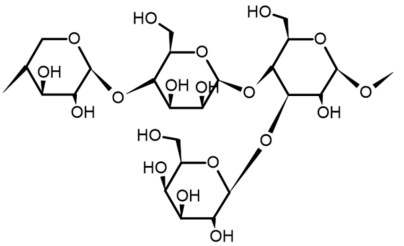

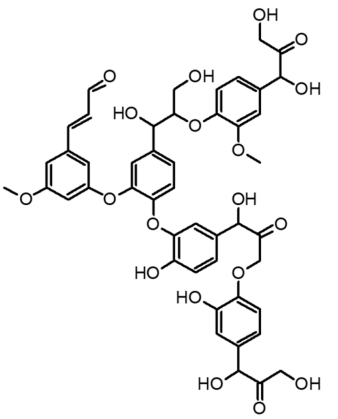

Figure 2. Structures of cellulose, hemicellulose, and lignin.

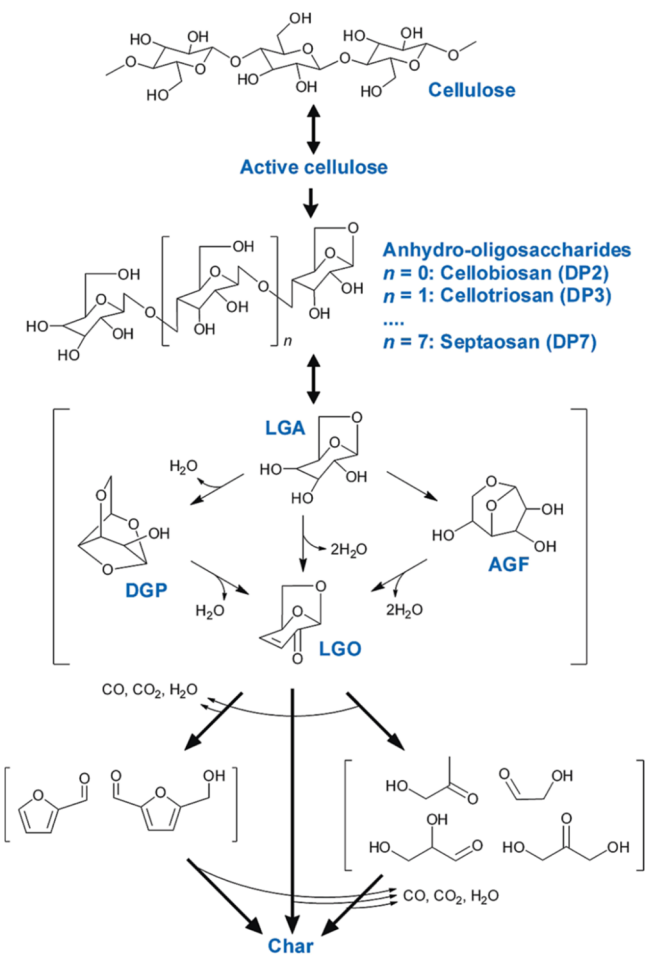

Figure 3. Proposed mechanism for cellulose pyrolysis reproduced from Lin et al.[40] Copyright 2009 American Chemical Society.

recent study presenting extensive speciation of products including furanoids such as 2-furanmethanol, 2-furfural, 2-methylfuran (2-MF), 2,5-dimethylfuran (2,5-DMF), 3-methylfuran (3-MF), and acetylfuran.[55]

In addition to biomass pyrolysis, furanoids have been observed as byproducts of combustion. Experiments have been conducted over a wide range of conditions, and the kinetics of combustion for furanoids has been a topic of many studies.[56−58] Currently accepted combustion pathways involve the formation of saturated cyclic ethers (QOs) from the combustion of linear, branched, and cyclic hydrocarbons, and related organic reactants, e.g., aliphatic ethers, esters, alcohols, (RH):

$$RH + {}^{\bullet}OH \rightleftarrows R^{\bullet} + H_2O \quad (1)$$

$$R^{\bullet} + O_2 \rightleftarrows ROO^{\bullet} \quad (2)$$

$$ROO^{\bullet} + HOO^{\bullet} \rightleftarrows ROOH + O_2 \quad (3)$$

$$ROO^{\bullet} + RH \rightleftarrows ROOH + R^{\bullet} \quad (4)$$

$$ROO^{\bullet} \rightleftarrows {}^{\bullet}QOOH \quad (5)$$

$${}^{\bullet}QOOH \rightleftarrows {}^{\bullet}OH + QO\ (\text{cyclic ether}) \quad (6)$$

Cyclic ethers (QOs), such as oxiranes, oxetanes, tetrahydrofurans, or tetrahydropyranes, can be formed depending on the size of the fuel and of the structure of $ROO^{\bullet}$ radicals.[59−61] Further oxidation can yield unsaturated cyclic products, such as dihydrofurans and furanoids, e.g.:

$$-CH_2-CH_2- + {}^{\bullet}OH \rightarrow -CH_2-{}^{\bullet}CH- + H_2O \quad (7)$$

$$-CH_2-{}^{\bullet}CH- + O_2 \rightarrow -CH=CH- + HOO^{\bullet} \quad (8)$$

where the −CH═CH− group is the unsaturated carbons in the heterocyclic ring. The combustion kinetics of furan derivatives has been investigated in part because they are potential fuel additives[62−65] and promising biofuels,[66−68] but is also relevant to the formation of complex furanoids observed in biomass burning.

3.2. Observations of Furanoid Emissions from Biomass Burning. The fundamental reactions described in Section 3.1 highlight that furanoids are key reaction products from biomass polymer pyrolysis and combustion. In open biomass burning (e.g., wild and prescribed fires) or residential

https://doi.org/10.1021/acsearthspacechem.3c00226
ACS Earth Space Chem. XXXX, XXX, XXX−XXX

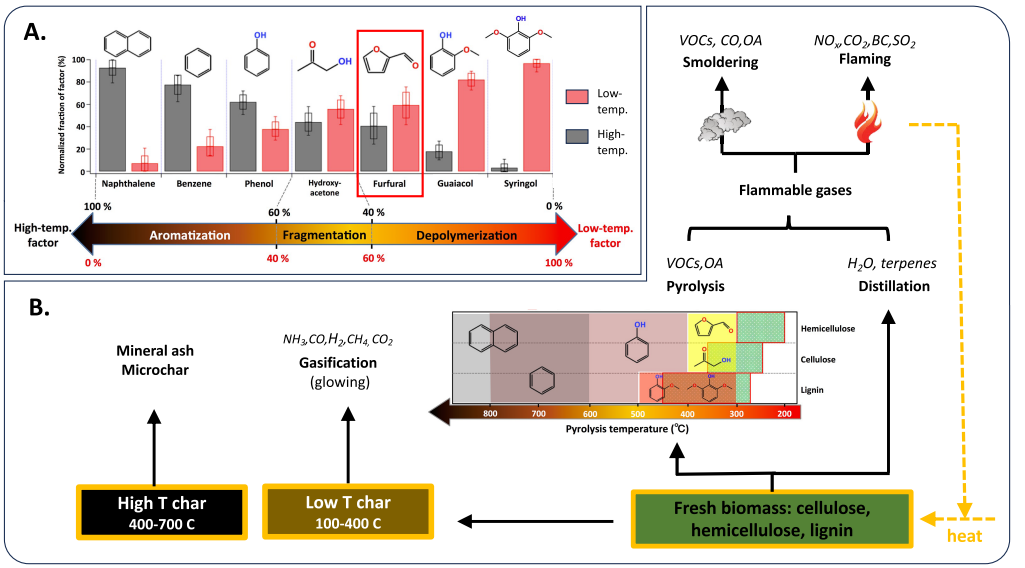

Figure 4. (A) Observed effect of pyrolysis temperature on BBVOC speciation from measurements of smoke emitted from open burning of temperature forest fuel types. (B) Process diagram showing the connection between pyrolysis, smoldering and flaming combustion, and release of gases and particles from open biomass burning. Graphs adapted with permission from Sekimoto et al.[35] under the creative commons attribution 4.0 License. Copyright 2018 The Authors, published by Copernicus Publications.

cooking/heating (e.g., woodstoves), pyrolysis occurs simultaneously with combustion under a range of temperatures, fuel to oxygen ratios, and fuel composition. These variable conditions lead to significant changes in BBVOC emissions. Given the wide variability in burning conditions and fuel composition, laboratory and field studies have quantified BBVOCs for a diverse spectrum of biomes, fuels, and burning conditions (e.g., open vs residential burning) in order to estimate emission factors (g of carbon emitted per kg of fuel consumed) that can be implemented in atmospheric models to evaluate the impacts of biomass burning on air quality and climate.[1,2] Below, studies are reviewed that have linked the fundamental processes described in Section 3.1 to the emissions of furanoids and other BBVOCs observed in open biomass burning. Furanoid emission factors and emission ratios to carbon monoxide (CO) are then compiled for various ecosystems and types of biomass burning

3.2.1. Biomass Burning Connections to Fundamental Pyrolysis Processes. Figure 4 summarizes the key processes controlling emissions from open biomass burning. Emissions of BBVOCs begin during distillation when oils and other higher volatility compounds evaporate. As the temperature rises, the pyrolysis of cellulose, hemicellulose, lignin, and proteins results in the breakdown of chemical bonds and release of volatile gases. In biomass burning, the BBVOCs formed by pyrolysis may undergo further transformations through combustion within the flames, leading to the formation of highly oxidized molecules, such as CO_2 and NO.[35,36] Generally, pyrolysis is considered to occur in the "smoldering" phase of burning and emits BBVOCs that escape flame processing, while combustion occurs during "flaming". The modified combustion efficiency (MCE), which relates the ratio between smoldering (CO) and flaming (CO_2) combustion tracers, is a quantity used to estimate the extent to which these different combustion processes contribute to observed trace gas and particle emissions.[69] Furanoid emissions, along with other BBVOCs, are inversely proportional to MCE, i.e., highest during smoldering combustion.[2,33,70−72] Observations of smoke from ambient wildfires and laboratory simulations of fuel mixtures typically observed in the field show that furanoid emissions are generally well-correlated to CO, regardless of fuel type.[33,72]

Further variability in furanoid emissions from biomass burning have been tied to differences in pyrolysis temperature.[35,73] For example, Sekimoto et al.[35] analyzed PTR-ToF-MS measurements of laboratory smoke from the open biomass burning of North American ecosystems using positive matrix factorization (PMF) source apportionment and found that the variability in BBVOCs could largely be explained by either high- or low-temperature pyrolysis (Figure 4A). Furanoid emissions were best explained by a linear combination of the high- and low-temperature PMF factors, which were interpreted to mean that furanoid emissions resulted from pyrolysis at intermediate temperatures. These results are consistent with the temperature-dependent furanoid emissions observed in laboratory pyrolysis studies,[17,18,39,40] as described in Section 3.1 and shown in Figure 4B.

3.2.2. Summary of Furanoid Emission Factors. Table 2 summarizes the reported emission factors for furanoids measured across ecosystems and other forms of biomass burning, including residential heating/cooking, dung burning, land/agricultural clearing, and garbage burning. A complementary table summarizing the individual measurements, instrumental techniques, and measurement environment (laboratory vs field) is provided in the supplement (Supporting Information Table S1). Figure 5 complements Table 2 and shows the distribution of furanoids measured for temperate forest, chaparral, and peat fuel types, which have the greatest number of reported furanoid emission factors. Other tables are included in the supplement which compile observed furanoid emission ratios to CO (ER = Δfuranoid/ΔCO, ppb ppm^{-1}), measurements of MCE, and corresponding emission factors of CO and CO_2 (Tables S2 and S3). Here, we focus on discussing observations of emission factors, which are most commonly reported in the literature.

Furan is the most commonly measured species across all forms of biomass burning. As shown in Table S1, this is partly due to the range of instruments capable of quantifying furan,

https://doi.org/10.1021/acsearthspacechem.3c00226
ACS Earth Space Chem. XXXX, XXX, XXX−XXX

Table 2. Emission Factors of Furanoids (g kg^{-1}, Avg ± Stdev) from Biomass Burning of Commonly Reported Fuel Types, Ecosystems, and Other Forms of Biomass Burning (Number of Studies *N*) [See References 21−24, 32, 33, 70−99[a]

Compounds		Savanna	Tropical Forest	Temperate Forest	Boreal Forest	Chaparral	Peat	Open Cooking	Cooking Stoves	Dung burning	Land Clearing / Ag Burning	Garbage Burning	References
Furan (C_4H_4O)	N	3	3	18	4	7	9	4	6	4	9	3	21, 22, 24, 32, 33, 70-72, 75-95
	Avg	0.32	0.46	0.36	0.59	0.16	0.88	0.72	0.26	0.59	0.30	0.13	
	Stdev	0.10	0.19	0.26	0.47	0.09	0.56	0.91	0.31	0.31	0.27	0.08	
2-methylfuran + 3-methylfuran (C_5H_6O)	N	3	3	12	2	4	7	2	4	2	6	1	21-24, 71, 76, 80-82, 85, 86, 89-96
	Avg	0.24	0.38	0.29	0.39	0.12	0.30	0.19	0.13	0.58	0.25	0.09	
	Stdev	0.18	0.43	0.17	0.12	0.05	0.20	0.04	0.09	0.47	0.30	---	
2-furfural + 3-furfural ($C_5H_4O_2$)	N	1	1	15	2	5	6	3	5	2	6	1	21, 22, 24, 32, 71, 72, 76, 80, 81, 85, 86, 88, 90-92, 94, 95, 97-99
	Avg	1.58	0.41	0.68	0.63	0.30	1.03	0.51	0.13	0.62	0.70	0.18	
	Stdev	---	---	0.76	0.04	0.21	0.85	0.37	0.10	0.64	0.52	---	
2,5-dimethylfuran + 2-ethylfuran + C2-substituted furan isomers (C_6H_8O)	N	2	1	12	2	4	5	1	1	1	6	1	21-24, 71, 72, 76, 80, 81, 85, 86, 90, 94-96
	Avg	0.08	0.03	0.15	0.20	0.05	0.16	0.04	0.05	0.68	0.21	0.03	
	Stdev	0.10	---	0.12	0.16	0.04	0.10	---	---	---	0.24	---	
Benzofuran (C_8H_6O)	N	2	1	10	2	4	5	1	1	1	6	2	21-24, 71, 72, 80, 81, 86, 90, 94-96
	Avg	0.02	0.02	0.06	0.03	0.05	0.22	0.05	0.00	0.07	0.07	0.13	
	Stdev	0.01	---	0.05	0.02	0.04	0.39	---	---	---	0.07	0.17	
2-furanmethanol ($C_5H_6O_2$)	N	1	0	6	2	2	3	1	1	1	5	1	22-24, 80, 86, 90, 94
	Avg	0.86	---	0.20	0.11	0.13	0.20	0.29	0.03	0.90	0.40	0.14	
	Stdev	---	---	0.16	0.08	0.12	0.17	---	---	---	0.38	---	
5-methyl furfural ($C_6H_6O_2$)	N	1	0	7	2	2	3	1	1	1	5	1	23, 24, 72, 80, 86, 88, 94, 95
	Avg	0.23	---	0.29	0.13	0.16	0.22	0.09	0.03	0.31	0.46	0.08	
	Stdev	---	---	0.18	0.11	0.13	0.17	---	---	---	0.42	---	
2(3H)-furanone ($C_4H_4O_2$)	N	1	0	7	2	2	3	1	1	1	5	1	23, 24, 32, 72, 80, 86, 90, 94, 95
	Avg	0.84	---	0.46	0.31	0.15	0.33	0.21	0.08	0.81	0.63	0.17	
	Stdev	---	---	0.10	0.21	0.06	0.24	---	---	---	0.35	---	
Methyl benzofuran (C_9H_8O)	N	0	0	6	2	3	4	0	0	1	3	0	21-24, 71, 86, 94
	Avg	---	---	0.04	0.04	0.06	0.06	---	---	0.10	0.06	---	
	Stdev	---	---	0.02	0.04	0.04	0.05	---	---	---	0.02	---	
Tetrahydrofuran (C_4H_8O)	N	1	1	5	0	2	1	0	0	0	3	0	21, 22, 71, 80, 96
	Avg	0.02	0.02	0.01	---	0.00	0.01	---	---	---	0.01	---	
	Stdev	---	---	0.01	---	0.00	---	---	---	---	0.02	---	
Dihydrofuran (C_4H_6O)	N	1	1	5	0	2	2	0	0	0	3	0	21, 22, 71, 80, 96
	Avg	0.01	0.01	0.01	---	0.01	0.01	---	---	---	0.05	---	
	Stdev	---	---	0.01	---	0.01	0.00	---	---	---	0.07	---	
2-propyl furan and other C3-substituted furans ($C_6H_6O_2$)	N	0	0	4	1	1	3	0	0	1	4	0	23, 24, 80
	Avg	---	---	0.04	0.15	0.03	0.07	---	---	0.31	0.06	---	
	Stdev	---	---	0.05	---	---	0.08	---	---	---	0.11	---	
5-(hydroxymethyl)-2-furfural ($C_6H_6O_3$)	N	0	0	3	2	1	2	0	0	1	2	0	23, 24, 80, 94
	Avg	---	---	0.24	0.21	0.07	0.16	---	---	0.38	0.23	---	
	Stdev	---	---	0.21	0.29	---	0.14	---	---	---	0.31	---	
5-hydroxy 2-furfural/2-furoic acid ($C_5H_4O_3$)	N	0	0	3	2	1	1	0	0	1	1	0	24, 80, 86, 94
	Avg	---	---	0.12	0.09	0.02	0.14	---	---	0.23	0.18	---	
	Stdev	---	---	0.05	0.06	---	---	---	---	---	---	---	

https://doi.org/10.1021/acsearthspacechem.3c00226
ACS Earth Space Chem. XXXX, XXX, XXX−XXX

Table 2. continued

Compounds		Savanna	Tropical Forest	Temperate Forest	Boreal Forest	Chaparral	Peat	Open Cooking	Cooking Stoves	Dung burning	Land Clearing / Ag Burning	Garbage Burning	References
5-hydroxymethyl-2[3H]-furanone ($C_5H_6O_3$)	N	0	0	2	1	1	1	0	0	1	1	0	24, 86
	Avg	---	---	0.08	0.13	0.05	0.10	---	---	0.29	0.58	---	
	Stdev	---	---	0.06	---	---	---	---	---	---	---	---	
5-hydroxymethyl tetrahydro 2-furanone + 5-hydroxy tetrahydro 2-furfural ($C_5H_8O_3$)	N	0	0	2	1	1	1	0	0	1	1	0	24, 86
	Avg	---	---	0.08	0.13	0.05	0.10	---	---	0.29	0.58	---	
	Stdev	---	---	0.06	---	---	---	---	---	---	---	---	
2,5-di(hydroxymethyl) furan + methyl hydroxy dihydrofurfural ($C_6H_8O_3$)	N	0	0	1	2	1	1	0	0	1	1	0	24, 94
	Avg	---	---	0.22	0.10	0.04	0.06	---	---	0.34	0.30	---	
	Stdev	---	---	---	0.13	---	---	---	---	---	---	---	

[a]Entries are ordered and colored by the furanoids most commonly reported in literature (darker colors correspond to a greater number of reported emission factors). A full table describing the individual measurements, instrumental techniques, and measurement environment (laboratory vs field) is provided in the Supporting Information (Table S1). Other supplemental tables summarize furanoid emission ratios to CO (ER = Δfuranoid/ΔCO, ppb ppm^{-1}), measurements of MCE, and corresponding emission factors of CO and CO_2 (Tables S2 and S3).

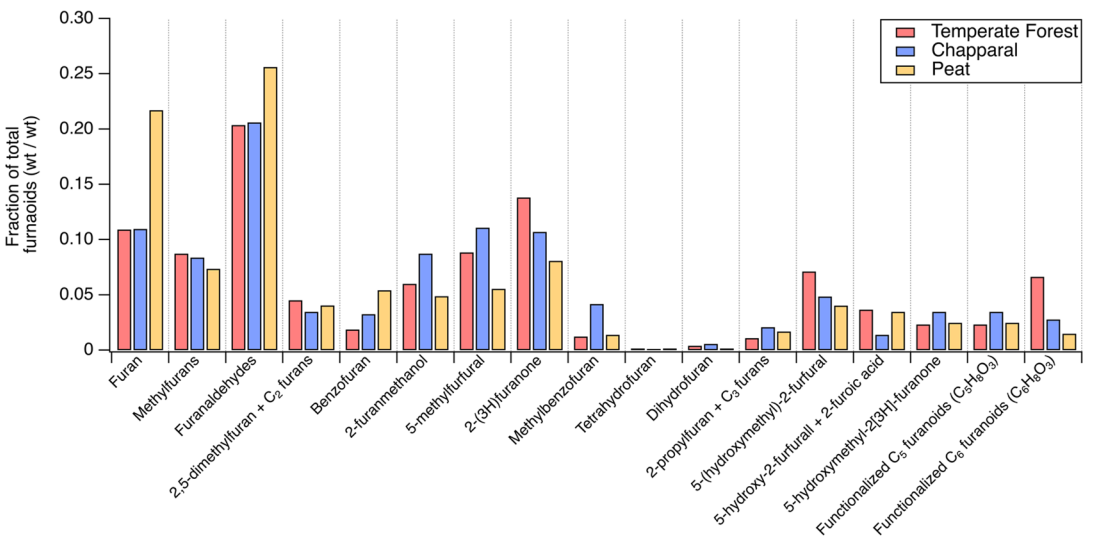

Figure 5. Distribution of furanoid mass for temperate forest, chapparal, and peat fuel types shown in Table 2. The fractions of total furanoids are calculated based on the emission factors reported in Table 2. Species are ordered by the furanoids most commonly reported in the literature.

including FTIR, GC-MS, and proton-transfer-reaction mass spectrometry (PTR-MS). Similarly, methylfurans (dominant isomer, 2-MF), furanaldehydes (dominant isomer, 2-furfural), and dimethylfurans (dominant isomer, 2,5-DMF) are commonly measured by GC-MS and PTR-MS. These species are also among the most abundant furanoids emitted from most fuel types, and their sum accounts for 48, 47, and 55% of the total furanoid emissions for temperate forest, chaparral, and peat emissions, respectively (Figure 5).

Functionalized furanoids such as 2-(3*H*)furanone, 5-methyl-2-furfural, 5-hydroxymethyl-2-furfural, and 2-furanmethanol are key products of cellulose pyrolysis.[18,40] These species have only recently been identified in the laboratory and ambient biomass burning smoke using advanced instrumentation such as two-dimensional gas chromatography mass spectrometry (GC×GC)[23] and high-resolution mass spectrometry (e.g., PTR-ToF-MS);[24] consequently, measurements of these species are limited (see Table S1). Laboratory studies such as those by Hatch et al.[22,23,74] suggest that these species are abundant. This is reflected in Figure 5, which shows that 2-(3*H*)-furanone, 5-methyl-2-furfural, 5-hydroxymethyl-2-furfural, and 2-furanmethanol represent 24−35% of the total measured furanoids emitted from well-characterized fuel types such as temperate forest, chapparal, and peat. Further characterization of these species by advanced gas chromatography may help to determine emission factors for lesser-studied fuel types.

3.2.3. Data Gaps and Measurement Uncertainties. Table 2 and Table S1 show that the determination of furanoid emission factors is limited for many fuel types. Recent field and laboratory efforts have expanded the characterization of smoke emitted from fuels common to the western and southeastern U.S.,[24,86,99] including temperate forest, chaparral, and agricultural refuse. Several laboratory and field campaigns have also been conducted to quantify peat emissions due to their seasonal impact on air quality in southeast Asia.[88−90] In contrast, furanoid emissions are not well quantified for relevant fuel types consumed by wildfires in Africa (e.g., Savanna), sources of urban and rural air pollution (e.g., residential wood burning and cooking), and other fuels (e.g., dung and garbage). It should be noted that the distribution of furanoids is similar across the well-studied fuel

https://doi.org/10.1021/acsearthspacechem.3c00226
ACS Earth Space Chem. XXXX, XXX, XXX−XXX

types shown in Figure 5. Consequently, it is likely that other types of biomass burning will also be characterized by high proportions of functionalized furanoids and would benefit from measurements using advanced instrumentation, including GC×GC-MS and chemical ionization mass spectrometry.

Table S1 shows that many of the highly functionalized furanoid emission factors reported in the literature result from measurements by PTR-ToF-MS. While this instrument is capable of quantifying a broad range of species, PTR-ToF-MS data alone cannot be used to quantify highly oxygenated species. For example, 5-methyl-2-furfural is isomeric with catechol, which is an abundant BBVOC in smoke. Koss et al.[24] leveraged GC preseparation followed by PTR-ToF-MS analysis to identify isomer distributions, and subsequent studies have used these distributions to estimate furanoid emission factors measured by PTR-ToF-MS.[72,86] However, these assignments were for a limited number of fuel types. More work is needed to expand the use of GC preseparation and improve the quantification of furanoids by PTR-ToF-MS.

Finally, many of the functionalized furanoids reported here are difficult to quantify due to a lack of unique standards or uncertainties in the delivery of quantifiable calibration gases. This uncertainty affects measurements by GC-MS, GC×GC-MS, and PTR-ToF-MS. Studies deploying GC-based instrumentation have estimated sensitivities by assuming that instrument responses to uncalibrated furanoids are the same as those of calibrated furanoids with similar structures.[22] Studies deploying PTR-ToF-MS have calculated sensitivities toward many important functionalized furanoids using proton-transfer rate constants, which typically have uncertainties exceeding 50%.[100] More work is needed to improve the quantification and reliable delivery of calibration standards of functionalized furanoids, e.g., 5-methyl-2-furfural, 5-hydroxymethyl-2-furfural, and 2-furanmethanol.

3.3. Estimated Global Flux of Furanoids from Biomass Burning. Atmospheric models use emission factors, such as those described in Section 3.2, to derive BBVOC emission fluxes.[101] Individual VOC emissions are estimated as the product of fuel-specific emission factors (EFs) and the amount of dry fuel consumed during combustion (F).

$$\text{emissions/g} = [\text{EF}/(\text{g kg}^{-1})](\text{F/kg})$$

where F can be estimated using satellite measures of fire radiative power or bottom-up estimates of the fire burned area. The Global Fire Emissions Database (GFED v4.1s) is a bottom-up inventory that estimates fire burned area from the Moderate Resolution Imaging Spectroradiometer (MODIS) satellite instrument.[102−104] Recent intercomparisons between emissions inventories have found that GFED provides conservative estimates of total biomass burning emissions and may represent a lower-limit estimate of fuel consumption.[104,105] For example, Stockwell et al.[105] recently compared GFED against aircraft observations of total carbon emissions from Western U.S. wildfires and showed that GFED was among the most reliable inventories to capture fire-to-fire variability in total carbon emission but underestimated total emissions by an average of ∼45%. Jin et al.[106] observed a similar underestimation for other biomass burning emissions inventories in model simulations of biomass burning across the Western U.S.

Using GFED and the biome-specific emission factors derived as part of this review (Table 2), it is estimated that furanoids were emitted to the atmosphere at an average rate of at least 9.4 Tg year^{-1} between 1997 and 2020. This global flux is comparable to the emissions of nonheterocyclic aromatic compounds from anthropogenic sources (∼23 Tg of C/year)[107] which are known to degrade urban air quality and modulate OH reactivity.[108] GFED exhibits interannual variability consistent with recent evaluations of total biomass burning emissions conducted by van Wees et al.[109]

4. GAS-PHASE TROPOSPHERIC DEGRADATION OF FURANOIDS

Once emitted to the atmosphere, furanoids may react with the major tropospheric oxidants, i.e., the hydroxyl radical (OH), nitrate radical (NO_3), ozone (O_3), and chlorine atom (Cl). These reactions lead to the formation of secondary pollutants that alter atmospheric composition. It is essential to review the reaction rate coefficients for furanoids with each of these oxidants in order to elucidate furanoid tropospheric lifetimes and evaluate their environmental impacts on local and regional scales. Likewise, a detailed description of the furanoid degradation pathways and reaction products is an essential input to air quality models used to evaluate the impact of pollutants on atmospheric photochemical cycles, air quality, and human health.

This section provides a detailed review of the kinetic and mechanistic data describing furanoid degradation with each of the major atmospheric oxidants. Section 4.1 reviews the kinetic data and the estimated lifetimes of furanoids observed in biomass burning plumes. Section 4.2 describes the reported chemical degradation pathways and subsequent gas-phase products. Finally, Section 4.3 summarizes the known secondary organic aerosol yields.

4.1. Furanoids Kinetics with Tropospheric Oxidants. This section provides a detailed review and a critical assessment of the kinetic data describing furanoids degradation with each of the major atmospheric oxidants. The kinetic data with OH radicals (the major day-time oxidant) are discussed first, followed by those of NO_3 (the dominant nighttime oxidant), and finally by those of O_3 and Cl atoms. It is worth noting that the relative loss of furanoids to OH, NO_3, and O_3 in biomass burning plumes depends on several parameters, such as the availability of OH precursors (e.g., HONO and formaldehyde), abundance of O_3, sufficient mixing ratios of NO_2 to produce NO_3, the actinic flux (e.g., day, night, transparent plumes, and opaque plumes), furanoid structure, etc. The available room-temperature (295 ± 5 K) rate coefficient values reported in each study are critically assessed and are averaged when multiple studies are available. When sufficient data are available, a non-Arrhenius equation is fit to temperature-dependent kinetic data using the following equation

$$k = A\left(\frac{T}{T_{\text{reference}}}\right)^{b} + C\left(\frac{T}{T_{\text{reference}_1}}\right)^{d} \exp\left(\frac{-E}{RT}\right)$$

where k is the rate coefficient (in cm^3 molecule^{-1} s^{-1}), A and C are factors that denote the temperature dependence of the pre-exponential factor, T is the temperature, $T_{\text{reference}}$ and $T_{\text{reference}_1}$) are reference temperatures used to fit the data, E is the activation energy, and R is the ideal gas constant. Throughout the discussion of the OH radical kinetics (Section 4.1.1), we discuss observations of rate coefficients relevant to atmospheric and combustion temperatures. Furanoid formation and OH chemistry occurs across these temperature ranges, and changes to kinetic data provide information about the temperature

https://doi.org/10.1021/acsearthspacechem.3c00226
ACS Earth Space Chem. XXXX, XXX, XXX−XXX

Table 3. Summary of Experimental Data for the Reaction of Furanoids with the Hydroxyl Radical (OH)[a]

Compound	Method/ technique	Temperature (K)	Pressure (Torr)	A (cm^3 $molecule^{-1}$ s^{-1})	E/R (K)	k (295 ± 5) (10^{-11} cm^3 $molecule^{-1}$ s^{-1})	References
				Unsubstituted Furanoids			
Tetrahydrofuran (THF)	RR-ASC/GC-FID	305 ± 2	760			1.4 ± 0.2	Winer et al.[110]
	AR-QR-FP/RF	298	20−200			1.63 ± 0.16 (20 Torr)	Ravishankara and Davis[111]
						1.59 ± 0.39 (200 Torr)	
	AR-PC-/RF	296	25−50			1.78 ± 0.16	Wallington et al.[112]
	RR-ASC/GC-FID	298 ± 2	760			1.80 ± 0.07	Moriarty et al.[113]
	AR-ASC/PLP-LIF	263−372	100	$(9.7 \pm 3.2) \times 10^{-12}$	−177 ± 67	1.67 ± 0.07	
	AR-ST/UV_{abs}	802−1338		$(1.50 \pm 0.01) \times 10^{-22}(T)^{3.407}$	−2436.7 ± 7.84	n.d.	Giri et al.[114]
	RR-QR/GC-FID	260−360	825 ± 75	$(5.7 \pm 3.2) \times 10^{-12}$	349 ± 168	1.73 ± 0.23	Illés et al.[115]
				$(1.66 \pm 0.80) \times 10^{-12}\left(\frac{T}{293}\right)^{1.77\pm0.26}$	684 ± 142	**1.66 ± 0.26**	**mean value**
Furan	AR-DFT/RF	295 ± 1	1.63−2.54			10.5 ± 0.8[b]	Lee and Tang[116]
	RR-ASC/GC-FID	298 ± 2	735			3.66 ± 0.26	Atkinson et al.[117]
	AR-PC-FP/RF	245−425	30−150	$(13.3 \pm 2.9) \times 10^{-12}$	333 ± 67	4.05 ± 0.26[c]	Wine and Thompson[118]
	RR-ASC/GC-FID	300 ± 2	760			4.19 ± 0.21	Bierbach et al.[119]
	AR-ST/UV_{abs}	924−1388	889−1482	$783.39T^3$	−1866.7	n.d.	Elwardany et al.[120]
	AR-PLP/LIF	294−595	3.8−7600	$3.5 \times 10^{-11}\left(\frac{T}{300}\right)^{-1.61} + 9.5 \times 10^{-11}\left(\frac{T}{100}\right)^{-0.44}$	−3079	3.34 ± 0.48 (P < 200 mbar)	Whelan et al.[121]
						3.45 ± 0.13 (P > 2 bar)	
	RR-ASC/SIFT-MS, FTIR	273−353	760	$(13.0 \pm 1.2) \times 10^{-12}$	336 ± 20	4.07 ± 0.32	Angelaki et al.[122]
	RR-PR/FTIR	254−1388	760	$\mathbf{4.03 \times 10^{-11}\left(\frac{T}{300}\right)^{-1.48} + 5.83 \times 10^{-11}\left(\frac{T}{1000}\right)^{2.18}}$	**−3416**	**3.79 ± 0.45**	**mean value**
				Methylfurans			
2-methylfuran (2-MF)	RR-ASC/GC-FID	300 ± 2	760			6.19 ± 0.30	Bierbach et al.[119]
	RR-ASC/GC-FID	296 ± 2	735			7.31 ± 0.35	Aschmann et al.[123]
	AR-PLP/LIF	295−350	9601−15826	$(1.23 \pm 0.37) \times 10^{-11}$	500	6.69 ± 0.37	Eble et al.[124]
	AR-ST/UV_{abs}	890−1327	798−1186	8.85×10^{13}	−2285	n.d.	Elwardany et al.[120]
	AR-PLP/LIF	296−668	3.8−7600	$7.3 \times 10^{-11}\left(\frac{T}{300}\right)^{-1.97} + 5.3 \times 10^{-8}\left(\frac{T}{100}\right)^{-4.19}$	−8756	7.34 ± 0.29 (P < 200 mbar)	Whelan et al.[121]
						6.80 ± 0.30 (P > 2 bar)	
						6.89 ± 0.70	**mean value**
3-methylfuran (3-MF)	RR-ASC/GC-FID	298 ± 2	740			9.35 ± 1.87	Atkinson et al.[11]
	RR-ASC/GC-FID	296 ± 2	735			8.73 ± 0.18	Aschmann et al.[123]
	RR-ASC-PC/GC-FID, CG-MS, FTIR	296 ± 2	760			10.7 ± 2.1	Tapia et al.[125]
	AR-DFT/LIF	273−368	2−6	$(3.2 \pm 0.4) \times 10^{-11}$	310 ± 40	9.1 ± 0.3	Liljegren and Stevens[126]
						9.47 ± 1.23	**mean value**

https://doi.org/10.1021/acsearthspacechem.3c00226
ACS Earth Space Chem. XXXX, XXX, XXX−XXX

Table 3. continued

Compound	Method/ technique	Temperature (K)	Pressure (Torr)	A (cm^3 $molecule^{-1}$ s^{-1})	E/R (K)	k (295 ± 5) (10^{-11} cm^3 $molecule^{-1}$ s^{-1})	References
				Dimethylfurans			
2,5-dimethylfuran (2,5-DMF)	RR-ASC/GC-FID	300 ± 2	760			14.63 ± 1.02[d]	Bierbach et al.[119]
	RR-ASC/GC-FID	296 ± 2	735			12.5 ± 0.4	Aschmann et al.[123]
	AR-PLP/LIF	295−350	5025−11701	$(3.38 \pm 1.00) \times 10^{-11}$	−219	7.04 ± 1.00[b]	Eble et al.[124]
	AR-ST/UV_{abs}	915−1278	904−1322	1.03×10^{14}	2182	n.d.	Elwardany et al.[120]
	AR-PLP/LIF	295−635	3.8−7600	$9.2 \times 10^{-11}\left(\frac{T}{300}\right)^{-1.78} + 2.0 \times 10^{-8}\left(\frac{T}{100}\right)^{-4.15}$	−7252	11.5 ± 0.7 (P < 200 mbar)	Wheln et al.[121]
						9.20 ± 0.40 (P > 2 bar)	
						11.96 ± 2.76	**mean value**
2,3-dimethylfuran (2,3-DMF)	RR-ASC/GC-FID	296 ± 2	735			12.6 ± 0.4	Aschmann et al.[123]
				Aldehydes			
2-furfural	RR-ASC/GC-FID	298 ± 2	750			3.51 ± 0.11	Bierbach et al.[127]
3-furfural	RR-ASC/GC-FID	298 ± 2	750			4.85 ± 0.16	Bierbach et al.[127]
5-methyl-2-furfural	RR-ASC/GC-FID	298 ± 2	750			5.10 ± 0.21	Bierbach et al.[127]
				Ketones/Dicarbonyls			
2-(3*H*)-furanone	RR-ASC/GC-FID	296 ± 2	750			4.45 ± 0.26	Bierbach et al.[128]
5-methyl-2-(3*H*)-furanone	RR-ASC/GC-FID	296 ± 2	750			6.90 ± 0.46	Bierbach et al.[128]
Maleic anhydride	RR-ASC/FTIR	296 ± 2	750			0.19 ± 0.01	Bierbach et al.[128]
	AR-PLP/LIF-FTIR	283−374	50−200	$(1.55 \pm 0.20) \times 10^{-12}$	−410 ± 44	0.0393 ± 0.0028	Chattopadhyay et al.[129]
				Benzofurans			
2,3-dihydrobenzofuran	RR-ASC/FTIR	298 ± 2	740			3.66 ± 0.56	Atkinson et al.[130]
2,3-benzofuran	RR-ASC/GC-FID	298 ± 2	740			3.73 ± 0.74	Atkinson et al.[130]
				Other Furanoids			
5-methyl-5-vinyltetrahydrofuran-2-ol	RR-ASC/FTIR	298 ± 5	740			7.40 ± 0.90	Calogirou et al.[131]
2,3-dihydrofuran	RR-PC/GC-FID	298 ± 2	800			11.95 ± 2.79	Alwe et al.[132]
2,5-dihydrofuran	RR-PC/GC-FID	298 ± 2	800			6.45 ± 1.69	Alwe et al.[132]
2-ethylfuran	RR-ASC/GC-FID	300 ± 2	760			10.77 ± 2.11	Bierbach et al.[119]

[a]Abbreviations for select species are shown in parentheses. Other abbreviations used in the table: RR, relative rate method; AR, absolute rate method; ASC, atmospheric simulation chamber—Teflon or glass made; DFT, discharge flow tube; ST, shocked tube; PC, Pyrex cell; QR, quartz reactor; PLP, pulse laser fluorescence; LIF, laser-induced fluorescence; RF, resonance fluorescence; FP, flash photolysis; GC-FID, gas chromatography-flame ionization detector; GC-MS, gas chromatography mass spectrometry; UV_{abs}, ultraviolet absorption; FTIR, Fourier-transform infrared spectroscopy; SIFT-MS, selected ion flow tube mass spectrometry. Table is organized first by abundance of observations, followed by chemical functionality. The errors reflect those reported from each study. The quoted error limits of the mean value encompass the range of measurements. [b]Data excluded from the mean value. [c]Value determined by averaging results at 298 ± 2 K. The quoted error limits of the mean value encompass the range of measurements. [d]Value scaled based on the current NASA JPL recommended rate coefficient of the reference molecule (*trans*-2-butene).

https://doi.org/10.1021/acsearthspacechem.3c00226
ACS Earth Space Chem. XXXX, XXX, XXX−XXX

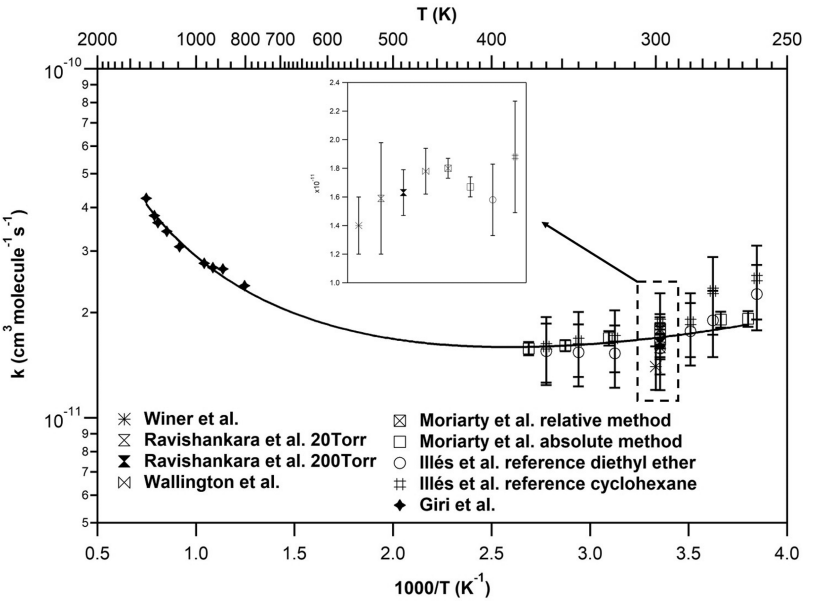

Figure 6. Summary of literature data for the reaction of THF with OH.[110−115] The solid line is a fit of results from Moriarty et al.[113] and from Giri et al.[114] and room-temperature experimental results to a modified Arrhenius expression: $k = A\left(\frac{T}{293}\right)^{b} \exp\left(\frac{-E}{RT}\right)$ (see Table 3).

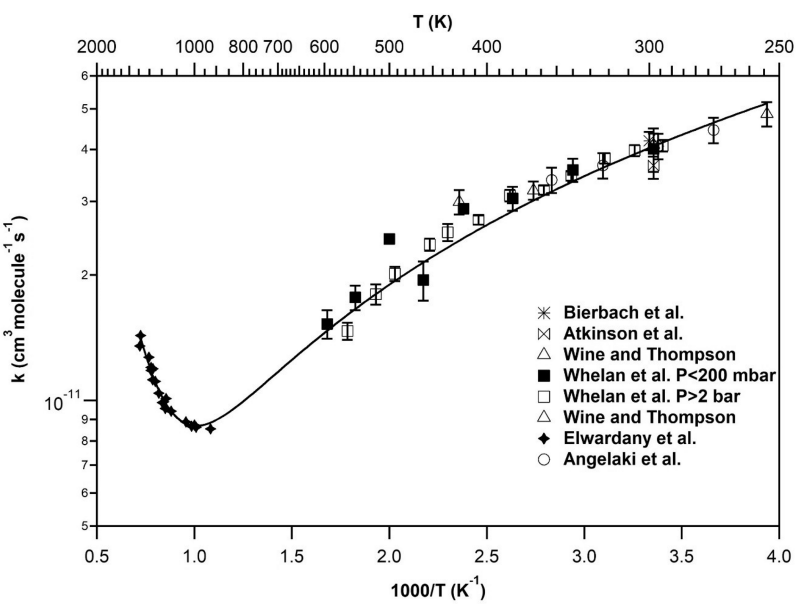

Figure 7. Summary of literature data for the reaction of furan with OH,[117−122] after scaling the values of Whelan et al.[121] and Wine and Thompson,[118] to those of Angelaki et al.[122] The solid line is a fit of the measurements to a modified Arrhenius expression $k = A\left(\frac{T}{300}\right)^{b} + C\left(\frac{T}{1000}\right)^{d} \exp\left(\frac{-E}{RT}\right)$ (see Table 3).

thresholds where different mechanistic processes, such OH-addition or H-abstraction pathways, dominate.

4.1.1. OH Radical Reaction Rate Coefficients. Presently, laboratory OH radical kinetic studies are not available for all of the furanoids listed in Table 1. There are several studies in the literature reporting rate coefficients for the OH radical reaction with tetrahydrofuran (THF), furan, and other furanoid derivatives. A summary of the published kinetic results is presented in Table 3 which includes the method/technique used in each study, the temperature of the measurements, room-temperature (295 ± 5 K) rate coefficients, and/or an Arrhenius expression. We organize this section by first describing the furanoids with the greatest number kinetic measurements. This section concludes with an outline of needs for future research.

4.1.1.1. Tetrahydrofuran + OH. There are six literature studies reporting the rate coefficient for the THF reaction with OH radicals.[111−115,118] Results are presented in Table 3 and Figure 6. Winer et al.,[110] Moriarty et al.,[113] and Illés et al.[115] used relative rate methods to determine the rate coefficient of THF + OH reaction at ambient temperature (296−307 K). Experiments were performed at atmospheric pressure (760−825 Torr) in smog chambers/photochemical reactors, and the gas mixture was monitored by GC-FID. Isobutene and methoxypropanol were used as reference compounds by Winer et al.[110] and Moriarty et al.,[113] respectively. Diethyl ether and cyclohexane

https://doi.org/10.1021/acsearthspacechem.3c00226
ACS Earth Space Chem. XXXX, XXX, XXX−XXX

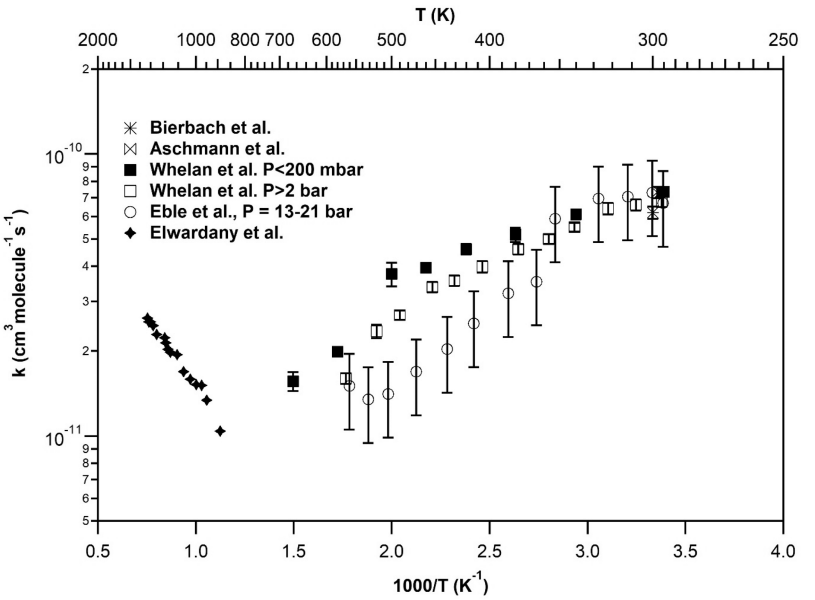

Figure 8. Summary of literature data for the reaction of 2-MF with OH.[119−121,123,124] Data points from Eble et al.[124] were extracted from the graph provided in their study.

were used by Illés et al.[115] The results from these studies agree to within 22%.

Ravishankara et al.,[111] Wallington et al.,[112] and Moriarty et al.[113] applied absolute methods to determine the room-temperature (296−300 K) rate coefficient of the THF + OH reaction under pseudo-first-order conditions in excess of THF. Ravishankara et al.[111] and Wallington et al.[112] performed experiments over the pressure ranges of 20−200 and 25−50 Torr, respectively. In both studies, no pressure dependence was observed and the rate coefficients agreed to within 12%.

Kinetic measurements at ambient temperature agree to within 22% with an average rate constant of $k(300\pm5\text{K}) = (1.66 \pm 0.26) \times 10^{-11}$ cm^3 molecule^{-1} s^{-1}. The quoted error encompasses the range of the measurements. This value is applicable in the temperature range 295 ± 5 K.

The temperature dependence of the THF + OH reaction has been reported by Moriarty et al.[113] (263−372 K), Illés et al.[115] (260−360 K), and Giri et al.[114] (802−1338 K). A slight negative temperature dependence is observed between 260 and 372 K, indicating that the reaction proceeds through a complex formation and an addition−elimination mechanism. This is also supported by the ab initio calculations reported by Giri et al.[114] In shock tube experiments at elevated temperatures, Giri et al.[114] show that the reaction exhibits a positive temperature dependence consistent with a direct H atom abstraction mechanism. Illés et al.[115] report high uncertainties in their temperature-dependent kinetic data; therefore, we recommend the results from Moriarty et al.[113] for the temperature range 263−372 K. At combustion-relevant temperatures, measurements are only available from Giri et al.,[114] and these dependencies are presented here in the absence of other measurements. Combining the data from Moriarty et al.,[113] Giri et al.,[114] and studies focused on the room-temperature kinetics, the following expression is proposed for the temperature-dependent rate coefficient at 760 Torr in the range of 263−1338 K:

$$k_{\text{THF+OH}}/(\text{cm}^3\ \text{molecule}^{-1}\ \text{s}^{-1}) = (1.66 \pm 0.80) \times 10^{-12}\left(\frac{T}{293}\right)^{1.77} \exp\left(\frac{685}{T}\right)$$

While the proposed expression captures the temperature dependencies currently reported in literature (Figure 6), there is a further need for temperature-dependent kinetic measurements in the intermediate range of 400−800 K to link the available low- and high-temperature data.

4.1.1.2. Furan + OH. There are seven studies reporting the rate coefficient for the OH + furan reaction. The literature results are presented in Table 3 and displayed in Figure 7. Atkinson et al.,[117] Bierbach et al.,[119] and Angelaki et al.[122] used relative rate methods to measure a room-temperature rate coefficient (296−302 K). Atkinson et al.[117] and Bierbach et al.[119] monitored the mixture by GC-FID and used *n*-hexane and propene as reference molecules, respectively. The value reported by Atkinson et al.[117] has been revised here using the most recent recommended *n*-hexane + OH rate constant reported by Atkinson.[133] The reference rate constant used by Bierbach et al.[119] is consistent with the latest NASA JPL evaluation[134] and was not revised. Angelaki et al.[122] performed kinetic measurements using atmospheric chambers with SIFT-MS and FTIR as detection techniques. Isoprene, *n*-butanol, THF, and trifluoroethylene (HFO-1123) were the reference molecules used. The results from these studies agree to within 10%.

Lee and Tang,[116] Wine and Thompson,[118] and Whelan et al.[121] measured the OH + furan rate coefficient at room temperature using absolute kinetic methods assuming pseudo-first-order decay. Lee and Tang[116] measured a significantly larger coefficient than all other studies. The reason for the discrepancy is unknown; however, as mentioned by Atkinson et al.,[117] a similar discrepancy was found for the analogous reaction of OH radicals with thiophene, suggesting the possibility of a systematic error in the discharge flow system deployed by Lee and Tang.[116] Therefore, the Lee and Tang[116] results are not considered further in this analysis. Whelan et al.[121] also conducted kinetic measurements over a wide pressure range

https://doi.org/10.1021/acsearthspacechem.3c00226
ACS Earth Space Chem. XXXX, XXX, XXX−XXX

(5 mbar to 10 bar). The rate coefficient exhibited no significant pressure dependence. The available studies show agreement to within 20% for the room-temperature rate coefficient with an average value of $k(297\pm3\text{K}) = (3.79 \pm 0.45) \times 10^{-11}$ cm^3 molecule^{-1} s^{-1}. The quoted error limits of the mean value encompass the range of measurements.

The temperature dependence of the OH + furan rate coefficient has been reported by Wine and Thompson[118] (254−425 K), Whelan et al.[121] (294−595 K), Angelaki et al.[122] (273−353 K), and Elwardany et al.[120] (924−1388 K). Angelaki et al.[122] applied the relative rate method to determine temperature-dependent rate coefficients. Furan and tetrahydrofuran were used as reference molecules. In all of the other studies, the temperature dependence of the rate coefficient was achieved using the absolute method. Over the 254−595 K temperature range, the reaction exhibits a negative temperature dependence consistent with an OH addition mechanism. In shock tube studies performed at elevated temperatures, Elwardany et al.[120] reported a positive temperature dependence consistent with an abstraction reaction. Whelan et al.[121] used a Rice−Ramsperger−Kassel−Marcus (RRKM) chemical reactivity analysis to demonstrate a consistency between their results and those of Elwardany et al.[120] Whelan et al.[121] proposed that the discrepancies between their results and those of Wine and Thompson[118] were due to secondary chemistry in the Wine and Thompson study. Nevertheless, the relative rate kinetic measurements reported by Angelaki et al.[122] are in excellent agreement with the absolute kinetic measurements of Wine and Thompson,[118] and hence contradict the assumption made by Whelan et al.[121] Angelaki et al.[122] scaled the Wine and Thompson[118] and Whelan et al.[121] data to their more precise room-temperature rate coefficient value and proposed the following modified Arrhenius expression, which is given here for the temperature range 254−1388 K at 760 Torr:

$$k_{\text{furan+OH}}/(\text{cm}^3\ \text{molecule}^{-1}\ \text{s}^{-1}) = 4.03 \times 10^{-11}\left(\frac{T}{300}\right)^{-1.48} + 5.83 \times 10^{-11}\left(\frac{T}{1000}\right)^{2.18} \exp\left(\frac{-3415}{T}\right)$$

4.1.1.3. 2-Methylfuran + OH. There are five studies investigating the rate coefficient for the OH + 2-methylfuran (2-MF) reaction. The results from these studies are summarized in Table 3 and displayed in Figure 8.[119−121,123,124] Bierbach et al.[119] and Aschman et al.[123] performed relative rate coefficient measurements at room temperature (294−302 K) using GC-FID.[119,123] Bierbach et al.[119] used propene as a reference compound, while Aschman et al.[123] used 1,3,5-trimethylbenzene. The rate coefficients used for these reference molecules are in excellent agreement with the NASA data evaluation[134] recommendations and revised kinetic evaluation studies.[135] The relative rate kinetic measurements agree to within 15%.

Absolute rate coefficient measurements of the 2-MF + OH radical reaction at room temperature are reported by Eble et al.[124] and Whelan et al.[121] Experiments were performed under pseudo-first-order conditions over a wide pressure range for Eble et al. (12.8−21.1 bar) and Whelan et al. (0.2−2 bar). No significant pressure dependence was observed. The room-temperature data are in agreement to within 18% with a mean value of $k(298\pm3\text{K}) = (6.89 \pm 0.70) \times 10^{-11}$ cm^3 molecule^{-1} s^{-1}. The quoted error limits of the mean value encompass the range of measurements.

Temperature-dependent measurements were performed by Eble et al.[124] (295−450 K), Whelan et al.[121] (296−668 K), and Elwardany et al.[120] (890−1333 K) using absolute methods. Eble et al.[124] observed an abrupt decrease (by a factor of ∼2.5) of the rate coefficients upon increase of temperature above 350 K. The reason for this sharp decrease was not explained. The authors only discussed their measurements below 350 K, and these results are considered here. Within the temperature range of 295−668 K, the reaction follows a negative temperature dependence, consistent with an OH addition reaction. The results presented in the works of Eble et al.[124] and Whelan et al.[121] are in a fairly good agreement in the overlapping temperature range (295−350 K). However, as shown in Figure 8, outside of these temperatures, significant discrepancies between the studies are observed. At higher temperatures, Elwardany et al.[120] reported a positive temperature dependence, indicating that the reaction proceeds mainly through an abstraction pathway. On the basis of RRKM calculations, Whelan et al.[121] demonstrated a consistency between their results and those of Elwardany et al.[120] However, as shown in Figure 8, the temperature-dependent data are not consistent above 360 K. Consequently, we do not provide an equation over the entire temperature range. Further work is needed to resolve these discrepancies.

4.1.1.4. 3-Methylfuran + OH. There are four studies in the literature that report kinetics for the 3-MF + OH reaction.[11,123,125,126] Relative rate coefficient measurements at room temperature (294−300 K) have been reported by Atkinson et al.,[11] Aschman et al.[123] and Tapia et al.[125] The first two studies were conducted in smog chambers using GC-FID, while Tapia et al.[125] carried out experiments in a Pyrex cell and Teflon bags using FTIR, GC-FID, and/or GC-MS, respectively. Atkinson et al.[11] and Aschman et al.[123] used 2,3-dimethyl-2-butene and 1,3,5-trimethylbenzene as reference molecules, respectively. Tapia et al.[125] selected *trans*-2-butene, propene, and 5-methylfurfural as references and applied a weighted average (based on experimental uncertainties) to obtain a mean rate coefficient.[125] The results from each study are summarized in Table 3. The results reported by Atkinson et al.[11] and Aschman et al.[123] are presented here as published since the reference rate coefficients values used in these studies are consistent with recent kinetic evaluations.[135,136] The results reported by Tapia et al.[125] have been revised using the current NASA recommended rate coefficients for the OH + *trans*-2-butene and propene reactions.[134]

Liljegren and Stevens[126] is the only study to use an absolute rate coefficient method to study the 3-MF + OH kinetics. Experiments were carried out at temperatures between 273 and 386 K in a discharge flow reactor using an excess of 3-methylfuran (see Table 3). The kinetics were assumed to follow pseudo-first-order conditions.

There is agreement to within 18% between the relative and absolute kinetic measurements at room temperature, with a mean value of $k(298\pm2\text{K}) = (9.47 \pm 1.23) \times 10^{-11}$ cm^3 molecule^{-1} s^{-1}. The reaction was also found to be independent of pressure between 2 and 760 Torr. Liljegren and Stevens[126] observed a negative temperature dependence for this reaction over the temperature range 273−386 K, which is consistent with an OH addition reaction.

4.1.1.5. 2,5-Dimethylfuran + OH. The kinetics of the 2,5-DMF + OH reaction has been reported in five studies,[119−121,123,124] and results are presented in Table 3. Relative rate kinetic measurements at room temperature (294−302 K) are reported by Bierbach et al.[119] and Aschmann et al.[123] Experiments were performed under atmospheric pressure in

https://doi.org/10.1021/acsearthspacechem.3c00226
ACS Earth Space Chem. XXXX, XXX, XXX−XXX

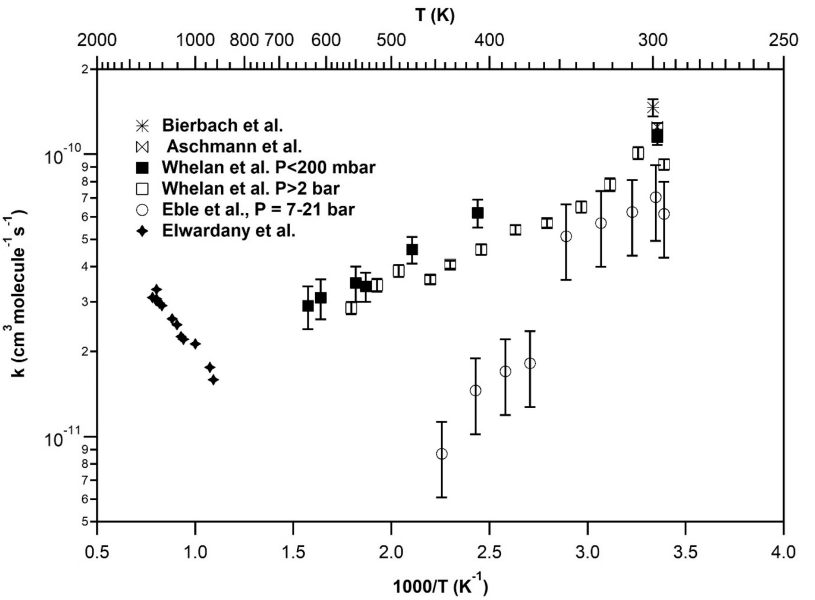

Figure 9. Summary of literature data for the reaction of 2,5-DMF with OH.[119−121,123,124] Data points from Eble et al.[124] were extracted from the graph provided in their study.

smog chambers, and the gas mixture was monitored by GC-FID. *trans*-2-Butene and 1,3,5-trimethylbenzene were the reference molecules used by Bierbach et al.[119] and Aschmann et al.,[123] respectively. The value reported by Bierbach et al.[119] has been revised from the original study using the current NASA recommended rate coefficients for the OH + *trans*-2-butene reaction. The relative rate coefficient measurements are in agreement to within 15%.

Eble et al.[124] and Whelan et al.[121] used absolute kinetic methods to measure the 2,5-DMF + OH reaction at room temperature in excess of 2,5-DMF. The authors assumed that the kinetics followed pseudo-first-order decay. Experiments were performed over a wide pressure range (5 mbar to 21 bar). The rate coefficient determined by Eble et al.[124] is 37% lower than those determined using relative rate methods, while the rate coefficient determined by Whelan et al.[121] is 50% lower. The reason for these discrepancies was not explained. The measurements by Eble et al.[124] are systematically lower than other studies over a wide temperature range (see below); therefore, these results are excluded from the average shown in Table 3. A mean value of $k(298\pm3\text{K}) = (12.0 \pm 2.80) \times 10^{-11}$ cm^3 molecule^{-1} s^{-1} is calculated for the 2,5-DMF + OH reaction, and the estimated uncertainties (~23%) encompass the range of the kinetic measurements.

Eble et al.[124] (295−578 K), Whelan et al.[121] (294−668 K), and Elwardany et al.[120] (915−1278 K) used absolute kinetic measurements to determine the temperature dependence of the 2,5-DMF + OH reaction (Figure 9). Eble et al.[124] observed an abrupt decrease (by a factor of ~2.5) in the rate coefficients upon increase in temperature above 350 K. The authors did not provide a clear explanation for this decrease and used results below 350 K to calculate the temperature dependence. The results from Eble et al.[124] are systematically lower than other literature studies. In Whelan et al.,[121] the low-pressure kinetic measurements (<200 mbar) are systematically higher by ~20% than their high-pressure data (except at room temperature). Although the reason for this discrepancy is unknown, it is likely attributed to differences between the two experimental setups used to evaluate the different temperature regimes. The reaction was found to be independent of pressure between 5 mbar and 10 bar and exhibited a negative temperature dependence between 294 and 668 K, which is consistent with an OH addition reaction. A positive temperature dependence was observed by Elwardany et al.[120] at elevated temperatures, indicating that the reaction proceeds mainly through an abstraction mechanism above 915 K. The temperature-dependent data are not consistent between these studies (see Figure 9), and thus an equation is not presented here. Further work is needed to resolve these discrepancies.

4.1.1.6. Maleic Anhydride + OH. There are two studies reporting the rate coefficient for reaction of maleic anhydride + OH (Table 3).[128,129] Bierbach et al.[128] performed relative rate coefficient measurements at ambient temperature in a quartz chamber and used *n*-butane as the reference molecule. The gases were monitored by a long path FTIR. The original rate constant reported by Bierbach et al.[128] has been revised here using the current NASA recommended rate coefficients for the *n*-butene + OH reaction.[134] Absolute kinetic measurements were carried out by Chattopadhyay et al.[129] at temperatures ranging between 283 and 374 K using pulse laser photolysis−laser-induced fluorescence (PLP-LIF). The kinetics followed pseudo-first-order conditions. The authors used FTIR to determine MA concentrations. Chattopadhyay et al.[129] reported a rate coefficient ~5 times lower than that of Bierbach et al.[128] The reason for this discrepancy was proposed by Chattopadhyay et al.[129] to be due to limitations in the experimental setup used by Bierbach et al.,[128] including (i) low loss of MA by OH (less than 4% chemical conversion), (ii) significant photolytic loss of MA, and (iii) significant dark (or wall) loss of MA. The kinetics exhibited a positive temperature dependence, and Chattopadhyay et al.[129] proposed a mechanism where OH added to the double bond of the heterocyclic ring. The temperature-dependent kinetics determined by Chattopadhyay et al.[129] were best described by an Arrehenius equation

https://doi.org/10.1021/acsearthspacechem.3c00226
ACS Earth Space Chem. XXXX, XXX, XXX−XXX

$$k_{MA+OH}(283-374K) = (1.55 \pm 0.2) \times 10^{-12} \exp\left(\frac{-410 \pm 44}{T}\right)$$

4.1.1.7. Other Furanoids + OH. There are several substituted furanoids where only one study has reported the kinetics with the OH radical, including 2,3-dihydrofuran and 2,5-dihydrofuran,[132] 5-methyl-5-vinyltetrahydrofuran-2-ol,[131] ethylfuran,[119] 2,3-benzofuran and 2,3-dihydrobenzofuran,[130] 2-(3*H*)-furanone and 5-methyl-2-(3*H*)-furanone,[128] 2-furfural, 3-furfural, and 5-methyl-2-furfural,[127] and 2,3-DMF.[123] Due to the limited number of studies, we refer the reader to Table 3 for the reported ambient temperature rate constants.

4.1.1.8. Data Gaps. For many furanoids, there is a need for additional OH kinetic measurements, in particular where there is only one reported study or where results are in poor agreement. Reliable ambient-temperature kinetic data for substituted furanoids are necessary to construct structure activity relationships (SARs), which are not currently available. In addition, there is a need for temperature-dependent kinetic data at (i) tropospheric relevant temperatures below 300 K, which will enable the more accurate determination of furanoid lifetimes and elucidate reaction mechanisms; (ii) combustion relevant temperatures, which are needed since furanoids are proposed biofuels;[7,8] and (iii) intermediate-temperature ranges (400−800 K) to link the cold- and hot-temperature regimes and enable comprehensive temperature-dependent expressions. Priority should be given to studies of the most abundant furanoids released to the atmosphere from biomass burning (see Table 2), or species considered as promising furanoid-based constituents of biofuels (e.g., methyl and dimethylfurans[7,8]).

4.1.2. NO_3 Radical Reaction Rate Coefficients. The NO_3 radical is a major nighttime tropospheric oxidant. The reaction of nitrate radical with different classes of organic compounds has been studied for more than four decades.[137] Nevertheless, there are gaps in kinetic data describing the atmospheric NO_3 oxidation of most organics, including furanoids. Table 4 summarizes the studies that have reported kinetics for the reactions of furanoid with NO_3, and the following discussion describes these results. Average rate coefficients are provided where possible. We begin by describing kinetic measurements of furanoids with the greatest number of observations and then end with an outline of needs for future research.

4.1.2.1. Tetrahydrofuran + NO_3. There are two studies reporting the rate coefficient for the THF + NO_3 reaction[138,139] (Table 4). Relative rate measurements were conducted by Atkinson et al.[138] at room temperature and atmospheric pressure using *trans*-2-butene as a reference molecule. The value reported by Atkinson et al.[138] has been updated using the IUPAC recommended rate coefficient for the NO_3 + *trans*-2-butene. Cabanas et al.[139] employed absolute rate methods at temperatures ranging between 287 and 340 K using a low-pressure (1.1−1.5 Torr) discharge flow tube reactor. These two studies show that ambient-temperature rate constants are independent of pressure between 1.1 and 740 Torr and in agreement to within 4%. Here, we report a mean value of $k(296\pm2K) = (5.02 \pm 0.1) \times 10^{-15}$ cm^3 molecule^{-1} s^{-1}. Cabanas et al.[139] studied the temperature-dependent kinetics between 287 and 340 K and showed that the reaction rate increases with temperature, which is consistent with an H-abstraction reaction mechanism. Cabanas et al.[139] determined an Arrhenius equation for this temperature range as

$$k_{THF+NO_3}(287-340K) = (2 \pm 2) \times 10^{-9} \exp\left(\frac{-3800 \pm 400}{T}\right)$$

More studies are needed to validate these measurements and extend the kinetics to atmospherically relevant temperatures below 287 K.

4.1.2.2. Furan + NO_3. There are five studies reporting rate coefficient data for the furan + NO_3 reaction.[139−143] The results are presented in Table 4 and Figure 10. Atkinson et al.,[140] Kind et al.,[141] Newland et al.,[142] and Al Ali et al.[143] used relative rate methods to measure a room-temperature (292−301 K) rate coefficient. GC-FID, FTIR, and PTR-MS were among the detection techniques used to monitor the kinetics. Atkinson et al.[140] and Kind et al.[141] used *trans*-2-butene as a reference molecule. Newland et al.[142] used four different reference molecules—cyclohexene, α-pinene, camphene, and α-angelicalactone. Finally, Al Ali et al.[143] used α-pinene and β-pinene. The value reported in Atkinson et al.[140] has been updated using the IUPAC recommended rate coefficient for the NO_3 + *trans*-2-butene reaction. The rate coefficients of the reference molecules used in the studies of Kind et al.,[141] Newland et al.,[142] and Al Ali et al.[143] are consistent with IUPAC recommendations and therefore have not been adjusted. The relative rate kinetic results agree to within 33% across all of these studies The rate constant reported by Kind et al.[141] is lower than others, and when excluded, the remaining studies agree to within 5%. We exclude the measurement from Kind et al.[141] from the averaged rate coefficient reported in Table 4.

Cabanas et al.[139] measured the NO_3 + furan rate coefficient at room temperature (298 K) using absolute kinetic methods in a low-pressure (1.1−1.5 Torr) discharge flow tube reactor. The measurement is in good agreement with the relative rate studies described above. When considered together, these studies show that the kinetics do not exhibit a significant pressure dependence between 1.1 and 740 Torr. The mean room-temperature rate coefficient for the NO_3 + furan reaction is $k(296\pm5K) = (1.44 \pm 0.14) \times 10^{-12}$ cm^3 molecule^{-1} s^{-1}. The error limits represent the range of the measurements.

Cabanas et al.[139] studied the temperature dependence of the NO_3 + furan rate coefficient between 260 and 345 K. The reaction exhibits a negative temperature dependence, consistent with an addition-dominated reaction mechanism. The fit these data to an Arrhenius equation and derived the following temperature dependence:

$$k_{furan+NO_3}(260-345K)/[\text{cm}^3\ \text{molecule}^{-1}\ \text{s}^{-1}] = (1.3 \pm 0.8) \times 10^{-13} \exp\left(\frac{700 \pm 200}{T}\right)$$

Additional studies are needed to confirm the reaction temperature dependence.

4.1.2.3. 2-Methylfuran + NO_3. Rate coefficient data for the 2-MF + NO_3 reaction has been reported by Kind et al.,[141] Newland et al.,[142] and Al Ali et al.[143] (see Table 4). These studies used relative rate methods to determine a room-temperature (292−301 K) rate coefficient. Kind et al. used 2,3-dimethyl-2-butene as a reference molecule, Newland et al.[142] used 2-carene, 2,3-dimethyl-2-butene, α-pinene, pyrrole, and 2,5-DMF, while Al Ali et al.[143] used 2-methyl-2-butene, 2,3-dimethyl-2-butene, and γ-terpinene. The rate coefficients reported by these studies agree to within 26%, and no significant

https://doi.org/10.1021/acsearthspacechem.3c00226
ACS Earth Space Chem. XXXX, XXX, XXX−XXX

Table 4. Summary of Available Literature Data for the Reaction of Furanoids with the Nitrate Radical (NO_3)[a]

Compound	Method/technique	Temperature (K)	Pressure (Torr)	A (cm^3 $molecule^{-1}$ s^{-1})	E/R (K)	k (295 ± 5) ($cm^3 molecule^{-1} s^{-1}$)	References
			Unsubstituted Furanoids				
Tetrahydrofuran (THF)	RR-ASC/GC-FID	296 ± 2	740	_		$(4.93 \pm 0.64) \times 10^{-15}$	Atkinson et al.[138]
	AR-DFT/LIF	287−340	1.1−1.5	$(2.0 \pm 2) \times 10^{-9}$	−3800 ± 400	$(5.1 \pm 0.2) \times 10^{-15}$	Cabañas et al.[139]
						$(5.02 \pm 0.1) \times 10^{-15}$	**mean value**
Furan	RR-ASC/GC-FID	295 ± 1	735	_		$(1.44 \pm 0.21) \times 10^{-12}$	Atkinson et al.[140]
	RR-FT/GC-FID	295 ± 2	5.1−150	_		$(9.98 \pm 0.62) \times 10^{-13}$[b]	Kind et al.[141]
	AR-DFT/LIF	260−345	1.1−1.5	$(1.3 \pm 0.8) \times 10^{-13}$	700 ± 200	$(1.3 \pm 0.2) \times 10^{-12}$	Cabañas et al.[139]
	RR-ASC/FTIR	299 ± 2	760			$(1.49 \pm 0.23) \times 10^{-12}$	Newland et al.[142]
	RR-ASC/PTR-MS	294 ± 2	760			$(1.51 \pm 0.38) \times 10^{-12}$	Al Ali et al.[143]
						$(1.44 \pm 0.14) \times 10^{-12}$	**mean value**
			Methylfurans				
2-methylfuran (2-MF)	RR-FT/GC-FID	295 ± 2	5.1−150			$(2.57 \pm 0.17) \times 10^{-11}$	Kind et al.[141]
	RR-ASC/FTIR	299 ± 2	760			$(2.26 \pm 0.52) \times 10^{-11}$	Newland et al.[142]
	RR-ASC/PTR-MS	294 ± 2	760			$(1.91 \pm 0.32) \times 10^{-11}$	Al Ali et al.[143]
						$(2.25 \pm 0.34) \times 10^{-11}$	**mean value**
3-methylfuran (3-MF)	RR-FT/GC-FID	295 ± 2	5.1−150	_		$(2.86 \pm 0.06) \times 10^{-11}$[b]	Kind et al.[141]
	RR-ASC/GC-FID	296 ± 2	740	_		$(1.31 \pm 0.46) \times 10^{-11}$	Alvarado et al.[144]
	RR-ASC/GC-FID, FTIR	296 ± 2	760	_		$(1.26 \pm 0.18) \times 10^{-11}$	Tapia et al. [125]
	RR-ASC/PTR-MS	294 ± 2	760			$(1.49 \pm 0.33) \times 10^{-11}$	Al Ali et al.[143]
						$(1.35 \pm 0.14) \times 10^{-11}$	**mean value**
			Dimethylfurans				
2,3-dimethylfuran (2,3-DMF)	RR-FT/GC-FID	295 ± 2	5.1−150			$(5.83 \pm 0.46) \times 10^{-11}$	Kind et al.[141]
2,4-dimethylfuran (2,4-DMF)	RR-FT/GC-FID	295 ± 2	5.1−150			$(2.72 \pm 0.46) \times 10^{-11}$	Kind et al.[141]
2,5-dimethylfuran (2,5-DMF)	RR-FT/GC-FID	295 ± 2	5.1−150			$(5.78 \pm 0.34) \times 10^{-11}$	Kind et al.[141]
	RR-ASC/FTIR	299 ± 2	760			$(1.02 \pm 0.31) \times 10^{-10}$	Newland et al.[142]
	RR-ASC/PTR-MS	294 ± 2	760			$(5.82 \pm 0.21) \times 10^{-11}$	Al Ali et al.[143]
			Tri- and Tetramethylfurans				
2,3,5-trimethylfuran	RR-ASC/PTR-MS	294 ± 2	760			$(1.66 \pm 0.69) \times 10^{-10}$	Al Ali et al.[143]
Tetramethylfuran	RR-FT/GC-FID	295 ± 2	5.1−150			$(1.18 \pm 0.16) \times 10^{-10}$	Kind et al.[141]
			Aldehydes				
2-furfural	RR-ASC/FTIR	298 ± 2	760			$(1.20 \pm 0.28) \times 10^{-12}$	Colmenar et al.[145]
	RR-ASC/FTIR	299 ± 2	760			$(9.07 \pm 2.30) \times 10^{-14}$	Newland et al.[142]
3-furfural	RR-ASC/FTIR	298 ± 2	760			$(3.41 \pm 0.79) \times 10^{-12}$	Colmenar et al.[145]
5-methyl-2-furfural	RR-ASC/FTIR	298 ± 2	760			$(5.51 \pm 1.27) \times 10^{-12}$	Colmenar et al.[145]
			Ketones				
γ-crotonolactone	RR-ASC/FTIR	299 ± 2	760			$<1 \times 10^{-16}$	Newland et al.[142]
5-methyl-2-(3*H*)-furanone (α-angelicalactone)	RR-ASC/FTIR	299 ± 2	760			$(3.01 \pm 0.45) \times 10^{-12}$	Newland et al.[142]
			Other Furanoids				
5-methyl-5-vinyltetrahydrofuran-2-ol	RR-ASC/FTIR	298 ± 5	740			$(2.0 \pm 0.9) \times 10^{-14}$	Calogirou et al.[131]

[a]Abbreviations for select species are shown in parentheses. Other abbreviations used: RR, relative rate method; AR, absolute rate method; ASC, atmospheric simulation chamber—Teflon or glass made; DFT, discharge flow tube; FT, flow tube; LIF, laser-induced fluorescence; GC-FID, gas chromatography-flame ionization detector; FTIR, Fourier-transform infrared spectroscopy; PTR-MS, proton transfer mass spectrometry (PTR-MS). Table is organized by chemical functionality. The errors reflect those reported from each study. The errors in the mean rate constant reflect the range of measured values [b]Data not included in the mean value determination.

https://doi.org/10.1021/acsearthspacechem.3c00226
ACS Earth Space Chem. XXXX, XXX, XXX−XXX

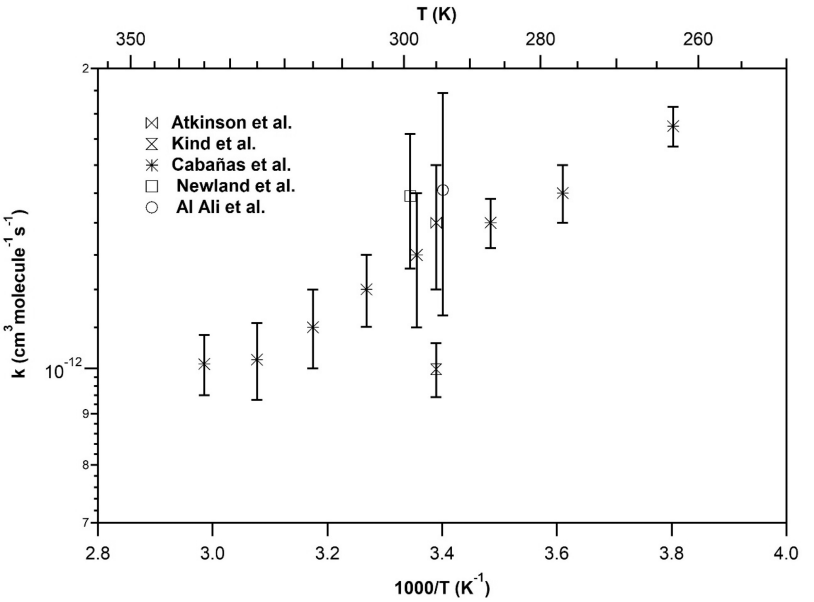

Figure 10. Summary of literature data for the furan + NO_3 radical reaction.[139−143]

Table 5. Summary of Available Literature Data for the Reaction of Furanoids with Ozone (O_3)[a]

Compound	Method/technique	Temperature (K)	Pressure (Torr)	k (295 ± 5) ($cm^3 molecule^{-1} s^{-1}$)	References
		Tetrahydrofuran and Methyl-Substituted Tetrahydrofurans			
Tetrahydrofuran (THF)	RR-QPR/FTIR	298 ± 3	700	$(7.12 \pm 2.11) \times 10^{-21}$	Andersen et al.[146]
	AR-QPR/FTIR	298 ± 3	700	$(4.69 \pm 1.60) \times 10^{-21}$	Andersen et al.[146]
				$(5.91 \pm 1.22) \times 10^{-21}$	**mean value**
2-methyltetrahydrofuran	RR-QPR/FTIR	298 ± 3	700	$(1.77 \pm 0.54) \times 10^{-20}$	Andersen et al.[146]
	AR-QPR/FTIR	298 ± 3	700	$(1.97 \pm 0.63) \times 10^{-20}$	Andersen et al.[146]
				$(1.87 \pm 0.10) \times 10^{-20}$	**mean value**
2,5-dimethyltetrahydrofuran	RR-QPR/FTIR	298 ± 3	700	$(5.00 \pm 1.48) \times 10^{-20}$	Andersen et al.[146]
	AR-QPR/FTIR	298 ± 3	700	$(4.15 \pm 1.55) \times 10^{-20}$	Andersen et al.[146]
				$(4.58 \pm 0.43) \times 10^{-20}$	**mean value**
		Methyl-Substituted Dihydrofurans			
2,3-dihydrofuran	RR-PC/GC-FID	298 ± 2	800	$(4.43 \pm 0.79) \times 10^{-15}$	Alwe et al.[132]
2,5-dihydrofuran	RR-PC/GC-FID	298 ± 2	800	$(1.65 \pm 0.31) \times 10^{-17}$	Alwe et al.[132]
		Furan and Methylfurans			
Furan	AR-ASC/GC-FID-O_3 analyzer	298 ± 2	735	$(2.42 \pm 0.28) \times 10^{-18}$	Atkinson et al.[117]
	RR-QPR/FTIR	298 ± 3	700	$(2.60 \pm 0.31) \times 10^{-18}$	Andersen et al.[146]
				$(2.51 \pm 0.09) \times 10^{-18}$	**mean value**
3-methylfuran (3-MF)	RR-ASC/GC-FID	296 ± 2	740	$(2.05 \pm 0.52) \times 10^{-17}$	Alvarado et al.[144]
2,5-dimethylfuran (2,5-DMF)	AR-FT/O_3 analyzer	295	n.d.	$(4.2 \pm 0.9) \times 10^{-16}$	Matsumoto[147]
		Benzofurans			
2,3-dihydrobenzofuran	AR-ASC/O_3 analyzer	298 ± 2	740	$<1 \times 10^{-19}$	Atkinson et al.[130]
2,3-benzofuran	AR-ASC/O_3 analyzer	298 ± 2	740	$(1.83 \pm 0.21) \times 10^{-18}$	Atkinson et al.[130]
		Other Furanoids			
5-methyl-5-vinyltetrahydrofuran-2-ol	RR-ASC/FTIR	298 ± 5	740	$(3.8 \pm 0.8) \times 10^{-18}$	Calogirou et al.[131]

[a]Abbreviations for select species are shown in parentheses. Other abbreviations used in the table: RR, relative rate method; AR, absolute rate method; ASC, atmospheric simulation chamber; PC, Pyrex cell; FT, flow tube; GC-FID, gas chromatography-flame ionization detector; FTIR, Fourier-transform infrared spectroscopy (FTIR). Table is organized by chemical functionality. The errors reflect those reported from each study. The errors in the mean rate constant reflect the range of measured values.

pressure dependence was reported over the range of 5−760 Torr. The average mean room-temperature rate coefficient between these studies is $k(296\pm5K) = (2.25 \pm 0.34) \times 10^{-11}$ cm^3 $molecule^{-1}$ s^{-1}. To our knowledge, no studies have investigated the temperature-dependent kinetics for the 2-MF + NO_3 reaction.

4.1.2.4. 3-Methylfuran + NO_3. The room-temperature (292−298 K) rate coefficient for the 3-MF + NO_3 reaction has been reported by Kind et al.,[141] Alvarado et al.,[144] Tapia et al.,[125] and Al Ali et al.[143] (Table 4). Each study determined rate coefficients using the relative rate method. Kind et al.[141] used 2,3-dimethyl-2-butene as a reference molecule, Alvarado et al.[144] used 2-methyl-2-butene and Tapia et al.[125] used α-pinene, while Al Ali et al.[143] used 2-methyl-2-butene, γ-terpinene, and α-pinene. Kind et al.[141] reported a rate coefficient that is independent of pressure between 5 and 150 Torr. Their value

https://doi.org/10.1021/acsearthspacechem.3c00226
ACS Earth Space Chem. XXXX, XXX, XXX−XXX

is a factor of 2 greater than those reported in other studies. The reason for this discrepancy is not known; therefore, the Kind et al.[141] results are not included in the average rate constant presented in Table 4. Overall, the agreement between the rate coefficient results of Alvarado et al.,[144] Tapia et al.,[125] and Al Ali et al.[143] is within 15%. The mean room-temperature rate coefficient of the NO_3 + 3-MF reaction is $k(295\pm3K) = (1.35 \pm 0.14) \times 10^{-11}$ cm^3 molecule^{-1} s^{-1}, where the error limits cover the range of the measurements. To our knowledge, no studies have investigated the temperature-dependent kinetics for the reaction of 3-MF with NO_3.

4.1.2.5. 2,5-Dimethylfuran + NO_3. The rate coefficient for the 2,5-DMF + NO_3 reaction has been measured by Kind et al.,[141] Newland et al.,[142] and Al Ali et al.[143] In all studies, measurements were performed at ambient-temperature (292−301 K) relative rate methods. Kind et al.[141] used 2,3-dimethyl-2-butene as the reference molecule, Newland et al. used 2-carene, 2,3-dimethyl-2-butene, pyrrole, and 2-MF, while Al Ali et al.[143] used 2,3-dimethyl-2-butene and γ-terpinene. There is a significant disagreement between these studies. In particular, the rate coefficient reported by Newland et al.[142] is a factor of 2 greater than those reported by Kind et al.[141] and Al Ali et al.[143] The reason for this discrepancy is unknown and additional studies are needed to clarify these differences.

4.1.2.6. Other Furanoids + NO_3. The reaction of NO_3 with other furanoids, including 2,3,5-trimethylfuran,[143] tetramethylfuran,[141] 2-furfural,[142,145] 3-furfural,[145] 5-methyl-2-furfural,[145] 5-methyl-2-(3*H*)-furanone,[142] and 4-methyl-5-vinyltetrahydrofuran-2-ol[131] have been measured and are presented in Table 4. Each species has only been investigated once at room temperature.

The kinetics of furan and methyl-substituted furanoids with NO_3 have been studied by multiple research groups using absolute and relative rate methods. Based on the available kinetic data, the rate coefficients for furanoid + NO_3 reactions seems to be independent of pressure between 1 and 760 Torr. The reaction mechanism could proceed by the addition of NO_3 to the C=C double bonds of furanoids forming stable reaction intermediates, or through H atom abstraction, a pathway that could also proceed through the formation of prereactive stable adducts. The reaction mechanism is discussed in Section 4.2. The reaction of NO_3 radicals with methyl-substituted furanoids is considerably faster when compared with the corresponding OH radical reaction rate coefficients (Table 3).

4.1.2.7. Data Gaps. In general, there are limited studies of furanoid reactions with NO_3, especially for substituted furanoids that have been identified in biomass burning (Table 2). Furthermore, there are few data describing temperature-dependent kinetics. For some furanoids, the reaction with NO_3 can compete with that of OH (see Section 4.1.6); therefore, it is important that the current database of NO_3 reaction with this class of compounds be extended with additional laboratory studies to better evaluate the impact of these reactions on tropospheric photochemistry and air quality.

4.1.3. O_3 Reaction Rate Coefficients. The ozonolysis of heterocyclic compounds, such as furanoids, has not been thoroughly studied. Presently, there are seven studies reporting kinetic data for furanoid + O_3 reactions at room temperature. The available kinetic data, method, and measurement technique used in each study are summarized in Table 5. Aside from furan, each species has only been investigated once. A brief discussion of these measurements is provided below.

4.1.3.1. Tetrahydrofuran and Methyl-Substituted Tetrahydrofurans + O_3. Andersen et al.[146] determined the room-temperature (298 ± 3 K) rate coefficient for the O_3 reaction with THF and methyl/dimethyl tetrahydrofurans, using both relative and absolute rate methods. Experiments were performed in a quartz photochemical reactor (QPR) at atmospheric pressure (700 Torr), and the reaction mixture was monitored by FTIR spectroscopy. Relative rate experiments were performed using acetylene and ethylene as reference compounds. Cyclohexane was used as an OH radical scavenger to minimize potential secondary chemistry. Absolute rate coefficient measurements were performed in an excess of O_3, and the kinetics were assumed to follow pseudo-first-order decay. There is an agreement between relative and absolute rate coefficient measurements for 2-methyltetrahydrofuran (to within 10%) and 2,5-dimethyltetrahydrofuran (to within 17%) and the corresponding mean values at room temperature (298 ± 3 K) are $(1.87 \pm 0.10) \times 10^{-20}$ and $(4.58 \pm 0.43) \times 10^{-20}$ cm^3 molecule^{-1} s^{-1}, respectively. The quoted error encompasses the range of the measurements. There is lower measurement agreement for THF, as Andersen et al.[146] report a relative rate coefficient that is 34% higher than the value determined by absolute methods. The reason for this discrepancy is unknown. The mean rate coefficient value at room temperature (298 ± 3 K) combining the relative and absolute rate measurements is $(5.91 \pm 1.22) \times 10^{-21}$ cm^3 molecule^{-1} s^{-1}.

4.1.3.2. Methyl-Substituted Dihydrofurans + O_3. The reaction kinetics of 2,3-dihydrofuran and 2,5-dihydrofuran with ozone were reported by Alwe et al.[132] Relative rate kinetic measurements were performed inside a Pyrex photochemical reactor, and the gases were monitored by GC-FID. 1,3-Cyclohexadiene and 1-butene were used as reference molecules for 2,3-dihydrofuran and 2,5-dihydrofuran, respectively. THF and tetrahydropyran were used as OH scavengers. The rate coefficients were determined to be $(4.43 \pm 0.79) \times 10^{-15}$and $(1.65 \pm 0.31) \times 10^{-17}$ cm^3 molecule^{-1} s^{-1} for 2,3-dihydrofuran and 2,5-dihydrofuran, respectively. These values indicate that the position of the double bond in dihydrofurans is a determinant factor of their reactivity, probably due to the stabilization of the resulting Criegee intermediate.

4.1.3.3. Furan and Methylfurans + O_3. Atkinson et al.[117] studied the kinetics of furan ozonolysis under atmospheric pressure and room temperature (298 ± 2 K) in a Teflon bag reactor. An absolute rate coefficient method was applied, where the concentration of furan was monitored with a GC-FID and that of ozone with a chemiluminescent analyzer. As part of their study, Andersen et al.[146] reported the room-temperature (298 ± 3 K) rate coefficient for the furan + O_3 reaction using a relative rate method and found it to agree to within 7% with the absolute rate coefficient measurements reported in Atkinson et al.[117] A mean value of $k(298\pm3K) = (2.51 \pm 0.09) \times 10^{-18}$ cm^3 molecule^{-1} s^{-1} is calculated here, where the estimated uncertainty covers the range of the kinetic measurements. The room-temperature kinetics of 3-MF and 2,5-DMF reaction with O_3 were reported by Alvarado et al.[144] and Matsumoto et al.,[147] respectively. Alvarado et al.[144] applied a relative rate method using propene as the reference molecule and cyclohexane as an OH radical scavenger to minimize secondary chemistry.[144] Matsumoto et al.[147] performed absolute rate coefficient measurements in a flow tube reactor in excess of 2,5-DMF.[147] The room-temperature rate coefficients reported in these studies were $(2.05 \pm 0.52) \times 10^{-17}$ and $(4.2 \pm 0.9) \times 10^{-16}$ cm^3 molecule^{-1} s^{-1} for 3-MF and 2,5-DMF, respectively.

https://doi.org/10.1021/acsearthspacechem.3c00226
ACS Earth Space Chem. XXXX, XXX, XXX−XXX

Table 6. Summary of Available Room Temperature Literature Data for the Reaction of Furanoids with Chlorine Atoms (Cl)[a]

Compound	Method/technique	Temperature (K)	Pressure (Torr)	k(295±5K) (10^{-10} cm^{3}molecule^{-1}s^{-1})	References
		Tetrahydrofuran and Methyl-Substituted Tetrahydrofurans			
Tetrahydrofuran (THF)	RR-QPR/FTIR	298 ± 3	700	1.96 ± 0.24	Andersen et al.[146]
	RR-PC/GC-FID	298 ± 2	800	2.50 ± 0.39	Alwe et al.[149]
				2.23 ± 0.27	**mean value**
2-methyltetrahydrofuran	RR-QPR/FTIR	298 ± 3	700	2.65 ± 0.43	Andersen et al.[146]
2,5-dimethyltetrahydrofuran	RR-QPR/FTIR	298 ± 3	700	2.84 ± 0.34	Andersen et al.[146]
		Methyl-Substituted Dihydrofurans			
2,3-dihydrofuran	RR-PC/GC-FID	298 ± 2	800	4.52 ± 0.99	Alwe et al.[149]
2,5-dihydrofuran	RR-PC/GC-FID	298 ± 2	800	4.48 ± 0.39	Alwe et al.[149]
		Furan, Methylfurans, Dimethylfuran, and Ethylfuran			
Furan	RR-ASC/GC-FID-MS			2.0 ± 0.2	Cabañas et al.[150]
	RR-QPR/FTIR	298 ± 3	700	2.39 ± 0.27	Andersen et al.[146]
				2.20 ± 0.20	**mean value**
2-methylfuran (2-MF)	RR-ASC/GC-FID-MS	298 ± 2	760	4.1 ± 0.2	Cabañas et al.[150]
3-methylfuran (3-MF)	RR-ASC/GC-FID-MS	298 ± 2	760	4.2 ± 0.3	Cabañas et al.[150]
2-ethylfuran	RR-ASC/GC-FID-MS	298 ± 2	760	4.6 ± 0.3	Cabañas et al.[150]
2,5-dimethylfuran	RR-ASC/GC-FID-MS	298 ± 2	760	5.7 ± 0.3	Cabañas et al.[150]
		Aldehyde Furanoids			
2-furfural	RR-QPR/GC-FID	298 ± 2	708.5	2.61 ± 0.27	Cabañas et al.[151]
3-furfural	RR-QPR/GC-FID	298 ± 2	708.5	3.15 ± 0.27	Cabañas et al.[151]
5-methyl-2-furfural	RR-QPR/GC-FID	298 ± 2	708.5	4.0 ± 0.5	Cabañas et al.[151]
Maleic anhydride	AR-PLP/RF	296	760	0.30	Chattopadhyay et al.[152b]
	RR-PPR/FTIR	296	620	0.287 ± 0.024[b]	

[a]Abbreviations for select species are shown in parentheses. Other abbreviations used in the table: AR, absolute rate method; RR, relative rate method; ASC, atmospheric simulation chamber; QPR, quartz photochemical reactor; PPR, Pyrex photochemical reactor; PC, Pyrex cell; GC-FID-MS, gas chromatography-flame ionization detector-mass spectrometry; SPME-GC-FID, solid-phase microextraction-gas chromatography-flame ionization detector; FTIR, Fourier-transform infrared spectroscopy; PLP, pulse laser fluorescence; RF, resonance fluorescence. The errors reflect those reported from each study. The errors in the mean rate constant reflect the range of measured values. [b]Study carried out as a function of pressure and temperature. Only the room temperature rate coefficient is presented; however, the pressure and temperature range where measurements were conducted are discussed in the main text. The room temperature value determined with the relative method is the mean value of the two reference molecules used (ethylene and acetylene). The estimated uncertainty covers the range of the kinetic measurements.

4.1.3.4. Benzofurans + O_3. The kinetics of the aromatic furanoids 2,3-dihydrobenzofuran and 2,3-benzofuran reaction with ozone were studied by Atkinson et al.[130] at room temperature (298 ± 2 K) in an atmospheric smog chamber. An absolute method was used by following the O_3 decay under known concentrations of the organic compound. An upper limit room-temperature rate coefficient for 2,3-dihydrobenzofuran was estimated to be $<10^{-19}$ cm^3 molecule^{-1} s^{-1}. The coefficient for 2,3-benzofuran was reported to be $1.83 \pm 0.21 \times 10^{-18}$ cm^3 molecule^{-1} s^{-1}.

4.1.3.5. Other Furanoids + O_3. The rate coefficient for the 5-methyl-5-vinyltetrahydrofuran-2-ol + O_3 reaction was measured by Calogirou et al.[131] Relative rate kinetic measurements were performed in an atmospheric simulation chamber using isobutene as the reference molecule, and the gas mixture was monitored by FTIR spectroscopy.

4.1.3.6. General Discussion and O_3 Reactivity Trends. The O_3 rate coefficients measured for THF and methyl derivatives are relatively slow, on the order of 10^{-20} cm^3 molecule^{-1} s^{-1}. The substitution of one or two H atoms in tetrahydrofuran with CH_3 group(s) substantially increases the rate coefficient by a factor of ∼10. The rate coefficients for furan and its methyl and dimethyl derivatives are several orders of magnitude greater than for the corresponding tetrahydrofuran analogs. This is primarily due to the presence of double bonds in the furanoid ring. It is well-established that ozone is a reactive electrophilic molecule attacking the C═C double bond of unsaturated organic compounds through the known "Criegee" mechanism.[26] The reaction would likely result in ring-opening products. The methyl and dimethyl substitution of H atoms in the base structure of furan increased the reaction rate coefficient by 1 and 2 orders of magnitude, most likely due to the stabilization of the corresponding Criegee intermediate formed. The latter was also discussed in the theoretical study of Li et al.,[148] where the rate coefficients of methylated furans, and furanaldehydes were calculated using density functional theory RRKM calculations.

The ozonolysis of tetrahydrofurans, furan, and single-methyl-substituted furanoids is expected to be a minor removal pathway under average ozone mixing ratios (∼30 ppb), though higher losses may be observed in biomass burning plumes where ozone mixing ratios are often elevated. Higher ozone losses are expected for multiply-substituted furanoids, e.g., dimethyl-, trimethyl-, or tetramethylfurans, since O_3 reactivity increases with higher substitution. For some species, such as trimethylfurans, the O_3 removal pathway could be comparable with that of OH radicals depending on the reaction rates inside biomass burning plumes (see Section 4.1.6). Dihydrofurans are found to be highly reactive with O_3, especially 2,3-dihydrofuran. The reported rate constants suggest that ozonolysis could be the dominant removal pathway, though more studies are needed to confirm these measurements.

4.1.3.7. Data Gaps. The available studies show that the O_3 rate coefficients with multi-methylated and oxygenated furanoids are lower than those for the reactions with OH and NO_3 radicals. For some species (such as dihydrofurans and trisubstituted furanoids), O_3 kinetics remain important and may require further evaluation in order to fully evaluate the oxidation chemistry of furanoids in fresh and aged biomass burning

https://doi.org/10.1021/acsearthspacechem.3c00226
ACS Earth Space Chem. XXXX, XXX, XXX−XXX

plumes. Therefore, considering the limited number of studies reporting the kinetics of O_3 reaction with furanoids, there is a need for room-temperature and temperature-dependent kinetic studies that would provide further insight into the reaction mechanisms.

4.1.4. Cl Radical Reaction Rate Coefficients. The kinetic data for furanoid + Cl atom reactions are relatively scarce. With the exception of THF and furan, only single kinetic measurements are reported at room temperature for the compounds given in Table 6. The vast majority of the available measurements have been carried out using relative rate methods at room temperature (295−301 K) and at atmospheric pressure.

4.1.4.1. Tetrahydrofuran and Methyl-Substituted Tetrahydrofurans + Cl. Andersen et al.[146] reported the Cl atom reaction rate coefficients for THF along with methyl- and dimethyltetrahydrofurans using a quartz photochemical reactor (QPR) with detection by FTIR spectroscopy. Ethane and propane were used as reference molecules. Alwe et al.[149] has also studied the relative rate kinetics of THF + Cl reaction. Experiments were performed inside a Pyrex photochemical reactor using nitrogen or air as bath gases, and the monitoring of THF and the corresponding reference molecule (*n*-pentane and *n*-hexane for THF kinetics) were monitored by GC-FID. The rate coefficients of THF reaction with Cl atoms determined by Andersen et al.[146] and Alwe et al.[149] agrees to within 22% with a mean value of $k(298\pm3K) = (2.23 \pm 0.27) \times 10^{-10}$ cm^3 molecule^{-1} s^{-1}. The rate coefficients reported by Andersen et al.[146] for methyltetrahydrofuran and dimethyl tetrahydrofuran were $k(298\pm3K) = (2.65 \pm 0.43) \times 10^{-10}$ and $(2.84 \pm 0.34) \times 10^{-10}$ cm^3 molecule^{-1} s^{-1}, respectively, showing a moderate increase in the rate coefficients with the substitution of one or two H atoms by CH_3 groups.

4.1.4.2. Methyl-Substituted Dihydrofurans + Cl. The kinetics of 2,3-dihydrofuran, and 2,5-dihydrofuran reaction with Cl were reported by Alwe et al.[149] Relative rate kinetic measurements were performed inside a Pyrex photochemical reactor using nitrogen or air as bath gases, and the mixture was monitored by GC-FID. The reference molecules used were cycloheptene, for 2,3-dihydrofuran kinetics, and *n*-pentane and 1-butene, for 2,5-dihydrofuran. The room-temperature rate coefficients reported were $k(298\pm3K) = (4.52 \pm 0.99) \times 10^{-10}$ and $(4.48 \pm 0.39) \times 10^{-10}$ cm^3 molecule^{-1} s^{-1} for 2,3-dihydrofuran, and 2,5-dihydrofuran, respectively, pointing out that the presence of the methyl group in position 3 or 5 of the furan ring does not impact the total reactivity.

4.1.4.3. Furan, Methylfurans, Dimethylfuran, and Ethylfuran + Cl. Andersen et al.[146] reported the relative rate reaction rate coefficient of Cl atom with furan using a quartz photochemical reactor (QPR). Propane was used as a reference molecule, and the relative rate kinetics were monitored with FTIR spectroscopy. Cabanas et al.[150] used relative rate measurements to determine the reaction of Cl with furan, 2-MF, 3-MF, 2-ethylfuran, and 2,5-DMF, at room temperature (298 ± 2 K). Experiments were performed in an atmospheric pressure smog chamber, and the reaction mixture was monitored by GC-FID-MS. The reference molecules used were propane, 1-butene, *n*-nonane, and E-2-butene for furan. *n*-Nonane was used as a reference for the methyl-substituted furanoids.

The rate coefficients for furan + Cl determined by Andersen et al.[146] and Cabanas et al.[150] agree to within 16%. Considering the large number of reference molecules used and the agreement between the measurements, we recommend a mean value of $k(298\pm3K) = (2.23 \pm 0.27) \times 10^{-10}$ cm^3 molecule^{-1} s^{-1} for the furan + Cl atom reaction. Considering the results of Cabanas et al.[150] 2,5-DMF exhibited the highest rate constant, followed by methyl- and ethylfurans, and then furan (see values in Table 6).

4.1.4.4. Aldehyde Furanoids + Cl. The room-temperature (298 ± 2 K) relative rate kinetics of 2-furfural, 3-furfural, and 5-methyl-2-furfural with Cl, were reported in the study of Cabanas et al.[151] Experiments were performed under atmospheric pressure in a smog chamber using GC-FID-MS as detection technique. The reference molecules used were nonane and ethylfuran.

4.1.4.5. Ketone Furanoids + Cl. Recently, Chattopadhyay et al.[152] studied the reaction maleic anhydride + Cl as a function of pressure (15−500 Torr) and temperature (283−323 K).[152] The authors determined the rate coefficient using absolute methods and monitored Cl atom kinetics using resonance fluorescence (RF). The authors provided a Troe falloff fit of the temperature and pressure dependence, yielding the following rate coefficient parameters:

$$k_0(T)/(\text{cm}^6\ \text{molecule}^{-2}\ \text{s}^{-1}) = (9.4 \pm 0.5) \times 10^{-29}\left(\frac{T}{298}\right)^{-6.3}$$

and

$$k_\infty(T)/(\text{cm}^3\ \text{molecule}^{-1}\ \text{s}^{-1}) = (3.4 \pm 0.5) \times 10^{-11}\left(\frac{T}{298}\right)^{-1.4}$$

Chattopadhyay et al.[152] performed complementary relative rate experiments at 296 K and 620 Torr using ethylene and acetylene as reference molecules. The room-temperature literature data are summarized in Table 6.

4.1.4.6. General Discussion and Cl Reactivity Trends. Despite the limited number of kinetic measurements, a brief comparison of the Cl reactivity trends for the reactivity of THF, furan, and their methylated derivatives is possible. The reaction of THF and its methylated derivatives with Cl atom is expected to proceed through H atom abstraction. An increase of around 30% in the rate coefficient with the substitution of one or two H atoms by CH_3 groups is observed in the rate coefficients shown in Table 6. Interestingly, the rate coefficient of Cl atom with 2-methyltetrahydrofuran and 2,5-dimethyltetrahydrofuran are almost identical, implying that further increases of CH_3 group substitution does not enhance the overall reactivity.

For furan and its methylated derivatives, the reaction of Cl atoms can proceed through Cl addition to the double bond as well as H abstraction. The substitution of one H atom in furan by a CH_3 group (i.e., 2- or 3-methylfuran) doubles the overall rate coefficient with Cl. The presence of a $-CH_3$ group in the case of 2-MF or 3-MF increased the electron density of the corresponding C=C double bond, and thus the addition of Cl atoms, as electrophile reagent, is expected to account for the increase in the overall rate coefficient. The latter could also reflect the energy of the adduct formed in the addition of Cl to the double bond. Considering the nonselective electrophilic addition preference of Cl atoms, the rate coefficients determined for 2-MF and 3-MF are similar. The rate coefficient of 2,5-DMF is ∼26% higher than monosubstituted methylfurans. The latter increase could also be attributed to an increased electron density of the C4=C5 double bond of 2,5-DMF.

https://doi.org/10.1021/acsearthspacechem.3c00226
ACS Earth Space Chem. XXXX, XXX, XXX−XXX

4.1.4.7. Data Gaps. Cl chemistry is expected to be a minor atmospheric loss process for furanoids, and Cl mixing ratios in smoke are generally low.[153] However, additional room-temperature, and pressure-dependent kinetic studies would provide further insight into furanoid atmospheric degradation mechanisms and the contribution of the H atom abstraction pathway to the overall rate coefficient.

4.1.5. UV–Vis Photochemistry. The UV photolysis of furanoids contributes to the production of new chemical species in the troposphere. Photolysis represents an irreversible loss process for furanoids and may lead to the formation of different intermediate and stable species than would otherwise be obtained via chemical reaction. Thus, photolysis and chemical reactions can have different atmospheric impacts depending on the fate of the subsequent degradation products.

Atmospherically relevant photodissociation of furanoids occurs primarily at wavelengths (λ) < 350 nm. The rate of atmospheric photolysis depends on the overlap of the absorption spectrum of the molecule with sunlight, the quantum yield for the dissociation process, and the solar flux. The first-order photolysis rate coefficient, J (s^{-1}), for the removal of a molecule via photolysis, is given by

$$J/s^{-1} = \int J(\lambda)\, d\lambda = \int \sigma(\lambda, T)\, \phi(\lambda, T)\, \psi(\lambda, Z, \chi)\, d\lambda \quad (9)$$

where $\sigma(\lambda,T)$ is the absorption cross-section at wavelength λ and temperature T, $\Phi(\lambda,P,T)$ is the molecules photolysis quantum yield at λ, pressure (P), and T, $\psi(\lambda,Z,\chi)$ is the solar flux (photons cm^{-2} s^{-1} nm^{-1}), which is a function of λ, altitude (Z), albedo, overhead column abundances of absorbing species, and solar zenith angle (SZA, χ). The solar flux term is obtained from radiative transfer models such as the NCAR TUV calculator.[154]

Laboratory measurements are needed to provide a quantitative absorption spectrum and photolysis quantum yields over a range of wavelengths, pressure, and temperature. UV photolysis in the actinic region, λ > 295 nm, represents a potentially significant tropospheric loss process for some of the furanoids listed in Table 1. The compounds of particular interest are the oxygenated furanoids, e.g., aldehydes and carbonyls, which exhibit significant absorption in the actinic region. For example, a photolysis quantum yield of unity would lead to a photolysis lifetime for maleic anhydride ($C_2H_2(CO)_2O$) on the order of an hour, which is faster than the loss by reaction with the OH radical (~8 days at $[OH] = 1.5 \times 10^6$ molecules cm^{-3}). This also implies that photolysis quantum yields of 0.01, or less, would still represent a significant furanoid loss process.

The accurate measurement of such small photolysis quantum yields represents a significant challenge for laboratory studies. The UV absorption spectra and photolysis quantum yields for the majority of the furanoids in Table 1 are presently not known, which is, in part, due to the lack of available high-purity samples. Another factor for quantum yield measurements in the actinic wavelength range is small absorption cross-sections, as well as suitable photolysis sources and sensitive detection methods. The available photochemical data for the furanoids given in Table 1 are reviewed below. In the following sections, the furanoids that have published spectra and possible photochemistry are listed in italics. We have organized these sections by chemical functionality, which significantly impacts the absorption properties for different furanoid classes. Note that the majority of the furanoid UV absorption spectra that are available in the literature are archived on the Mainz database.[155]

4.1.5.1. Methyl-Substituted Furanoids + hν: Tetrahydrofuran, 2-Methyltetrahydrofuran, 2,5-Dimethyltetrahydrofuran-(E,Z), 2,3-Dihydrofuran, 2,5-Dihydrofuran, Furan, 2-Methylfuran, 3-Methylfuran, 2,3-Dimethylfuran, 2,4-Dimethylfuran, 2,5-Dimethylfuran, Tetramethylfuran, 2-Ethylfuran, 3-Ethylfuran, 2-Propylfuran, and 2-Ethyl-5-methylfuran. THF, furan, and methyl- and ethyl-substituted derivatives do not have measured absorption in the actinic region, and therefore photodissociation in the troposphere is not expected to be an important loss process. For example, Figure 11 shows the VUV/UV absorption spectrum of furan, which shows the significant onset of absorption around 220 nm.

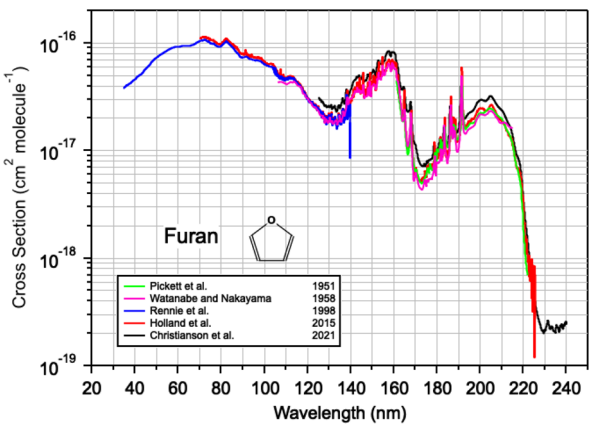

Figure 11. VUV/UV absorption spectrum of furan, C_4H_4O. Data of Pickett et al.,[156] Watanabe and Nakayama,[157] Rennie et al.,[158] Holland et al.,[159] and Christianson et al.[160] were taken from the Mainz database.[155]

4.1.5.2. Aldehyde Furanoids + hν: 2-Furfural, 3-Furfural, 5-Methy-2-furfural, 5-Hydroxy-2-furfural, and 5-Hydroxymethyl-2-furfural. The furanoid aldehydes listed in Table 1 (2-furfural, 3-furfural, and 5-methy-2-furfural) have reported VUV/UV absorption spectra. The aldehyde chromophore yields strong absorption in the actinic region, where diffuse structure is observed on top of a broad continuum (Figure 12). As a result, the absorption in the actinic region is expected to have wavelength- and pressure-dependent photolysis quantum yields. To date, there are no quantum yield or photolysis product

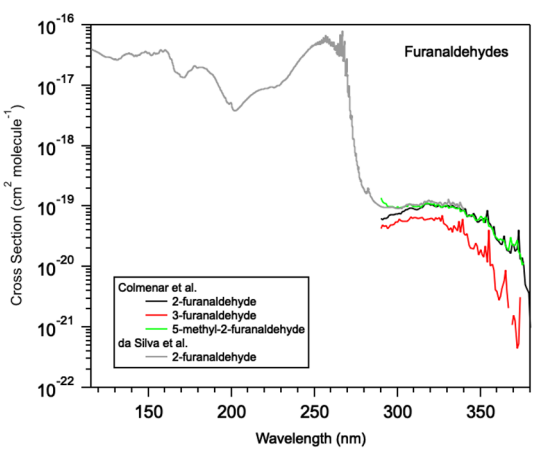

Figure 12. VUV/UV absorption spectra of 2-furfural, 3-furfural, and 5-methyl-2-furfural. Data of Colmenar et al.[161] and da Silva et al.[162] were taken from the Mainz database.[155]

https://doi.org/10.1021/acsearthspacechem.3c00226
ACS Earth Space Chem. XXXX, XXX, XXX−XXX

studies available in this wavelength range. Colmenar et al.[161] estimated summer solstice equatorial boundary layer photolysis lifetimes of <1 h for these compounds for a photolysis quantum yield of unity. Wavelength-, pressure-, and temperature-dependent quantum yield measurements are needed to quantify this potentially important atmospheric loss process.

4.1.5.3. Ketone/Anhydride Furanoids + hν: Maleic Anhydride, 2-(3H)-Furanone, 2-(5H)-Furanone, and 5-Methyl-5-vinyltetrahydrofuran-2-ol. Back and Parsons[163] and Marshall et al.[164] have reported the UV absorption spectrum of maleic anhydride (Figure 13). The agreement between these studies

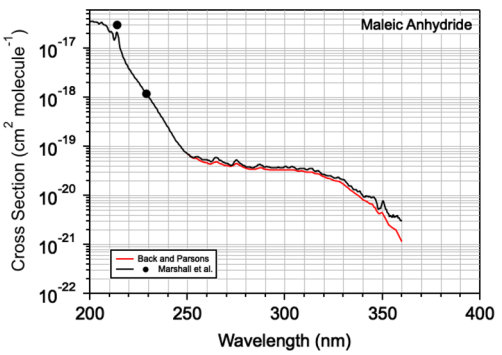

Figure 13. UV absorption spectra of maleic anhydride, $C_4H_2O_3$. Data from Back and Parsons[163] and Marshall et al.[164] are available on the Mainz database.[155]

over a common wavelength range is relatively good considering the difficulties in handling and quantifying maleic anhydride (see Marshall et al.[164] for details). The spectrum displays several electronic transitions in the 200−350 nm region with prominent diffuse structure in the long wavelength region. Back and Parsons assigned the electronic transitions to a strong $\pi \leftarrow \pi^*$ transition (200−260 nm) and overlapping weaker $\pi \leftarrow n^+$ and $\pi \leftarrow n^-$ transitions at longer wavelengths.

Marshall et al.[164] also reported the maleic anhydride photolysis quantum yield and product yields following 248 nm pulsed laser photolysis. The maleic anhydride photolysis quantum yield was determined to be 0.85 ± 0.20, independent of pressure. CO, CO_2, and acetylene (C_2H_2) were observed using infrared detection as photolysis products. The products were formed with a 1:1:1 stoichiometric ratio with 1 ± 0.15 yield, independent of total pressure (100−600 Torr, zero air). These observations are consistent with a photolysis mechanism involving ring rupture and the release of CO and CO_2. Photolysis quantum yield and product studies at wavelengths more relevant to tropospheric photolysis are needed.

The other furanoid ketones included in Table 1, such as 2-(3*H*)-furanone, are expected to also have absorption in the tropospheric actinic region. Therefore, UV absorption laboratory studies are needed for this class of furanoids.

There are no UV spectra or photolysis product yield data currently available for the alcohols (2-furanmethanol) and acids (2-furoic acid) included in Table 1. The chromophores in these classes of compounds are not expected to lead to significant absorption in the actinic region, and thus UV photolysis is not expected to be a significant tropospheric loss process. However, this expectation needs to be validated with quantitative laboratory studies.

4.1.5.4. Benzofurans + hν: 2,3-Dihydrobenzofuran, 2,3-Benzofuran, 2-Methylbenzofuran, and 3-Methylbenzofuran. There are no UV spectra or photolysis product yield data currently available for the benzofuranoids listed in Table 1. Strong absorption in the UV region is expected and laboratory studies are needed to evaluate absorption and photolysis in the actinic region.

4.1.5.5. Nitrate Photochemical Products + hν. Nitrate and PAN type compounds are potential wildfire/biomass burning degradation products, although field observations and laboratory studies are extremely limited. Furoyl peroxynitrate ($C_4H_3O-C(O)-OONO_2$), formed following the atmospheric degradation of 2-furfural,[165] is the only furanoid nitrate to be reported in wildfire plumes to date. UV spectra or photolysis product studies of furanoid nitrates are currently not available, but it is expected that initial photolysis occurs at the $O-NO_2$ bond.

4.1.5.6. Data Gaps. The furanoid photochemistry database, i.e., spectra and quantum yield data, is presently understudied. There are many furanoids in biomass burning smoke with aldehyde and ketone functionality that would result in strong UV absorption (Table 2). Likewise, products of furanoid chemistry might also exhibit strong absorption. For example, fur-PAN shares similar functionality with strong UV absorbers like 2-furfural and 5-methylfurfural. Shortened lifetimes of NO_x reservoirs, such as nitrates, could have implications on downwind ozone formation via re-introduction of NO_x.

Table 7. Estimated Gas-Phase Atmospheric Lifetimes of Selected Furanoids with Major Atmospheric Oxidants[a]

compd	τ_{OH}(day)[b]	τ_{NO_3} (night)[c]	τ_{NO_3}(day)[d]	τ_{O_3}[e]	τ_{Cl}(average)[f]	τ_{Cl}(coastal/urban)[g]
tetrahydrofuran	3.3 h	12 days	231 days	5.4 years[k]	141 h[k]	23 h[k]
furan	89 min	58 min	19.3 h	5 days	126 h	21 h
2-methyl furan	48 min	3.7 min	1.2 h		68 h[n]	11 h[n]
3-methyl furan	35 min	6.2 min	2.1 h	13.6 h[l]	66 h[n]	11 h[n]
2,5-dimethylfuran	29 min	1.4 min[i]	28.7 min[i]	40 min[m]	48 h[n]	8 h[n]
2-furfural	1.6 h[h]	15.3 h[j]	12.8 days[j]		106 h[o]	18 h[o]

[a]Unless noted, the mean values of the room temperature (295 ± 5 K) rate coefficients of furanoids proposed in the current study are used to estimate the lifetimes. [b]Estimated using an average daytime OH radical concentration of 5×10^6 radical cm^{-3}.[166] [c]Estimated using an average nighttime NO_3 radical concentration of 2×10^8 radical cm^{-3}.[167] [d]Estimated using an average daytime NO_3 radical concentration of 1×10^7 radical cm^{-3}.[167] [e]Estimated using an average O_3 concentration of 1×10^{12} molecules cm^{-3}.[168] [f]Estimated using an average Cl atom concentration of 1×10^4 atom cm^{-3}.[169] [g]Estimated using an average Cl atom concentration in coastal or urban areas of 6×10^4 atom cm^{-3}.[170,171] [h]Estimated using the rate coefficient determined by Bierbach et al.[127] [i]Estimated using an average value of $k = 5.8 \times 10^{-11}$ cm^3 molecule^{-1} s^{-1} from Kind et al.[141] and Al Ali et al.[143] [j]Estimated using the rate coefficient determined by Newland et al.[142] [k]Estimated using the rate coefficient determined by Andersen et al.[146] [l]Estimated using the rate coefficient determined by Alvarado et al.[144] [m]Estimated using the rate coefficient determined by Matsumoto.[147] [n]Estimated using the rate coefficient determined by Cabañas et al.[150] [o]Estimated using the rate coefficient determined by Cabañas et al.[151]

https://doi.org/10.1021/acsearthspacechem.3c00226
ACS Earth Space Chem. XXXX, XXX, XXX−XXX

Laboratory studies are needed to quantitatively evaluate the relative significance and potential environmental impact of furanoid photolysis.

4.1.6. Atmospheric Lifetimes of Furanoids. Knowledge of the kinetics and degradation mechanisms of furanoids enables an estimation of their atmospheric lifetime, atmospheric fate, and potential to form secondary pollutants. Table 7 summarizes the estimated atmospheric lifetimes of selected furanoids assuming room-temperature (295 ± 5 K) rate coefficients and mean daytime/nighttime concentrations of atmospheric oxidants. The atmospheric lifetime relative to a given oxidant is determined by the following equation:

$$\tau_{\text{oxidant}} = 1/k_{\text{oxidant}}[\text{oxidant}]$$

where k_{oxidant} is the reaction rate coefficient for a furanoid reaction with a given oxidant. Here, lifetimes are calculated assuming daytime $[NO_3] = 1 \times 10^7$ radicals cm^{-3},[166] nighttime $[NO_3] = 2 \times 10^8$ radicals cm^{-3},[167] ozone average concentrations of $[O_3] = 1 \times 10^{12}$ molecules cm^{-3},[168] daytime rural $[Cl] = 1 \times 10^4$ atoms cm^{-3},[169] and daytime coastal/urban $[Cl] = 6 \times 10^4$ atoms cm^{-3}.[170,171] We note that gradients in oxidants would change the lifetimes reported here, especially for NO_3 and Cl which may vary significantly based on the available emission sources of NO_x and chloride.

The atmospheric lifetime of THF (~3 h) is mainly determined by its reaction with OH radicals. The lifetime for furan is a factor of 3 shorter than THF and is mainly determined by its reaction with OH (~90 min) and NO_3 (~60 min) radicals during daytime and nighttime, respectively. In general, the rate coefficients of methyl- and dimethyl-substituted furanoids with all of the atmospheric oxidants are higher compared to unsubstituted furanoids; thus, their lifetimes are shorter. In the case of methyl-substituted furanoids, the NO_3 reaction is likely to be competitive with the OH reaction even during daytime under low-NO_x environments. At night, 2-MF, 3-MF, and 2,5-DMF react very rapidly with NO_3, leading to estimated lifetimes < 10 min. It is worth mentioning that O_3 reactivity becomes more important with the degree of methyl substitution of furan and, in the case of 2,5-DMF, becomes comparable with OH and NO_3 daytime reaction. The latter implies that O_3 chemistry with trimethyl- or tetramethyl-substituted furanoids could be the dominant atmospheric degradation pathway for these compounds. For 2-furfural, the reactivity with OH radicals is the dominant gas-phase reaction pathway with an estimated lifetime of 1.6 h. The NO_3 nighttime chemistry is less important and likely leads to an atmospheric lifetime of ~15 h. Field observations and modeling of furan oxidation (discussed in Section 5) from biomass burning plumes emphasizes the point that OH, NO_3, and O_3 simultaneously compete in furan chemistry and the dominant loss pathway is dependent on the photolysis rates (i.e., time of day and the location within a biomass burning plume).

Table 7 shows that furan and methylated furanoids react rapidly with atmospheric oxidants, which quickly leads to the production of secondary pollutants. Current knowledge suggests that gas-phase reactions are the major removal processes for furanoids, though more work is needed to describe deposition processes, specifically aqueous solubilities and liquid-phase reaction rates. The reaction mechanism and product analysis of furan and methylated furanoids with atmospheric oxidants is discussed in Section 4.2. Table 7 does not consider losses due to UV photolysis, which may be important for strongly absorbing chromophores described in Section 4.1.5, such as aldehydes, ketones, and anhydrides.

4.2. Gas-Phase Products Formed by Atmospheric Oxidation. The tropospheric oxidation of furanoids leads to a variety of gas-phase degradation products. Presently, the OH-initiated oxidations of furan and its methyl derivatives are the most studied systems and include quantitative assessments of gas-phase products. Detailed data for the reaction mechanisms of furanoids with other oxidations—i.e., NO_3 radical, O_3, and Cl atoms—are more limited.

In this section, we present furanoid oxidation product yields as defined by the following equation

$$\text{molar yield}/\% = \frac{[\text{product formed}]}{[\text{reactant consumed}]} \times 100$$

where [product formed] and [reactant consumed] correspond to the concentrations of products formed and reactants consumed, respectively. Where available, we present proposed multigeneration chemistry that describes the degradation of secondary products formed from furanoid oxidation. Section 4.2.1 describes the products observed formed from OH oxidation along with a general degradation for furans and methylated furans. Section 4.2.2 describes the products formed from NO_3 oxidation. Section 4.2.3 describes the products observed from O_3 and Cl oxidation

4.2.1. OH-Initiated Degradation. There are several experimental and theoretical literature studies investigating the atmospheric degradation mechanism and gas-phase products formed by the reactions of furan and methylfurans with the OH radical.[123,127,172−175] All experimental studies have been conducted under ambient temperature and atmospheric pressure.

Bierbach et al.[127] performed a product analysis of the OH radical reaction with furan and 2-MF in the absence of NO_x. Experiments were carried out in a glass simulation chamber, and the gas mixture was monitored in situ by FTIR spectroscopy. Gomez Alvarez et al.[172] studied the reaction mechanism and products of furan, 2-MF, and 3-MF oxidation initiated by the OH radical in the presence of NO_x in the 200 m^3 EUPHORE simulation chamber. PTR-MS, GC-FID, and solid phase microextraction (SPME) were used to monitor reactants and products. The products of the 3-MF + OH reaction with OH was also studied by Tapia et al.[125] in (i) a Teflon chamber with products detected by SPME and GC-MS/FID and (ii) a glass chamber with in situ IR spectroscopy detection. Aschmann et al.[123] investigated the mechanism of 2,5-DMF photooxidation with OH in the presence and absence of NO_x in Teflon chambers using GC-FID, GC-MS, and API-MS. The same group later extended their study to investigate the degradation pathways of furan, 2-MF 3-MF, 2,3-DMF, and 2,5-DMF by OH.[173] The oxidation mechanism of furan/methylfurans has also been studied using high-level quantum calculations, which showed agreement with experimental data.[174,175]

These studies show that the reaction primarily proceeds by the addition of OH to the C2 and C5 positions of the furan ring (Figure 1). These observations are supported by the negative temperature dependence observed in the reaction rate coefficient of furan and its methylated derivatives (see Section 4.1). The radical formed from the addition of OH can either undergo ring-opening and formation of an unsaturated dicarbonyl or be stabilized (thermally or with collisions with a third body) and undergo alkoxy decomposition to form ring-retaining hydroxyfuranones and epoxides. The product yields

https://doi.org/10.1021/acsearthspacechem.3c00226
ACS Earth Space Chem. XXXX, XXX, XXX−XXX

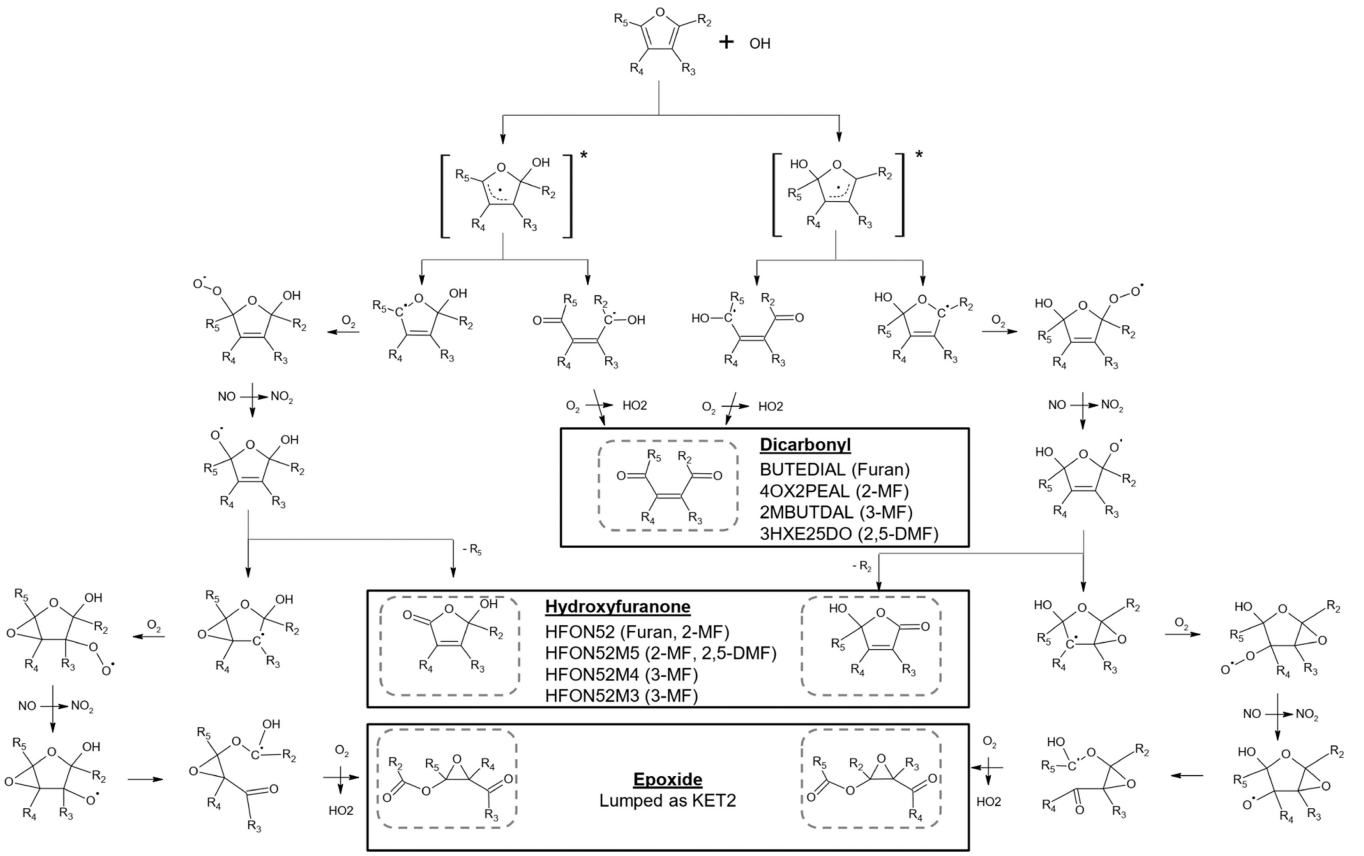

Figure 14. Reaction mechanism proposed by Aschmann et al.[173] and Jiang et al.[176] for the room-temperature degradation of furan and methyl-substituted furanoids by OH radicals in the presence of NO_x. Reproduced with permission from Jiang et al.[176] Copyright 2020 American Chemical Society.

depend on the presence of NO_x, which enhances the reaction pathway leading to the formation of ring-retaining products. Figure 14, adapted from Jiang et al.,[176] reports the dominant OH pathways for furan and methyl-substituted analogs. Table 8 summarizes the experimental conditions, analytical methods, and the yields of dicarbonyl compounds formed by ring-opening. The results for each compound are briefly discussed below, and a recommended product yield value of the dicarbonyl formed is provided.

4.2.1.1. Furan + OH Products. There are three experimental studies reporting the oxidation products formed by the reaction of furan with OH radicals under atmospheric pressure and ambient temperature.[127,172,173] Only the yield of 1,4-butenedial has been quantitatively determined, and results from all studies are in a relatively good agreement. Bierbach et al.[119] reported a lower limit of 1,4-butenedial formation (>70%) in the absence of NO_x. Gomez Alvarez et al.[172] reported yields of 1,4-butenedial to be 109 ± 41 and 90 ± 36%, with an average value 100 ± 39%. Gomez Alvarez et al. quantified the relative abundance of 1,4-butenedial isomers and observed a higher contribution of the trans (76%) compared to the cis (24%) isomer. Aschmann et al.[173] determined the yield of 1,4-butenedial to be 75 ± 5%, which accounted for possible secondary losses of the dicarbonyls to photolysis and/or reaction with OH. Considering the uncertainties in the IR cross-section values reported by Bierbach et al.[127] and the analytical limitations in the collection and derivatization efficiency described by Gomez Alvarez et al.,[172] the 1,4-butenedial yield reported by Aschmann et al.[173] (75 ± 5% in the presence of NO_x) and the isomer distributions reported by Gomez Alvarez et al.[172] (76 and 24% for trans and cis isomers, respectively) are most likely. In the absence of NO_x, the yield of 1,4-butenedial is expected to be higher (Figure 14).[173] Other reaction products with lower yields (<10%) were identified in the absence of NO_x, including hydroxyfuranones, glyoxal, formic acid, and maleic anhydride.[127,173] In the presence of NO_x, glyoxal and a carbonyl compound at m/z 92 were reported with a positive chemical ionization GC-MS.[79]

4.2.1.2. 2-Methylfuran + OH Products. There are three experimental studies reporting the oxidation products formed from the reaction of 2-MF with the OH radical reaction under atmospheric pressure and temperature.[127,172,173] The dominant carbonyl formed from these reactions is 4-oxo-2-pentenal. In the absence of NO_x, Bierbach et al.[127] reported a yield of ∼70%. In the presence of NO_x, Gómez Alvarez et al.[172] and Aschmann et al.[173] reported 4-oxo-2-pentenal yields of 60 ± 24 and 31 ± 5%, respectively. Aschmann et al.[173] argued that the discrepancy between the two studies was due to uncertainties associated with the SPME GC-FID response factors applied by Gómez Alvarez et al.[172] Nevertheless, more studies are necessary to better quantify the yield of 4-oxo-2-pentenal. Other products identified in the presence of NO_x were glyoxal, methyl glyoxal, and hydroxyfuranones. In the absence of NO_x, the yields of glyoxal and methylglyoxal were reported by Bierbach et al.[127] to be between 1.5 and 4.8% and between 1.6 and 2.3%, respectively. Aschmann et al.[173] reports observations of hydroxyfuranones by atmospheric pressure ionization tandem mass spectrometry (API-MS and API-MS/MS), though the yields were not determined quantitatively.

https://doi.org/10.1021/acsearthspacechem.3c00226
ACS Earth Space Chem. XXXX, XXX, XXX−XXX

Table 8. Experimentally Determined Yields of the Dicarbonyls Formed from the Oxidation of Furan/Methylfurans by OH Radicals at Room Temperature and Ambient Pressure[a]

				Unsaturated dicarbonyl		
Compound	Method/technique	Temperature (K)	Pressure (Torr)	Canonical SMILES	Yield (%)[b]	References
Furan	ASC/FTIR	298 ± 2	750	C(=CC=O)C=O 2-butenedial	[>70]	Bierbach et al., 1995[127]
	ASC/PTR-MS, GC-FID	n.g[c]	n.g		100 ± 39[2]	Gómez Alvarez et al., 2009[172]
	ASC/PCI GC-MS, API-MS/MS	296 ± 2	735		75 ± 5	Aschmann et al., 2014[173]
					75 ± 5	**Recommended value**
2-methylfuran (2-MF)	ASC/FTIR	298 ± 2	750	CC(=O)C=CC=O 4-oxo-2-pentenal	[~70]	Bierbach et al. 1995[127]
	ASC/PTR-MS, GC-FID	n.g[c]	n.g		60 ± 24	Gómez Alvarez et al., 2009[172]
	ASC/PCI GC-MS, API-MS/MS	296 ± 2	735		31 ± 5	Aschmann et al., 2014[173]
					31 ± 5	**Recommended value**
3-methylfuran (3-MF)	ASC/PTR-MS, GC-FID	n.g[c]	n.g	CC(=CC=O)C=O 2-Methyl-butenedial	83 ± 33	Gómez Alvarez et al., 2009[172]
	ASC/GC-FID, CG-MS, FTIR	296 ± 2	760		1.4 ± 0.3	Tapia et al., 2011[125]
	ASC/PCI GC-MS, API-MS/MS	296 ± 2	735		38 ± 2	Aschmann et al., 2014173
					38 ± 2	**Recommended value**
2,3-dimethylfuran (2,3-DMF)	ASC/PCI GC-MS, API-MS/MS	296 ± 2	735	CC(=CC=O)C(=O)C 3-methyl-4-oxo-2-pentenal	8 ± 2	Aschmann et al., 2014173
2,5-dimethylfuran (2,5-DMF)	ASC/GC-FID, GC-MS, API-MS/MS	296 ± 2	735	CC(=O)C=CC(=O)C 3-hexene-2,5-dione	24 ± 3 [34 ± 3]	Aschmann et al., 2011[123]
	ASC/PCI GC-MS, API-MS/MS	296 ± 2	735		27	Aschmann et al., 2014173
					25 ± 4	**Recommended value**

[a]Abbreviations for select species are shown in parentheses. Other abbreviations used in the table: ASC, atmospheric simulation chamber—Teflon or glass made; GC-FID, gas chromatography-flame ionization detection; FTIR, Fourier-transform infrared spectroscopy; PTR-MS, proton transfer mass spectrometry; PCI GC-MS, positive chemical ionization gas chromatography−mass spectrometry; API-MS/MS, atmospheric pressure ionization tandem mass spectrometry. [b]The recommended values for the yield of dicarbonyls correspond to conditions in the presence of NO_x. The yields of dicarbonyl formed in the absence of NO_x are shown in brackets. These values are expected to be higher than in the presence of NO_x.[173] [c]Not given. However, experiments were performed in an EUPHORE atmospheric simulation chamber and thus conditions should be close to ambient temperature and atmospheric pressure.

4.2.1.3. 3-Methylfuran + OH Products. Gómez Alvarez et al.,[172] Tapia et al.,[125] and Aschmann et al.[173] studied the reaction mechanism of 3-MF oxidation initiated by the OH radical reaction under atmospheric pressure and ambient temperature conditions. The primary dicarbonyl formed is 2-methylbutenedial. In the presence of NO_x, the yields reported by Gómez Alvarez et al.[172] and Aschmann et al.[173] were 83 ± 33[35] and 38 ± 2%, respectively. The yield obtained by Tapia et al.[125] is significantly lower in comparison with that of other studies (1.4 ± 0.3%). Tapia et al.[125] results were impacted by analytical artifacts and are not considered further. As described earlier, the results by Gómez Alvarez et al.[172] were likely limited by uncertainties in the dicarbonyl derivatization efficiency and the applied SPME GC-FID response factor. Consequently, we recommend the 2-methylbutenedial yield determined by Aschmann et al.[173] (38 ± 2%). Other identified products included acetic acid, 3-furfural, 3-methyl-2,5-furandione, 3-methyl-2-(3*H*)-furanone, 2-hydroxy-3-methyl-5-(2*H*)-furanone,[125] glyoxal, and methylglyoxal.[173]

4.2.1.4. Dimethy-Substituted Furanoid + OH Products. Aschmann et al.[123,173] studied the reaction mechanism for 2,3-DMF and 2,5-DMF + OH radicals. The observed yields for dicarbonyl products in the presence of NO_x were as follows: 8 ± 2% for 3-methyl-4-oxo-2-pentenal (2,3-DMF) and 25 ± 4% for 3-hexene-2,5-dione (2,5-DMF). In the absence of NO_x, Aschmann et al.[123] observed an increase in the yield for 3-hexene-2,5-dione to 34 ± 3%.

4.2.1.5. 2-Furfural + OH Products. Besides furan and its methyl derivatives, the reaction mechanism of 2-furfural with the OH radical has been studied by Colmenar et al.[177] Experiments were carried out at room temperature (297 ± 2 K) and atmospheric pressure (700 ± 1 Torr) inside glass and Teflon simulation chambers. FTIR was used to monitor reactants and products. The gas mixture from the chamber was also sampled using SPME and then injected onto a column for further analysis with time-of-flight mass spectrometer (GC-ToF-MS). The authors observed only maleic anhydride in the gas-phase with the GC-ToF-MS. The FTIR spectra were not interpreted further due to the overlap of the injected OH precursors (CH_3ONO + NO) and the decomposition products (formaldehyde, CO, and NO_2). The authors observed IR bands associated with the presence of $-ONO_2$ and $-OONO_2$ groups, suggesting the formation of organic nitrates. It is likely that these products include furoyl peroxynitrate (fur-PAN), which has been observed in aged biomass burning plumes and whose properties have been studied by Roberts et al.[165] Other furanaldehydes, including 3-furfural and 5-methyl-2-furfural, are also likely to form peroxynitrates, though no studies have experimentally evaluated the product yields of these potential NO_x reservoirs.

The 2-furfural + OH reaction has also been studied with quantum chemical calculations by Zhao et al.[137] The reaction was calculated to primarily occur via OH addition to the furan ring at the C2 and C5 positions. Similar to the reactions observed for methylated furanoids, this oxidation is expected to result in a mixture of ring-opening and ring-retaining products. The main products were calculated to be 2-oxo-3-pentene-1,5-dialdehyde, 5-hydroxy-2-(5*H*)-furanone, 4-oxo-2-butenoic acid, and 2,5-furandione. Hydrogen abstraction from the aldehyde group was estimated to be a minor pathway (3%), though this reaction is the likely route for the formation of fur-PAN observed in ambient smoke.[165] 2-Furfural is an important furanoid emitted from biomass burning (Table 2), and experimental studies are needed to evaluate its reaction with OH radicals.

https://doi.org/10.1021/acsearthspacechem.3c00226
ACS Earth Space Chem. XXXX, XXX, XXX−XXX

4.2.1.6. Furan and Methylated Furan OH Oxidation Mechanism. Aschmann et al.[173] and Jiang et al.[176] proposed a general scheme for the tropospheric degradation of furan and methyl-/dimethyl-substituted furanoids in the presence of NO_x, as shown in Figure 14. It should be noted that the mechanism only considers the addition of OH to the C2 or C5 positions. Pathways leading to organic nitrates are not included. Moreover, the H atom abstraction (direct or addition−elimination) has not been evaluated, although it is expected to be of minor importance under tropospheric relevant pressures and temperatures.[175]

Table 9 compares the experimental product yields of dicarbonyls herein with the theoretical calculations of Yuan et al.[174] and the those estimated by Jiang et al.[176] using the SAPRC-18 mechanism generator. Generally, the product yields determined experimentally agree with those calculated via quantum chemistry. Furthermore, Table 9 and results from Aschmann et al.[173] show that the dicarbonyl yield decreases with increasing methyl substitution. Consequently, ring-retaining compounds, such as hydroxyfuranones, or expoxides are expected to be products formed from substituted furanoids.

Table 9. Product Yields (%) of Dicarbonyls for Furan and Methylated Derivatives with OH Radicals Determined from Experiments, Quantum Chemical Calculations, and the SAPRC-18 Mechanism Generator

compd	exptl yield	quantum mechanical theor calc[174]	SAPRC-18 mechanism generator[176]
furan	75 ± 5	76	76
2-methylfuran	31 ± 5	44	44
3-methylfuran	38 ± 2	28	27
2,5-dimethylfuran	25 ± 4	28	28

4.2.1.7. Data Gaps. The mechanisms for furanoid degradation by OH radicals are understudied and there remains a number of research needs. First, only a small number of furanoid + OH mechanisms have been studied, yet there remain a number of highly reactive furanoids in biomass burning smoke that would benefit from mechanistic studies (e.g., 2-furanone, 2-furanmethanol, and 5-methyl-2-furfural; Table 2). Second, atmospheric observations show that there are first-generation products, such peroxynitrates[165] and hydroxyfuranones,[31] whose yields have not been quantified in the laboratory. These products would continue to react in the atmosphere to form highly oxygenated molecules and water-soluble organics, such as maleic anhydride.[31] The reactions for key dicarbonyls, such as 1,4-butenedial, have been studied and are presently incorporated into chemical mechanisms such as the Master Chemical Mechanism (MCM v3.3.1).[178,179] Gas-phase reactions and possible heterogeneous chemistry of key hydroxyfuranones, such as 5-hydroxy-2-(5*H*)-furanone, are presently unknown. Hydroxyfuranones are likely formed at yields that are equivalent to dicarbonyls; therefore, additional work is needed to determine their reaction pathways. Finally, the properties of secondary species formed from multigenerational chemistry are not well studied. For example, maleic anhydride is likely to be lost to hydrolysis and contribute to the formation of aqueous carbon.[180] Studies focused on characterizing the deposition rates, solubility, and UV absorption of secondary species would better constrain the fate of furanoid carbon.

4.2.2. NO_3-Initiated Degradation. There are limited studies investigating furanoid degradation mechanisms by reaction with NO_3.[125,140,177,181−183] This pathway is an important atmospheric loss process for certain species with high NO_3 rate coefficients, including methylated furanoids (Table 7). Except for furan, there are few quantitative and/or qualitative assessments of the resulting gas-phase products. Here, we review the known literature describing the products from furanoid reactions with NO_3. A mechanism for furan is provided based on available quantitative assessments.

4.2.2.1. Furan + NO_3 Products. Atkinson et al.[140] first proposed a reaction mechanism describing furan oxidation by NO_3 radicals. Although the authors did not identify or quantify

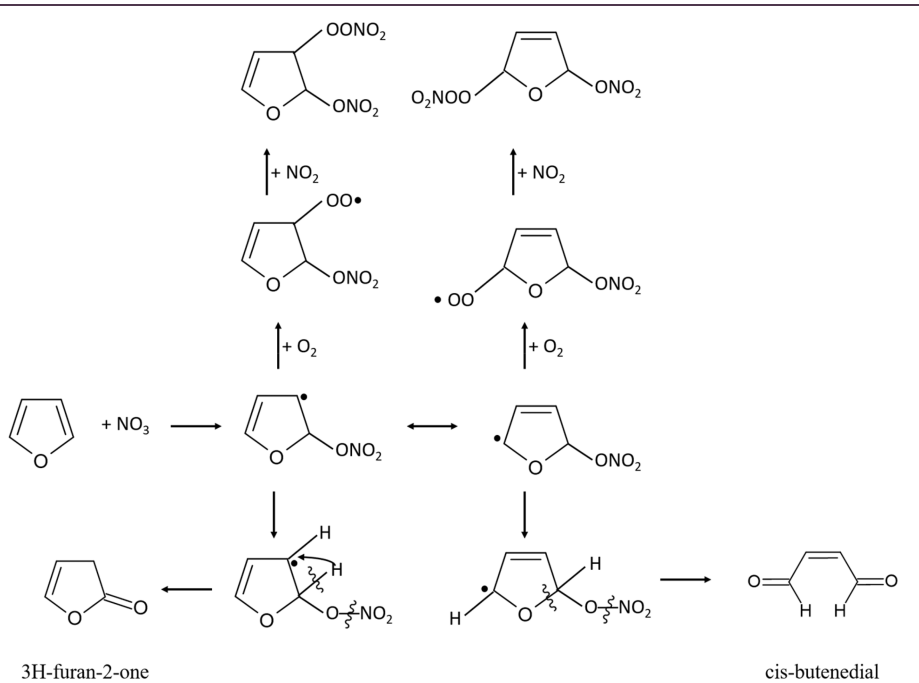

Figure 15. Proposed reaction mechanism for the addition of NO_3 radical to the olefinic double bonds of furan.

https://doi.org/10.1021/acsearthspacechem.3c00226
ACS Earth Space Chem. XXXX, XXX, XXX−XXX

products, they suggested that the dominant reaction pathway is the NO_3 addition to the olefinic double bonds, which in the presence of O_2 and NO_2 could lead to the formation of thermally unstable peroxynitrates. This expectation is consistent with observed nitrates formed from the NO_3 reactions with methylfurans described in the following sections.

Berndt et al.[181] investigated the NO_3-initiated oxidation of furan inside a low-pressure flow tube reactor (3.75−75 Torr) under a range of synthetic air mixtures (100% N_2 to 67% O_2/N_2). The gases were monitored by electron impact mass spectrometry (EI-MS), GC-MS/FID, and FTIR. The major products identified by FTIR were *cis*-butenedial and 3*H*-furan-2-one at yields of 77 and 19%, respectively. Product formation was found to be independent of pressure between 3.75 and 75 Torr. An increase of the 3*H*-furan-2-one yield was observed with increasing O_2 concentrations and a maximum value of 38% was observed in the 67% O_2/N_2 mixture. The authors determined that *cis*-butenedial and 3*H*-furan-2-one accounted for >90% of the total carbon from NO_3-initiated oxidation of furan. To explain these measurements, Berndt et al.[181] suggested that NO_3 adds to the C2 position to form a resonance-stabilized radical. The localization of the radical at C5 and loss of NO_2 leads to *cis*-butenedial formation. Localization of radical at C3, followed by NO_2 loss and intramolecular H-transfer from C2 to C3, leads to 3*H*-furan-2-one formation. Figure 15 shows a proposed mechanistic scheme based on the conclusions drawn by Atkinson et al.[140] about the formation of peroxynitrates and the conclusions drawn by Berndt et al.[181] about the formation of *cis*-butenedial and 3*H*-furan-2-one.

4.2.2.2. 2-Methylfuran + NO_3 Products. The products of 2-MF reaction with NO_3 radical have been reported by Al Ali et al.[183] Experiments were performed under atmospheric pressure and room temperature in two different atmospheric simulation chambers (stainless steel and Teflon made, respectively), and the reaction mixture was monitored using mass spectrometry. The identification of the gas-phase products was performed via offline GC-EI-MS after trapping the gas-phase mixture on adsorbents. 4-Oxo-2-pentenal was identified as the principal ring-opening product, while several other ring-retaining aldehydes, ketones, and nitrates were observed. In their experiments, the authors combined the information provided in the two simulation chambers and the real-time monitoring of the gas mixture with PTR-ToF-MS and SIFT-MS to quantify the yields of the products formed, aiming to address the reaction mechanism and the relative contribution of the addition and abstraction pathways. The two major products of the NO_3 addition to the C2/C5 double bond of 2-MF were 4-oxo-2-pentenal (ring-opening pathway) and 2-(5*H*)-furanone, 5-methyl, 5-nitrooxy ($(CH_3)C(ONO_2)(C_4H_2O_2)$) (ring-retaining pathway) with yields of 61.5 ± 14.7 and 26 ± 3%, respectively. The yield of 2-furanaldehyde, a product related to the H-abstraction pathway, was estimated to be less that 1%.

To evaluate the end-products and the formation yields of organic nitrates, Al Ali et al.[183] studied the 2-MF reaction in an optical cell coupled with in situ FTIR spectroscopy and combined the experimental observations with ab initio calculations. Organic nitrate formation was in the range of ∼30%. The authors propose the formation of organic dinitrates as possible end-oxidation products of the 2-MF reaction with NO_3.

4.2.2.3. 3-Methylfuran + NO_3 Products. The gas-phase products resulting from the 3-MF + NO_3 reaction have been reported by Tapia et al.[125] and Joo et al.[182] Tapia et al.[125] studied the reaction in atmospheric simulation chambers (Teflon chamber, Pyrex cell), and the gas mixture was sampled onto a 30/50 μm SPME fiber and subsequently quantified by GC-MS and GC-FID. Complementary gas-phase FTIR analysis was applied for the detection of organic nitrates. The authors report observations of 2-methylbutenedial, 3-furfural-3-methyl-2-(3*H*)-furandione, and 3-methyl-2-(3*H*)-furanone. The reported yield for 2-methyl butenedial was unexpectedly low (<1%) due to analytical artifacts. The yield for 3-furfural was below 1%, indicating that the H atom abstraction pathway from the methyl group is of minor importance. The yields for 3-methyl-2-(3*H*)-furandione and 3-methyl-2-(3*H*)-furanone were ∼30 and 2%, respectively. FTIR analysis demonstrated the presence of various furanoid nitrates, i.e., nitroperoxy and nitrooxy compounds. Finally, Tapia et al.[125] proposed that the dominate reaction pathway is NO_3 addition to the double bond of 3-MF at the C2 or C5 position.

Joo et al.[182] conducted experiments in a smog chamber and monitored the gas mixture using an iodide high-resolution time of flight-chemical ionization mass spectrometer (HR-TOF-CIMS). The particulate matter composition was analyzed with a high-resolution time-of-flight aerosol mass spectrometer (HR-TOF-AMS). Eighteen different C2−C5 oxygenated and nitro-containing products were identified with the HR-ToF-CIMS, with masses ranging between m/z 45 and m/z 192. The product peaks with the highest intensities were attributed to a cyclic nitrooxy carbonyl ($C_5H_5NO_5$) and an organic acid ($C_5H_6O_3$). Similar to Tapia et al.,[125] Joo et al.[182] proposed that the reaction proceeds mainly with the addition of NO_3 to the C2 or C5 position of the furan ring. The H-abstraction pathway was considered minor. The resulting radical can either react with O_2 to form a cyclic nitrooxyperoxy radical (RO_2) or lose NO_2 and yield 2-methylbutenedial. Further details of the reaction mechanism are provided by Joo et al.[182]

4.2.2.4. 2-Furfural + NO_3 Products. Colmenar et al.[184] reported the reaction mechanism of 2-furfural + NO_3. Experiments were carried out at room temperature (297 ± 2 K) and atmospheric pressure (700 ± 1 Torr) inside glass and Teflon simulation chambers. Products were monitored in situ by FTIR and sampled onto 30/50 μm SPME with offline analysis by GC-MS.

Maleic anhydride and 2-nitrofuran were identified by GC-MS with molar yields of 58.6 ± 8.6 and 20 ± 3%, respectively. A third product was observed and attributed to a ketone (identified as 2-furylnitroketone by Colmenar et al.[184]), but the retention time was not confirmed with standards. Several nitroperoxy and nitrooxy compounds were observed by FTIR. The authors assigned the IR bands to the presence of 5-hydroxy-2-(5*H*)-furanone, maleic anhydride, or 5-nitrate-2-(5*H*)-furanone and 2-furylacetone, but these compounds were not confirmed due to the unavailability of standards.

Colmenar et al.[184] proposed a general scheme where NO_3 oxidation begins with an addition to the C5 position or hydrogen abstraction from the aldehyde group, although this reaction pathway is anticipated to be of minor importance.[185] Hydrogen abstraction from the furan ring was also considered to be a minor pathway. The presence of maleic anhydride was attributed to both addition and abstraction pathways, while that of organic nitrates was mainly associated with the abstraction pathway.

Besides these experiments, 2-furfural oxidation by NO_3 radicals has been studied by Huang et al.[185] using quantum chemical calculations. The calculated major products were

https://doi.org/10.1021/acsearthspacechem.3c00226
ACS Earth Space Chem. XXXX, XXX, XXX−XXX

Table 10. Experimentally Determined Yields of the Major Products Formed from the Photooxidation of Furanoids by Cl Atoms at Room Temperature and Ambient Pressure (See References 125, 184, 186, and 187)[a]

Compound	Products identified or proposed		
	Addition pathway	Abstraction pathway	Other or secondary products
Furan	• *E*-butenedial(11 ± 2%)[b] • *Z*-butenedial(1.6 ± 0.4%)[c] • 5-chloro-2-(5*H*)-furanone[b](68 ± $\frac{17}{20}$%)	• 5-hydroxy-2-(5*H*)-furanone (≤2.4%)[c] • Hydrogen Chloride (21 ± 3%)[d] • Maleic Anhydride (<8%)[b,f]	• 2-(3*H*)-furanone (3 ± 1%)[c],
2-methylfuran (2-MF)	• 4-oxo-2-pentenoyl chloride (36 ± 4%)[d] • Formaldehyde (31 ± 7%)[d] • 5-chloro-2-(5*H*)-furanone (24 ± $\frac{6}{14}$%)[e,b] • *E*/*Z*-4-oxo-2-pentenal (<10%)[f]	• 2-furfural (11 ± 3%)[b] • 5-hydroxy-2-(5*H*)-furanone[c] • Hydrogen Chloride (33 ± 4%)[d]	• 4-cyclopenten-1,3-dione (2.9 ± 0.6)[c,g] • Maleic Anhydride (3 ± 1%)[c,g] • 4-oxo-2-pentenoic acid[c] • Carbon Monoxide[d]
3-methylfuran (3-MF)	• 5-chloro-3-methyl-2-(5*H*)-furanone (81 ± 9%)[d] • 5-hydroxy-2-(5*H*)-methylfuranones[c] • 2-methylbutenedial (4 ± 1%)[c]	• 3-furfural (8 ± 3%)[b] • Hydrogen Chloride (34 ± 4%)[d]	• 3-methyl-2-(5*H*)-furanone (2 ± 1)[c] • 3-methyl-2,5-furanodione • Carbon Monoxide[d]
2,5-dimethylfuran (2,5-DMF)	• 4-oxo-2-pentenoyl chloride (34 ± 5%) • Formaldehyde (34 ± 5%)[d] • E/Z-3-hexene-2,5-dione (11 ± 2)[b]	• 5-methylfurfural (8 ± 2%)[c] • Hydrogen Chloride (66 ± 8%)[d]	• 4-cyclopenten-1,3-dione (8 ± 1%)[c,g] • 4-oxo-2-pentenoic acid[c]
2-ethylfuran	• 4-oxo-2-hexenoyl chloride or 4-oxo-2-pentenoyl chloride • Acetaldehyde (31 ± 6%)[d] • 5-chloro-2(5H)-furanone (23 ± 14 %)[b] • *E*/*Z*-4-oxo-2-hexenal (4 ± 1%)[c]	• 2-vinylfuran (9 ± 2%)[c] • 2-acetylfuran (2 ± 1%)[c] • hydrogen chloride (27 ± 3%)[d] • 5-hydroxy-2-(5*H*)-furanone[c] • 2-(1- hydroxyethyl)furan[c]	• 2-cyclohexen-1,4-dione • Maleic Anhydride[c] • 4-oxo-2-hexenoic acid[c]
2-furfural	• 5-chloro-2-(5*H*)-furanone (6.8 ± 1.0)[b,e]	• Hydrogen Chloride (72.9 ± 0.9%/56.6 ± 2.1%)[e,d]	• Maleic Anhydride (6.4 ± 0.8%)[c] • Carbon Monoxide (22.9 ± 0.4%/11.4 ± 0.4%)[e,d] • 2-nitrofuran (10.8 ± 0.5)[c,e]

[a]Abbreviations for select species are shown in parentheses. [b]Product identified/average value of the yield from SMPE and FTIR. The quoted error encompasses the full range of uncertainties denoted for each quantification experiments. [c]Quantified/identified with SMPE-GC/MS. [d]Quantified with FTIR. [e]Products observed in the presence of NO_x. In cases where the yield has been determined, it is given. [f]Significant variation was noted for the yields of the products using different analytical techniques, and thus only an upper limit is presented. [g]Secondary product.

found to be in good agreement with those observed by Colmenar et al.[184]

4.2.2.5. Data Gaps. Atmospheric losses of furanoids to NO_3 are expected to be important for select species, even during the day when OH oxidation is expected to dominate (Table 7). More studies are needed to clarify the NO_3 oxidation mechanism of methylated furanoids, which have the highest reported rate coefficients and whose reactivity increases with the degree of methyl substitution. Systematic studies of NO_3 reaction with furan and methylated furan derivatives may help to elucidate trends in reaction pathways. The contribution of the H-abstraction pathway from the methyl-substituted furanoids or furanaldehydes should also be evaluated with experimental data. Further investigation is also needed to understand the formation of organic nitrates. Identifying organic nitrates is challenging and theoretical studies could provide insights into the formation of these species and aid in determining compound structures. Expanded use of iodide adduct chemical ionization mass spectrometers (I-CIMS) may also help to improve the quantification of organic nitrates. I-CIMS is more sensitive to nitrates than other mass spectrometry techniques (e.g., PTR-ToF-MS) and has been used to identify important nitrated species, such as a fur-PAN.[165]

4.2.3. O_3 and Cl-Initiated Degradation. The reaction of O_3 with furanoids could be an important atmospheric loss process, especially for dihydrofurans and methylated furanoids (see Section 4.1.6). Studies reporting the reaction mechanism or the gas-phase products are, however, scarce. Alvarado et al.[144] discussed the possible reaction mechanism of O_3 with furan and 3-MF. Based on the observed increase in reactivity of 3-MF compared to furan, the authors proposed that the reaction proceeds mainly via O_3 addition to the C2−C3 bond of the furan ring, followed by a decomposition of the primary ozonide leading to energy-rich biradicals. Li et al.[148] have also provided theoretical insights regarding the O_3-initiated degradation pathways of furan, methylfurans, and furanaldehydes. These authors observed that furanoids ozonolysis forms a primary ozonide which decomposes to form predominantly β-unsaturated Criegee intermediates. The Criegee intermediates can either isomerize to dioxirane and dioxolene or dissociate to form a vinoxy-type radical and an OH. Dioxolenes would further isomerize to either products containing another two carbonyl groups or one carbonyl group and one epoxide group. The estimated OH radical formation yields from the ozonolysis of 2-MF, 3-MF, 2,3-DMF, and 2,5-DMF were 1.4, 30.5, 12.6, and 1.8%, respectively.

The Cl atmospheric degradation of furanoids is not expected to be a significant tropospheric loss, though the detection of chlorinated compounds may serve as tracers for this chemistry.[153] There are a few studies that have reported gas-phase products and proposed reaction mechanisms for Cl-addition and H-abstraction pathways.[125,184,186,187] All studies have been performed at room-temperature (296 ± 2 K) and atmospheric-pressure (1000 ± 20 mbar) conditions in smog

https://doi.org/10.1021/acsearthspacechem.3c00226
ACS Earth Space Chem. XXXX, XXX, XXX−XXX

Table 11. SOA Yields from Furanoid Reactions with Various Atmospheric Oxidants

Compound	SOA yield (%)	Initial VOC (ppb)	Initial NO_x (ppb)	Seed[a]	RH	References
			OH Experiments			
Furan	0.04−5	700−780	16−97	NaCl + $NaNO_3$	dry−85%	Jiang et al.[191]
	1.9−7.2	633−830	50	none	dry	Gomez Alvarez et al.[172]
2-methylfuran (2-MF)	5.5	750	70	none	dry	Gomez Alvarez et al.[172]
3-methylfuran (3-MF)	9	640	120	none	dry	Gomez Alvarez et al.[172]
3-methylfuran	9−15	10000	10000	DOS or AS	dry−50%	Strollo and Ziemannn[190]
2,5-dimethylfuran (2,5-DMF)	1.4−3.7	300−800	<1	none or AS	dry−25%	Jiang et al.[192]
2,5-dimethylfuran	4−16	10−1000	<5 ppb	AS or $CaCl_2$	dry −59%	Trajuello et al.[189]
2-furfural	0.3	1860−1376	not noted	none	dry	Colmenar et al.[184]
			NO_3 Experiments			
Furan	4−10	200		none	dry	Jiang et al.[193]
2-methylfuran	1.0−2.2	80−531		none	dry	Al Ali et al.[183]
3-methylfuran	1.6−2.4	96−560		AS	dry	Joo et al.[182]
			O_3 Experiments			
2,5-dimethylfuran	<1	50−500		AS or $CaCl_2$	dry	Trajuelo et al.[189]
2-furfural	0.5	1860−1376		none	dry	Colmenar et al.[184]

[a]AS = ammonium sulfate; DOS = dioctyl sebacate.

chambers. FTIR and SPME-GC/FID-ECD and SPME-GC/MS were used as detection techniques for the identification and quantification of the products from the Cl-addition and H-abstraction pathways. In several cases where standards were not available or synthesis of standards was not possible, the authors estimated yields using instrument response factors of similar compounds. Table 10 summarizes the products quantified or identified from the Cl-initiated degradation of furanoids. The products and mechanism of the Cl-initiated atmospheric oxidation of furan have been also studied using theoretical methods.[188]

4.3. Secondary Organic Aerosol Yields. Products of furanoid oxidation may partition to atmospheric particles to form secondary organic aerosols (SOAs). SOA is hazardous to human health and the formation of absorbing constituents, such as brown carbon, can alter aerosol optical properties. SOA formation from biomass burning plumes is not well understood, in part due to an incomplete knowledge of SOA yields from biomass burning constituents such as furanoids. Here, we review literature that has studied SOA formed from furanoid reactions with the key atmospheric oxidants.

SOA formation is typically studied using environmental chambers and flow tube reactors where VOCs are volatilized into air and mixed with oxidant precursors, NO_x, and seed aerosols. For OH experiments, the reaction mixture is exposed to artificial or natural UV light to generate radicals. Nitrate and ozonolysis experiments are performed under dark conditions, where O_3 is typically injected from a generator and NO_3 is produced from the thermal decomposition of N_2O_5. As the reactions proceed, products from furanoid oxidation may nucleate or partition to seed aerosol and the resulting change to aerosol mass, composition, and size are monitored using a suite of particle instrumentation. Most laboratory studies determine the aerosol yield, which is defined by the mass of aerosol formed per gram of VOC reacted.

$$\text{SOA yield}/(\text{g/g}) = \frac{\Delta(\text{aerosol mass})}{\Delta\text{VOC}}$$

Table 11 summarizes the experimental conditions and SOA yields reported from laboratory studies of furanoid oxidation by OH, NO_3, and O_3. Overall, the available studies suggest that SOA yields from furanoids are low for all the atmospheric oxidants (<16%). Below, studies are summarized that have investigated the SOA formation from furanoid reactions with OH, NO_3, and O_3 and explored the SOA relationships associated with changes to environmental conditions (e.g., relative humidity (RH) and NO_x mixing ratios).

4.3.1. SOA Yield and Products from Furanoids + OH. Most SOA experiments have focused on furan and methylated furan reactions with OH (Table 11). The highest yields have been reported for 2,5-DMF by Trajuelo et al.[189] (16%) and 3-MF by Strollo and Ziemann[190] (12−15%). All other studies report OH yields < 10%, with the lowest yields for furan under dry chamber conditions (yield, 0.04−1%).[191] In general, there is agreement across studies for the SOA yield from 3-MF and furan, while a wider range of yields have been observed for 2,5-DMF. The number of studies on SOAs formed from multisubstituted furanoids are limited, so further investigation is needed to resolve these differences.

Several studies have conducted detailed chemical analyses of furanoid SOA to determine the products that likely partition or react in atmospheric particles to form organic aerosols. Strollo and Ziemann[190] analyzed aerosol produced from the reaction of 3-MF+ OH using online thermal desorption mass spectrometry and offline analysis of filter extracts by UV absorption and electrospray ionization mass spectrometry. The authors found that gas-phase oxidation of 3-MF resulted in 1,4-dialdehydes, hydroxyfuranones, and 1,4-aldoacids consistent with the expected oxidation mechanism presented in Figure 14. The dialdehydes and aldoacids then participate in heterogeneous/multiphase acid catalyzed reactions to form C_{10} hemiacetals, acetals, and ester oligomers. The presence of monomers in SOAs was minimal. At higher relative humidity, the presence of acid-catalyzed oligomers was replaced by the dominance of gem-diol oligomers formed by the reactions of dialdehydes and aldoacids. Jiang et al.[191] observed similar oligomers in the SOAs formed from the OH oxidation of furan in the presence of NO_x, but also measured organonitrates likely formed by the reactions of alkoxy radicals with NO_2, which subsequently partition to aerosol and contribute to SOA mass.

4.3.2. SOA Yield and Products from Furanoids + NO_3 and O_3. Several studies have investigated the SOA yields from furanoid reactions with NO_3 and O_3 (Table 11). Losses to NO_3 are competitive with OH for many furanoids, and the resulting

https://doi.org/10.1021/acsearthspacechem.3c00226
ACS Earth Space Chem. XXXX, XXX, XXX−XXX

organic nitrates formed from the addition of NO_3 to the furan ring is a possible source of brown carbon.[193,194] Furanoid oxidation by NO_3 generally results in SOA yields that are comparable to those from OH oxidation, whereas oxidation by O_3 results in significantly lower yields. Disubstituted furanoids, such as 2,5-DMF, have ozone losses that are competitive with other oxidants (Table 7), yet the SOA yields from ozonolysis are at least four times lower than those by OH. Consequently, SOA formed by furanoid ozonolysis are not expected to be significant in the atmosphere.

Joo et al.[182] measured SOA for 3-MF + NO_3 using a high-resolution aerosol mass spectrometer and filter inlet for a gas and aerosol (FIGAERO) system coupled to a iodide chemical ionization mass spectrometer. The authors observed the formation of organic nitrates consistent with those produced in the gas phase from NO_3 addition to the furan ring (Figure 15), which then partitioned to form SOA. C_{10} oligomers were also observed and likely formed by the heterogeneous processes described by Strollo and Ziemann[190] for the reaction of 3-MF with OH. Joo et al.[182] estimated that organonitrates composed ~40% of the total SOA formed by this reaction.

Al Ali et al.[183] studied the SOA formation yields from the 2-MF + NO_3 reaction as a function of the initial 2-MF concentration using PTR-ToF-MS and a scanning mobility particle sizer-condensation particle counter (SMPS). The SOA formation yields ranged between 1.0 and 2.2%, and the experimental data were fitted using a one product model (i.e., the Odum fit[195]) to determine the mass-based stoichiometric coefficient of the semivolatile organic compounds SVOC (α) and the gas-particle partitioning equilibrium constants (K, m^3 μg^{-1}), respectively.[183] The chemical composition of the SOA formed was chemically characterized using electrospray ionization-liquid chromatography-quadrupole-time of flight-tandem mass spectrometry (ESI-LC-QToF-MS/MS) and revealed the formation of oligomers, e.g., highly oxygenated molecules (HOMs).[183] Attenuated total reflection infrared spectroscopy was used to identify the presence of characteristic infrared bands attributed to organic nitrate formation.

4.3.3. SOA Dependencies to RH and NO_x. The aerosol products of furanoid oxidation change depending on environmental conditions, which is also reflected in the SOA yield. Jiang et al.[191] observed higher SOA yields from the OH oxidation of furan when NO_x and relative humidity were increased. The higher yields with increased relative humidity were partly attributed to greater OH production, but also to the enhanced formation of multiphase products in the presence of aerosol water. This mechanism is consistent with the observation of C_{10} oligomers in deliquesced aerosol particles formed from the OH oxidation of 3-MF.[190] Higher yields at higher NO_x were attributed to the formation of organic nitrates. The increase in yields from changes to atmospheric conditions were modest—for example, SOA yields under dry conditions were 0.04−1%, but increased to 5% when the relative humidity was higher (RH ~ 85%). Though the absolute yields at higher relative humidity were small, the relative change from dry conditions suggests that multiphase reactions are likely key processes in determining SOA formed from furanoid systems. Higher-carbon or multifunctional furanoids—such as 2-furfural, 5-methyl-2-furfural, and 5-hydroxymethyl-2-furfural—may also undergo similar reactions, and thus further research should be aimed at studying furanoid oxidation under varying relative humidity and NO_x conditions.

4.3.4. Data Gaps. In general, SOA yields are low and furanoids are unlikely to be significant sources of SOAs in the atmosphere beyond concentrated wildfire plumes. Changes to SOA yields in response to NO_x and water content afford opportunities to study the role of multiphase chemistry in altering aerosols formed from furanoids. Likewise, there remain a number of higher molecular weight furanoids, such as 5-methyl-2-furfural, 2-furanmethanol, and 5-hydroxymethyl-2-furfural, for which SOA yields have not been determined. A systematic study of furanoids might elucidate the dependence of furanoid functionality on SOA formation.

5. FIELD OBSERVATIONS AND CHEMICAL MODELING OF FURANOID ATMOSPHERIC CHEMISTRY

Field observations of furanoids and their gas-phase products are typically performed using gas-chromatography and mass spectrometry techniques, which include PTR-MS and iodide−adduct chemical ionization mass spectrometry (I-CIMS). In situ measurements are often coupled with modeling techniques to study how biomass burning plumes chemically evolve and impact air quality and climate. Furanoid chemistry is not widely represented in chemical transport models, yet recent work has expanded the chemical mechanisms used to represent the gas-phase evolution of biomass burning plumes. The following discussion summarizes studies that have characterized the atmospheric chemistry of furanoids using ambient field observations and chemical transport modeling. Section 5.1 discusses the techniques employed to quantify furanoid mixing ratios in the field. Section 5.2 describes studies that have evaluated the contributions of furanoids to radical reactivity in biomass burning plumes. Finally, Section 5.3 reviews studies that have used models to evaluate the atmospheric impact of furanoids on air quality.

5.1. Techniques to Measure Furanoid Mixing Ratios in Biomass Burning Plumes. Furan is the most commonly observed furanoid in ambient biomass burning plumes. To our knowledge, the first field measurement of furan was reported by Greenberg et al.[82] in a wildfire plume in Brazil's cerrado and selva regions in 1979 and 1980. The authors sampled smoke using whole air sampling (WAS) and detected furan and 2-MF using both gas chromatography-flame ionization detector (GC-FID) and gas chromatography-mass spectrometry (GC-MS). In the early 2000s, Bertschi et al.[77,196] made the first in situ measurement of furan by open-path Fourier transform infrared (OP-FTIR) spectroscopy while sampling wood and charcoal cooking fires and an earthen charcoal-making kiln in Zambia. In these in situ experiments, the smoke age was <1 s, suggesting that the observed furan is directly emitted as opposed to formed via secondary chemistry.[77,196]

Later studies deployed FTIR-based instrumentation to quantify furan emission factors in ambient smoke.[75,76,78,79,88,89] Quantification by FTIR has been conducted via ground (e.g., Stockwell et al.[88]) and aircraft (e.g., Akagi et al.[75]) observations for a wide variety of fuels described in Table 2. Similarly, GC-MS has been deployed on ground and mobile platforms to quantify furan, furanaldehydes, methylated furanoids, and benzofurans.[76,81,82,87,89,91,93,96−98]

Furanoids are also detectable by PTR-MS, which has the capability to measure a wide range of functionalized furanoid.[24] These instruments have become more commonly deployed on aircraft due to their capabilities to perform measurements at high time resolution. Initial PTR-MS measurements were performed using quadrupole or low mass resolution time-of-flight mass

https://doi.org/10.1021/acsearthspacechem.3c00226
ACS Earth Space Chem. XXXX, XXX, XXX−XXX

spectrometers with a focus on quantifying furan. For example, during the 2008 ARCTAS campaign, a WAS and PTR-MS aboard the NASA DC-8 aircraft measured furan emissions from multiple biomass burning plumes.[197] The PTR-MS did not have a sufficient mass resolution to differentiate furan and isoprene signals which are detected at the same nominal mass (m/z 69). The authors combined the PTR-MS measurements with those from WAS with GC-MS analysis to deduce that roughly half of the signal is attributed to furan within BB plumes, consistent with laboratory burns. An analogous detection method was used to measure furan from the California Rim Fire during the 2013 SEAC^{4}RS campaign.[198]

Developments in PTR-MS designs as well as the use of high-resolution time-of-flight (ToF) mass spectrometers (termed PTR-ToF-MS) have improved the quantification of functionalized furanoids. Müller et al.[32] first used a PTR-ToF-MS onboard the NASA DC-8 aircraft to separate isobaric species (e.g., isoprene and furan) and quantify furan, 2-MF, and furanaldehydes. More recent deployments of PTR-ToF-MS instruments on the NCAR C-130 during the 2018 Western wildfire Experiment for Cloud chemistry, Aerosol absorption and Nitrogen (WE-CAN) and the NASA DC-8 during the 2019 Fire Influence on Regional to Global Environments and Air Quality (FIREX-AQ) have expanded the quantification of important furanoids such as 5-methylfurfural and 2-(3*H*)-furanone.[72,86] The assignments of various PTR-ToF-MS signals to furanoids and other BBVOCs have largely been based on the laboratory work conducted at the Missoula, MT Fire Sciences Laboratory (Firelab).[22−24] Gkatzelis et al.[72] compared aircraft observations from PTR-ToF-MS to those from co-located GC-MS instruments and found that the PTR-ToF-MS masses assigned to furanoids may include interferences from compounds produced from chemical oxidation within the plume. Consequently, more work is needed to improve the quantification of functionalized furanoids measured in ambient smoke by mass spectrometry.

5.2. Evaluation of Furanoid Chemistry in Biomass Burning Plumes. Literature describing the atmospheric chemistry of biomass burning smoke has mostly focused on OH chemistry and corroborated laboratory findings that furanoids are highly reactive toward OH during the daytime. Studies evaluating furanoid reactions with O_3 and NO_3 are more limited, yet Table 7 shows that the atmospheric lifetime of many furanoids also depends on reactions with NO_3 and O_3. The relative loss of furanoids in biomass burning plumes to OH, O_3, and NO_3 depends on the available actinic flux (e.g., day, night, transparent plumes, opaque plumes), availability of OH precursors (e.g., HONO, formaldehyde), abundance of O_3, and sufficient mixing ratios of NO_2 to produce NO_3.

Below, we discuss the current understanding of furanoid chemical evolution in biomass burning plumes as determined by the combination of field and modeling studies. Many studies quantify radical reactivity (k_x in s^{-1}) as a proxy for determining the potential of BBVOCs to form ozone or other secondary pollutants.

$$k_x = \sum_{i=1}^{n} k_{X+BBVOC_i} \times [BBVOC_i]$$

where $k_{X+BBVOC_i}$ (in cm^3 $molecule^{-1}$ s^{-1}) is a bimolecular rate coefficient for the reaction of an oxidant (X) with a given BBVOC, and $[BBVOC_i]$ is the molecular concentration (in molecules cm^{-3}). Radical reactivity is a useful measure to compare furanoid reaction rates with OH, NO_3, or O_3 against those of other BBVOCs. We also discuss a proxy for BBVOC oxidation termed the oxidation rate (R_x, in molecules cm^{-3} s^{-1})

$$R_x = \sum k_{X+BBVOC_i}[BBVOC_i][X]$$

where [X] is the concentration of given oxidant (in molecules cm^{-3}). The oxidation rate considers the concentration of OH, O_3, or NO_3 measured or modeled in smoke and can therefore give a more accurate picture of the evolution of BBVOCs in real plumes. Oxidation rate is a useful measure for comparing furanoid losses due to the reaction with each of the atmospheric oxidants. We note that OH concentrations are not commonly measured in smoke; consequently, this proxy relies on modeled OH mixing ratios[30] or average OH mixing ratios estimated based on the decay of reactive VOCs[199]

5.2.1. Daytime Evolution of Furanoid Chemistry. The first airborne measurements capable of quantifying furan chemical oxidation occurred during the 2013 DISCOVER-AQ mission when a PTR-ToF-MS with sufficient mass resolution was deployed on the NASA DC-8 aircraft to differentiate furan from other isobaric species.[200] From these observations, Müller et al.[32] reported mixing ratios of furan and 2-furfural during sunlit hours from a small understory fire. The authors interpreted the aircraft measurements with a 0D box model and were able to reproduce the observed furan and 2-furfural decay with only OH as the chemical oxidant. The expectation that OH is the main sink of furan during daytime was first noted by Bertschi et al.[196] The model and observations by Müller et al.[32] provided the first in situ evidence for furan and 2-furfural oxidation.

To evaluate the potential for other furanoids to react with OH, Coggon et al.[31] studied the oxidation of biomass burning emissions using an OH oxidation chamber. These experiments were leveraged to further evaluate the field measurements presented by Müller et al.[32] The authors focused on two fuel types during laboratory experimentation: ponderosa pine and Engelman spruce duff. While these fuels are both characteristic of temperate forests, they were chosen because they represented extreme cases of low-NO_x emitting smoldering combustion (Engelmann case) and a typical mixture of flaming and smoldering (Ponderosa case). PTR-ToF-MS measurements determined that furanoids were one of two classes of compounds with the greatest measured carbon loss from OH oxidation. Bottom-up OH reactivity calculations placed 2,5-DMF, 5-hydroxymethyl-2-furfural, furan, 2-furfural, 2-MF, and furanone in the top 20 compounds with the highest reactivity. In total, furanoids accounted for ∼30% of the total OH reactivity estimated for all measured BBVOCs.

The result by Coggon et al.[31] is consistent with a similar calculation by Decker et al.[30] who compiled an emissions database from both the 2016 Firelab and 2012 FLAME-4 laboratory campaigns and used these emissions to interpret field observations from a plume sampled at night during the 2013 Southeast Nexus (SENEX) campaign. In this estimate, furanoids accounted for ∼25% of total OH reactivity. This study also determined that furanoid chemistry with NO_3 and O_3 could also be significant. Furanoids accounted for 19% of total NO_3 reactivity (second to phenolics) and 7% of total O_3 reactivity (second to alkenes and terpenes).

It is important to note here that laboratory-derived emission ratios are important to understand the chemistry of fresh smoke (i.e., smoke observed within minutes of emission). The studies described above provide information to understand the

https://doi.org/10.1021/acsearthspacechem.3c00226
ACS Earth Space Chem. XXXX, XXX, XXX−XXX

initiation of smoke chemistry. In contrast, observations of smoke outside of a laboratory typically capture aged emissions—i.e., a mixture of emission losses and secondary product formation. As the emissions undergo atmospheric chemistry, the oxidant reactivity will also change.

A detailed accounting of the OH reactivity from ground-site[15] and airborne observations[30,201] of smoke illustrate how furanoid reactivity evolves with smoke age. Liang et al.[15] used ground-site observations of the 2017 Northern California wildfire smoke for bottom-up OH reactivity calculations and found that furanoids accounted for four of the five compounds with the highest contribution to total OH reactivity. Specifically, in smoke that was ∼3 h old, furanoids accounted for 18% of total OH reactivity, but for plumes with an age >6 h, furanoids accounted for only 8%. The authors conclude that the contribution of furanoids to total OH reactivity decreases with age due to a decrease in furan mixing ratios.[15] Airborne studies by Xu et al.[199] and Gkatzelis et al.[72] from the 2019 FIREX-AQ campaign similarly found that, on average, furanoids accounted for 20% of OH reactivity in one fire plume <4 h old but that the contribution decreases in smoke downwind of the fire. Similarly, Permar et al.[201] used airborne measurements from the 2018 WE-CAN campaign to calculate OH reactivity for young (<130 min) smoke and aged (>3 days) smoke. On average furanoids account for ∼20% of total OH reactivity for young smoke, but 13% for aged smoke. The authors note that a large fraction of furanoid OH reactivity in aged smoke is due to the production of secondary VOCs, including maleic anhydride.

A 0D box model constrained to aircraft observations from FIREX-AQ by Decker et al.[15] details how the oxidation rate of furanoids (R_x) evolves with plume age. The authors investigated four wildfire plumes but note that all were sampled in the afternoon or evening when actinic flux (and, thus, OH production) was past its peak and decreasing. Observations of furanoid mixing ratios were as large as 20 ppbv (∼3.5 ppbv furan ppmv CO^{-1}) as measured by PTR-ToF-MS. The calculated oxidation rate (R_x) showed that furanoids were mainly consumed by O_3, in contrast to the OH-dominated losses observed in other plumes (e.g., Müller et al.[32]). That was attributed, in part, to the size and emission time of the plumes studied by Decker et al.[15] For example, in a relatively small and optically transparent plume, roughly 70% of furanoid oxidation rate was attributed to OH at emission but then decreased to 20% by sunset 1.25 h later. In a significantly larger and optically thick plume, only ∼25% of furanoids reacted with OH while the remaining fraction was oxidized by O_3. These results suggest that O_3 and OH may be equally important for furanoid oxidation in some plumes, with the former more important in large optically dense plumes or plumes emitted near sunset.

5.2.2. Nighttime Evolution of Furanoid Chemistry. Nighttime observations of furanoids are limited. Two ground-based[15,202] studies and one airborne[203] measurement of furanoids in nighttime smoke have been reported. However, the airborne measurement of furan was limited to the sum of isoprene + furan as the instrument was a quadrupole PTR-MS.[203] Even so, two box model analyses have explored the expected nighttime oxidation of furanoids using daytime aircraft observations.[30,203]

Box models by Decker et al.[30] show that nighttime oxidation (furanoids or otherwise) proceeds more slowly relative to daytime plumes. This is due to the lower oxidant concentration at night (when oxidation proceeds by mainly O_3 and NO_3) compared to the day (when all oxidants take part: OH, NO_3, and O_3). As such, the models suggest more furanoids survive nighttime oxidation and thus retain reactivity by sunrise the following day. For some furanoids, more than 50% of nighttime emissions remain by sunrise.[30,203] The "preservation" of reactivity overnight was also suggested by Mouat et al.[202] who report ground-site nighttime observations of smoke in North South Wales, Australia during the COALA 2020 campaign.

Nighttime observations by Mouat et al.[202] of aged plumes found that furan remains mostly unchanged until sunrise after which concentrations decreased to background levels within hours. While the authors only consider OH reactivity, they found that the reactivity reaches a minimum at night, but that the nighttime transport adds additional reactivity to daytime smoke and that the largest group contributing to reactivity was furanoids. It should be noted that the greatest contribution (69%) to furanoid reactivity was attributed to PTR-MS measurements at m/z 85, which includes contributions from both furanone and butenedial. While butenedial is a furan oxidation product, it is not a furanoid and may overestimate the OH reactivity budget here. The total furanoid contribution to OH reactivity at night was determined to be 1.24−3.93 s^{-1}.

During ground-site observations, Liang et al.[15] showed that OH reactivity budgets for an observed nighttime plume (∼3 h old) were similar to fresh (∼3 h) and aged (>6 h) daytime plumes (22.5−25.8 s^{-1}). The nighttime plume had the greatest furan reactivity to OH (31%) compared to the fresh (18%) and aged (8%) plumes. While it is difficult to compare the plume ages, it is likely the nighttime plume was emitted after sunset. Considering the results by Decker et al.[30] and Mouat et al.,[202] it is likely that the large furan reactivity to OH at night observed by Liang et al.[15] is the result of minimal furan oxidation since emission, relative to the daytime plumes.

There are no reports of NO_3 or O_3 reactivity calculations from nighttime observations of furanoids. In two model analyses of nighttime plumes by Decker et al.,[30] the authors report furanoid oxidation rates with NO_3, O_3, and OH for daytime and nighttime plume models constrained to aircraft observation. Note that the models incorporated furanoid emissions based on laboratory emission ratios. Model results suggest that the fraction of furanoids oxidized by OH during the daytime is replaced by O_3 oxidation at night. Further, oxidation by NO_3 was estimated to be minimal (<5%) owing to the high loss of NO_3 radicals to other BBVOCs (e.g., phenolic compounds).

In a separate analysis by Decker et al.,[204] the authors used aircraft observations of biomass burning plumes from FIREX-AQ to investigate differences in daytime plume chemistry at the plume center and plume edge. Typical aircraft sampling of biomass burning plumes was done using cross-wind transects; that is, crossing the plume in a direction perpendicular to the prevailing wind direction. Measurements of the furan oxidation product maleic anhydride clearly show a dependence on the location within the plume due to variations in photolysis rates. Using a novel method to analyze 430 daytime cross-wind transects, the authors defined plume shapes relative to CO by "plume width" and "plume center" and found maleic anhydride exhibited, on average, wider plume widths relative to CO. This is interpreted to indicate enhanced maleic anhydride formation on plume edges from OH oxidation or less formation at the plume center. The authors further show that the maleic anhydride plume width decreases and becomes more similar to CO as the plume ages over 3 h. The authors found similar results using an established OH oxidation proxy, namely, acetyl peroxynitrate (PAN), suggesting that maleic anhydride may be used as an

https://doi.org/10.1021/acsearthspacechem.3c00226
ACS Earth Space Chem. XXXX, XXX, XXX−XXX

indicator for OH oxidation chemistry. These observations demonstrate that non-OH chemistry at the center of a plume may contribute to furanoid losses during daytime hours.

5.3. Modeling Furanoid Atmospheric Chemistry. Recent modeling work has explored the impacts of furanoid oxidation on the formation of ozone, secondary VOCs, and PM2.5. While this work is limited and additional modeling studies are needed, these results show that furanoids can be an important contributor to atmospheric pollutants in biomass burning plumes.

Explicit reactions describing furanoid oxidation have been implemented into chemical mechanisms, including the master chemical mechanism (MCM v 3.3.1).[178] Coggon et al.[31] modified the MCM to include the reactions and products formed from the OH oxidation of furan, 2-MF, 2,5-DMF, 2-furfural, and 5-methyl-2-furfural based on laboratory work by Aschmann et al.[123,173] and quantum chemical reactions proposed by Zhao and Wang.[137] The mechanism was applied to box models of biomass burning plumes and was shown to reproduce observations of secondary VOCs, including hydroxyfuranones and maleic anhydride. The inclusion of furanoid chemistry increased modeled ozone by 10−20% and resulted in better model agreement with aircraft ozone observations.

The products of furanoid oxidation—i.e., hydroxy furanones and maleic anhydride—were shown by Coggon et al.[31] to be useful markers for identifying aged biomass burning plumes. Maleic anhydride has been observed in young[15,16,31,32,72] (<1day) and long-lived plumes[31] (∼1 week), and is expected to be predominantly formed from OH oxidation of furan, methylated furanoids, and 2-furfural.[31] OH production occurs quickly in biomass burning smoke, and strong gradients in photolysis rates lead to higher OH oxidation at the edges of plumes where smoke is optically thin vs the center of plumes where smoke is optically thick. Wang et al.[205] applied a large eddy simulation (LES) model to simulate the chemical topography of a wildfire plume sampled during the FIREX-AQ campaign. The authors used a simplified furan mechanism derived from explicit chemistry used by Coggon et al.[31] and showed that maleic anhydride produced at the edges of wildfire plumes directly correlated with higher OH production. This modeling work was consistent with the observations made by Decker et al.[204] described above, which showed that chemical gradients could be described by changes to secondary products such as maleic anhydride. The authors proposed that the furanoid system could be useful for deriving OH exposures from aircraft observations.

Furanoid chemistry has recently been included into reduced chemical mechanisms used for regional air quality modeling, such as and Statewide Air Pollution Center chemical mechanism (SAPRC)[206] and Community Regional Atmospheric Chemistry Mechanism (CRACMM),[207] as well as global modeling via GEOS-Chem.[208] Traditionally, reduced mechanisms have assumed that furanoids react similarly to nonheterocyclic aromatics. Jiang et al.[176] included explicit furanoid chemistry into SAPRC using a mechanism generator and then evaluated model performance against photooxidation experiments of furan, 2-MF, 3-MF, and 2,5-DMF. The model reliably reproduced ozone observations under a wide range of NO_x conditions. The reactions and updated mechanism outperformed simulations where furanoids were treated as nonheterocyclic aromatics, which shows that reduced mechanisms should consider including reactions specific to furanoids in order to capture their potential impacts on ozone formation from biomass burning plumes.

Pye et al.[207] recently included a reduced scheme for furanoid oxidation into CRACMM, which is a new mechanism developed for the U.S. Environmental Protection Agency's Community Multiscale Air Quality Modeling System (CMAQ). The reactions follow the same scheme used by Wang et al.[205] for LES modeling. This mechanism has yet to be evaluated against field observations, and future studies may consider using CMAQ to evaluate the impacts of furanoids on regional air quality.

Carter et al.[208] recently implemented furanoid emissions and simplified furanoid chemistry into the global climate model GEOS-Chem. BBVOC emissions were included based on the emission factors compiled in Andreae's work,[2] and furanoids were explicitly represented as a lumped tracer that reacts with OH radicals to form butenedial. This simplified scheme was used to track furanoid contributions to OH reactivity throughout the global simulations. The author found that updates to GEOS-Chem substantially increased global simulated nonmethane organic gases mixing ratios and that biomass burning contributed as much as 75% of the total OH reactivity in regions prone to wildfires. These results are consistent with the GEOS-Chem simulations performed by Jin et al.[106] who showed that BBVOCs contributed more than 45% to the total primary VOCs emitted during the 2018 wildfire season in the Western U.S. Among the non-methane organic gases modeled by Carter et al.,[208] furans were highlighted as significant contributors to global OH reactivity.

5.3.1. Data Gaps. The modeling studies described above demonstrate that furanoids are important contributors to the chemical evolution of ozone and other secondary pollutants in biomass burning smoke. Furthermore, these studies highlight that furanoid chemistry impacts global atmospheric reactivity.

There remain a number of major knowledge gaps that need to be addressed in chemical transport models in order to evaluate furanoid impacts on air quality and global climate. First, most inventories used to evaluate biomass burning impacts do not include the highly functionalized furanoids reported in Table 2. For example, the GEOS-Chem simulations described by Carter et al.[208] included emissions from furan, 2-MF, and 2,5-DMF, which represent ∼20−30% of the total furanoid emissions across common fuel types (Figure 5). Inclusion of furanaldehydes, 2-(3*H*)-furanone, and other oxygenated furanoids would likely increase the reactivity of smoke in global and regional models.

Next, most reduced chemical mechanisms used in 3D models do not represent the chemical degradation of furanoids by atmospheric reactions that are consistent with laboratory mechanism studies. Jiang et al.[176] show that lumping furanoids to nonheterocyclic aromatics (the typical assumption) underestimates potential contributions of furanoids to the formation of secondary pollutants, such as ozone. To date, only Pye et al.[207] and Wang et al.[205] have incorporated a simplified reaction scheme that can be used in 3D models to represent the multigenerational OH chemistry of furanoids. More work is needed to include the chemistry of furanoids with other oxidants (e.g., NO_3 and O_3) and refine reduced mechanisms to include the chemistry of important oxygenated furanoids (e.g., furfural). This is especially relevant to global simulations, as multigenerational furanoid chemistry may perpetuate radical reactivity through the formation of highly reactive VOCs (e.g., dialdehydes and hydroxyfuranones) and lead to longer-lived species, such a maleic anhydride. Maleic anhydride has been observed in biomass burning plumes transported in the remote

https://doi.org/10.1021/acsearthspacechem.3c00226
ACS Earth Space Chem. XXXX, XXX, XXX−XXX

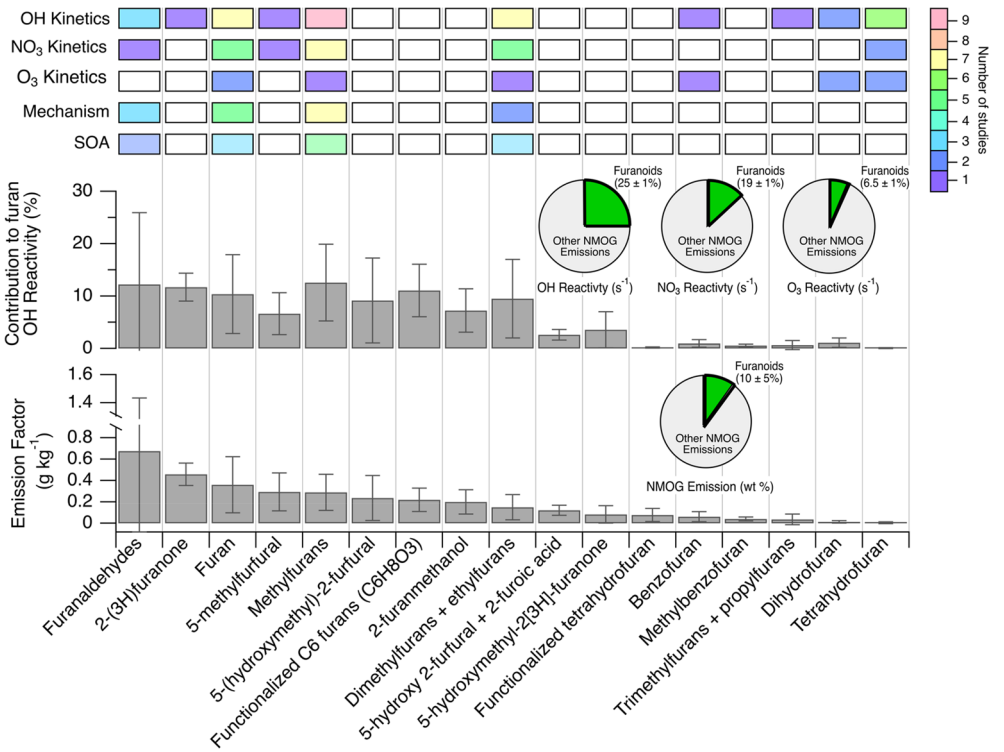

Figure 16. (Bottom) Furanoid emission factors for temperate forests compiled as part of this review (Table 2). (Middle) Contributions of each species to total furanoid OH reactivity, calculated using OH rate constants reported in the literature or calculated by Koss et al.[24] using structurally similar furanoids. Error bars reflect the standard deviation in emission factors reported in Table 2. The boxes above each species highlight the number of studies for which kinetic, mechanistic, or SOA studies have been performed. The pie charts show the contribution of furanoids to total non-methane organic gas (NMOG) emissions based on the distribution BBVOC reactivity to OH, NO_3, and O_3 reported by Decker et al.[30] for western U.S. wildfires.

atmosphere from distant sources,[31] and incorporation of furanoid chemistry may help to explain these observations.

Finally, furanoid emissions and mechanism updates are both needed to fully capture biomass burning impacts on global ozone formation. Biomass burning is a significant source of ozone, and VOCs observed in the remote atmosphere[20,106,208] and the OH reactivity estimates from Carter et al.[208] suggest that furanoids may play an important role.

6. PERSPECTIVES

This review presents an assessment of the emissions, kinetics, and atmospheric chemistry of furanoids primarily derived from biomass burning smoke. To date, there have been major advancements in the characterization of furanoid emissions and atmospheric chemistry. New developments in instrumental techniques have enabled the quantification of multifunctional furanoids, and recent field deployments have shown that these species are important contributors to the reactivity of biomass burning smoke. Laboratory experiments have shown that furanoids are highly reactive with the major atmospheric oxidants, and mechanistic/SOA studies of select furanoids indicate that the carbon that evolves from furanoid reactions is largely retained in the gas phase. Modeling efforts show that furanoids are an important contributor to the ozone and secondary pollutants formed from biomass burning smoke.

There remain open questions about the emissions and atmospheric fate of furanoids. Figure 16 summarizes key observations from this assessment and illustrates the distributions of furanoid emissions and reactivity toward atmospheric radicals based on the data summarized as part of this work (Tables 2, 3, 4, 5, and 6). The grid at the top of Figure 16 is colored by the number of studies that have characterized the emissions, kinetics, and mechanism of each species. This figure, along with the tables presented in this review, illustrates several key research opportunities that may help to better characterize the atmospheric fate, air quality implications, and climate impacts of furanoids.

First, atmospheric observations of highly functionalized furanoids remain limited (Table 2). These molecules have the potential to impact air quality through ozone or SOA formation. Deployment of advanced gas chromatography and mass spectrometry instrumentation may improve observations of functionalized furanoids. Additional observations are also needed for most furanoids emitted from different fuel types, e.g., savanna, dung burning, and trash burning, Table 2.

The chemistry of many furanoids emitted from biomass burning remains understudied, especially for reaction with NO_3 radicals and O_3. Key species—including 2-(3*H*)-furanone, 2-furanmethanol, and functionalized furanaldehydes—would benefit from research aimed at characterizing their degradation by UV photolysis and reactions with OH, NO_3, and O_3. Furthermore, cross-validation of kinetic results is essential for many furanoids where single measurements exist or where results disagree. Laboratory studies have already shed light on the degradation mechanism of methyl-substituted furanoids by OH radicals, but further research is needed to elucidate the reaction mechanism of other functionalized furanoids by OH, NO_3, and O_3. The formation of organic nitrates by the atmospheric degradation of furanoids is also understudied. Organic nitrates are temporary reservoirs of nitrogen which can impact ozone formation over longer time scales and in remote atmospheres. The reaction mechanism of furanoids degradation

https://doi.org/10.1021/acsearthspacechem.3c00226
ACS Earth Space Chem. XXXX, XXX, XXX−XXX

by UV photolysis and NO_3 oxidation are likely to impact the atmospheric lifetimes of reactive and photosensitive species, such as furanaldehydes (Table 7).

Laboratory studies are also needed to study the SOA formation potential of functionalized furanoids and provide quantitative yields that could be used in atmospheric models to interpret field observations. The available literature data on SOA are scarce, and there is a need to investigate the impact of relative humidity and effect of mixtures (i.e., oxidation of multiple furanoids) on the formation of SOA, especially in biomass burning plumes. There is also a significant lack of laboratory data regarding the hygroscopicity and optical properties of the SOA formed by furanoid oxidation. These are essential pieces of information necessary to evaluate the impact of furanoid SOA on climate. The presence of multifunctional organic nitrates in the particulate phase is expected to strongly absorb in the actinic range reaching earth's atmosphere.

Finally, the atmospheric chemistry of furanoids have only recently been implemented into atmospheric models. Reduced mechanisms have been developed for large-eddy simulations and regional chemical models (e.g., CRACMM[207]), but similar mechanisms for global models have not been fully implemented. More model development is needed in order to determine the regional and global impacts of furanoids on atmospheric composition. This will become even more important as climate change exacerbates biomass burning in drought-prone regions and economies shift toward renewable fuels which may contain furanoids such as methyl and dimethylfurans.[7,8]

■ ASSOCIATED CONTENT

Supporting Information

The Supporting Information is available free of charge at https://pubs.acs.org/doi/10.1021/acsearthspacechem.3c00226.

Detailed description of the tables in the other SI file (PDF)

Summaries of individual emission factor measurements (Table S1), emission ratios (Table S2), and corresponding measures of MCE and CO/CO_2 emission factors (Table S3), organized by furan functionality, molecular weight, and then measurement type (laboratory vs field); full reference to each measurement and reference ID number which can be used to identify corresponding measurements among the tables (Table S4) (XLSX)

■ AUTHOR INFORMATION

Corresponding Authors

Manolis N. Romanias − *IMT Nord Europe, Institut Mines-Télécom, University of Lille, Centre for Energy and Environment, F-59000 Lille, France;* orcid.org/0000-0002-9049-0319; Email: emmanouil.romanias@imt-nord-europe.fr

Matthew M. Coggon − *Chemical Sciences Laboratory, National Oceanic and Atmospheric Administration, Boulder, Colorado 80305, United States;* orcid.org/0000-0002-5763-1925; Email: matthew.m.coggon@noaa.gov

Authors

Fatima Al Ali − *IMT Nord Europe, Institut Mines-Télécom, University of Lille, Centre for Energy and Environment, F-59000 Lille, France; Laboratoire de Physico−Chimie de l'Atmosphère (LPCA), Université du Littoral Côte d'Opale, 59140 Dunkerque, France*

James B. Burkholder − *Chemical Sciences Laboratory, National Oceanic and Atmospheric Administration, Boulder, Colorado 80305, United States;* orcid.org/0000-0001-9532-6246

Philippe Dagaut − *Institut de Combustion, Aérothermique, Réactivité, Environnement (ICARE), CNRS, 45071 2 Orléans Cedex, France;* orcid.org/0000-0003-4825-3288

Zachary Decker − *Laboratory of Atmospheric Chemistry, Paul Scherrer Institut (PSI), 5232 Villigen, Switzerland;* Present Address: (Z.D.) Cooperative Institute for Research in Environmental Sciences, University of Colorado, 216 UCB, Boulder, CO 80305, USA; Present Address: (Z.D.) Chemical Sciences Laboratory, National Oceanic and Atmospheric Administration, 325 Broadway, Boulder, CO 80305, USA.; orcid.org/0000-0001-9604-8671

Carsten Warneke − *Chemical Sciences Laboratory, National Oceanic and Atmospheric Administration, Boulder, Colorado 80305, United States;* orcid.org/0000-0003-3811-8496

Chelsea E. Stockwell − *Chemical Sciences Laboratory, National Oceanic and Atmospheric Administration, Boulder, Colorado 80305, United States;* orcid.org/0000-0003-3462-2126

James M. Roberts − *Chemical Sciences Laboratory, National Oceanic and Atmospheric Administration, Boulder, Colorado 80305, United States;* orcid.org/0000-0002-8485-8172

Alexandre Tomas − *IMT Nord Europe, Institut Mines-Télécom, University of Lille, Centre for Energy and Environment, F-59000 Lille, France;* orcid.org/0000-0002-0125-581X

Nicolas Houzel − *Laboratoire de Physico−Chimie de l'Atmosphère (LPCA), Université du Littoral Côte d'Opale, 59140 Dunkerque, France*

Cecile Coeur − *Laboratoire de Physico−Chimie de l'Atmosphère (LPCA), Université du Littoral Côte d'Opale, 59140 Dunkerque, France;* orcid.org/0000-0002-5643-5148

Steven S. Brown − *Chemical Sciences Laboratory, National Oceanic and Atmospheric Administration, Boulder, Colorado 80305, United States;* orcid.org/0000-0001-7477-9078

Complete contact information is available at: https://pubs.acs.org/10.1021/acsearthspacechem.3c00226

Notes

The authors declare no competing financial interest.

■ ACKNOWLEDGMENTS

This work was achieved in the frame of Labex CaPPA, funded by ANR through the PIA under contract ANR-11-LABX-0005-01, CPER ECRIN project, funded by the Hauts-de-France Regional Council. This work was also supported by the French National program LEFE (Les Enveloppes Fluides et l'Environnement), in the framework of the FiLL project.

■ REFERENCES

(1) Akagi, S. K.; Yokelson, R. J.; Wiedinmyer, C.; Alvarado, M. J.; Reid, J. S.; Karl, T.; Crounse, J. D.; Wennberg, P. O. Emission factors for open and domestic biomass burning for use in atmospheric models. *Atmos. Chem. Phys.* **2011**, *11* (9), 4039−4072.

(2) Andreae, M. O. Emission of trace gases and aerosols from biomass burning − an updated assessment. *Atmos. Chem. Phys.* **2019**, *19* (13), 8523−8546.

(3) McDonald, B. C.; de Gouw, J. A.; Gilman, J. B.; Jathar, S. H.; Akherati, A.; Cappa, C. D.; Jimenez, J. L.; Lee-Taylor, J.; Hayes, P. L.; McKeen, S. A.; et al. Volatile chemical products emerging as largest petrochemical source of urban organic emissions. *Science* **2018**, *359* (6377), 760−764.
(4) Hoa Van, B.; Inho, H.; Dawoon, J.; Amna, T. Principle of Meat Aroma Flavors and Future Prospect. In *Latest Research into Quality Control*; Isin, A., Ed.; IntechOpen, 2012; p Chapter 7.
(5) Wailzer, B.; Klocker, J.; Wolschann, P.; Buchbauer, G. Structural features for furan-derived fruity and meaty aroma impressions. *Nat. Prod. Commun.* **2016**, *11* (10), 1934578X1601101.
(6) Crews, C.; Castle, L. A review of the occurrence, formation and analysis of furan in heat-processed foods. *Trends Food Sci. Technol.* **2007**, *18* (7), 365−372.
(7) Román-Leshkov, Y.; Barrett, C. J.; Liu, Z. Y.; Dumesic, J. A. Production of dimethylfuran for liquid fuels from biomass-derived carbohydrates. *Nature* **2007**, *447* (7147), 982−985.
(8) Tuan Hoang, A.; Viet Pham, V. 2-Methylfuran (MF) as a potential biofuel: A thorough review on the production pathway from biomass, combustion progress, and application in engines. *Renew. Sust. Energy Rev.* **2021**, *148*, No. 111265.
(9) Lange, J.-P.; Price, R.; Ayoub, P. M.; Louis, J.; Petrus, L.; Clarke, L.; Gosselink, H. Valeric biofuels: a platform of cellulosic transportation fuels. *Angew. Chem., Int. Ed. Engl.* **2010**, *49* (26), 4479−4483.
(10) Dauenhauer, P. J.; Huber, G. W. Biomass at the shale gas crossroads. *Green Chem.* **2014**, *16* (2), 382−383.
(11) Atkinson, R.; Aschmann, S. M.; Tuazon, E. C.; Arey, J.; Zielinska, B. Formation of 3-methylfuran from the gas-phase reaction of OH radicals with isoprene and the rate constant for its reaction with the OH radical. *Int. J. Chem. Kinet.* **1989**, *21* (7), 593−604.
(12) Birmili, W.; Daniels, A.; Bethke, R.; Schechner, N.; Brasse, G.; Conrad, A.; Kolossa-Gehring, M.; Debiak, M.; Hurraß, J.; Uhde, E.; et al. Formaldehyde, aliphatic aldehydes (C2-C11), furfural, and benzaldehyde in the residential indoor air of children and adolescents during the German Environmental Survey 2014−2017 (GerES V). *Indoor Air* **2022**, *32* (1), No. e12927.
(13) Liu, Y.; Misztal, P. K.; Xiong, J.; Tian, Y.; Arata, C.; Weber, R. J.; Nazaroff, W. W.; Goldstein, A. H. Characterizing sources and emissions of volatile organic compounds in a northern California residence using space- and time-resolved measurements. *Indoor Air* **2019**, *29* (4), 630−644.
(14) Coggon, M. M.; Veres, P. R.; Yuan, B.; Koss, A.; Warneke, C.; Gilman, J. B.; Lerner, B. M.; Peischl, J.; Aikin, K. C.; Stockwell, C. E.; et al. Emissions of nitrogen-containing organic compounds from the burning of herbaceous and arboraceous biomass: Fuel composition dependence and the variability of commonly used nitrile tracers. *Geophys. Res. Lett.* **2016**, *43* (18), 9903−9912.
(15) Liang, Y.; Weber, R. J.; Misztal, P. K.; Jen, C. N.; Goldstein, A. H. Aging of volatile organic compounds in October 2017 northern California wildfire plumes. *Environ. Sci. Technol.* **2022**, *56* (3), 1557−1567.
(16) Rickly, P. S.; Coggon, M. M.; Aikin, K. C.; Alvarez, R. J.; Baidar, S.; Gilman, J. B.; Gkatzelis, G. I.; Harkings, C.; He, J.; Lamplugh, A.; et al. Influence of Wildfire on Urban Ozone: An Observationally-Constrained Box Modeling Study at a Site in the Colorado Front Range. *Environ. Sci. Technol.* **2023**, *57*, 1257−1267.
(17) Collard, F.-X.; Blin, J. A review on pyrolysis of biomass constituents: Mechanisms and composition of the products obtained from the conversion of cellulose, hemicelluloses and lignin. *Renew. Sust. Energy Rev.* **2014**, *38*, 594−608.
(18) Wang, Q.; Song, H.; Pan, S.; Dong, N.; Wang, X.; Sun, S. Initial pyrolysis mechanism and product formation of cellulose: An experimental and density functional theory (DFT) study. *Sci. Rep.* **2020**, *10* (1), 3626.
(19) Jones, M. W.; Abatzoglou, J. T.; Veraverbeke, S.; Andela, N.; Lasslop, G.; Forkel, M.; Smith, A. J. P.; Burton, C.; Betts, R. A.; van der Werf, G. R.; et al. Global and regional trends and drivers of fire under climate change. *Rev. Geophys.* **2022**, *60* (3), No. e2020RG000726.
(20) Bourgeois, I.; Peischl, J.; Neuman, J. A.; Brown, S. S.; Thompson, C. R.; Aikin, K. C.; Allen, H. M.; Angot, H.; Apel, E. C.; Baublitz, C. B.; et al. Large contribution of biomass burning emissions to ozone throughout the global remote troposphere. *Proc. Natl. Acad. Sci. U. S. A.* **2021**, *118* (52), No. e2109628118.
(21) Gilman, J. B.; Lerner, B. M.; Kuster, W. C.; Goldan, P. D.; Warneke, C.; Veres, P. R.; Roberts, J. M.; de Gouw, J. A.; Burling, I. R.; Yokelson, R. J. Biomass burning emissions and potential air quality impacts of volatile organic compounds and other trace gases from fuels common in the US. *Atmos. Chem. Phys.* **2015**, *15* (24), 13915−13938.
(22) Hatch, L. E.; Luo, W.; Pankow, J. F.; Yokelson, R. J.; Stockwell, C. E.; Barsanti, K. C. Identification and quantification of gaseous organic compounds emitted from biomass burning using two-dimensional gas chromatography−time-of-flight mass spectrometry. *Atmos. Chem. Phys.* **2015**, *15* (4), 1865−1899.
(23) Hatch, L. E.; Yokelson, R. J.; Stockwell, C. E.; Veres, P. R.; Simpson, I. J.; Blake, D. R.; Orlando, J. J.; Barsanti, K. C. Multi-instrument comparison and compilation of non-methane organic gas emissions from biomass burning and implications for smoke-derived secondary organic aerosol precursors. *Atmos. Chem. Phys.* **2017**, *17* (2), 1471−1489.
(24) Koss, A. R.; Sekimoto, K.; Gilman, J. B.; Selimovic, V.; Coggon, M. M.; Zarzana, K. J.; Yuan, B.; Lerner, B. M.; Brown, S. S.; Jimenez, J. L.; et al. Non-methane organic gas emissions from biomass burning: identification, quantification, and emission factors from PTR-ToF during the FIREX 2016 laboratory experiment. *Atmos. Chem. Phys.* **2018**, *18* (5), 3299−3319.
(25) Calvert, J. G.; Atkinson, R.; Becker, K. H.; Kamens, R. M.; Seinfeld, J. H.; Wallington, T. H.; Yarwood, G. *The Mechanisms of Atmospheric Oxidation of the Aromatic Hydrocarbons*; Oxford University Press, 2002. DOI: 10.1093/oso/9780195146288.001.0001.
(26) Mellouki, A.; Wallington, T. J.; Chen, J. Atmospheric chemistry of oxygenated volatile organic compounds: impacts on air quality and climate. *Chem. Rev.* **2015**, *115* (10), 3984−4014.
(27) Calvert, J. G.; Mellouki, A.; Orlando, J. J.; Pilling, M.; Wallington, T. J. *Mechanisms of Atmospheric Oxidation of the Oxygenates*; Oxford University Press, 2011. DOI: 10.1093/oso/9780199767076.001.0001.
(28) Fuentes, J. D.; Lerdau, M.; Atkinson, R.; Baldocchi, D.; Bottenheim, J. W.; Ciccioli, P.; Lamb, B.; Geron, C.; Gu, L.; Guenther, A.; et al. Biogenic hydrocarbons in the atmospheric boundary layer a review. *Bull. Am. Meterol. Soc.* **2000**, *81* (7), 1537−1575.
(29) Wennberg, P. O.; Bates, K. H.; Crounse, J. D.; Dodson, L. G.; McVay, R. C.; Mertens, L. A.; Nguyen, T. B.; Praske, E.; Schwantes, R. H.; Smarte, M. D.; et al. Gas-phase reactions of isoprene and its major oxidation products. *Chem. Rev.* **2018**, *118* (7), 3337−3390.
(30) Decker, Z. C. J.; Robinson, M. A.; Barsanti, K. C.; Bourgeois, I.; Coggon, M. M.; DiGangi, J. P.; Diskin, G. S.; Flocke, F. M.; Franchin, A.; Fredrickson, C. D.; et al. Nighttime and daytime dark oxidation chemistry in wildfire plumes: an observation and model analysis of FIREX-AQ aircraft data. *Atmos. Chem. Phys.* **2021**, *21* (21), 16293−16317.
(31) Coggon, M. M.; Lim, C. Y.; Koss, A. R.; Sekimoto, K.; Yuan, B.; Gilman, J. B.; Hagan, D. H.; Selimovic, V.; Zarzana, K. J.; Brown, S. S.; et al. OH chemistry of non-methane organic gases (NMOGs) emitted from laboratory and ambient biomass burning smoke: evaluating the influence of furans and oxygenated aromatics on ozone and secondary NMOG formation. *Atmos. Chem. Phys.* **2019**, *19* (23), 14875−14899.
(32) Müller, M.; Anderson, B. E.; Beyersdorf, A. J.; Crawford, J. H.; Diskin, G. S.; Eichler, P.; Fried, A.; Keutsch, F. N.; Mikoviny, T.; Thornhill, K. L.; et al. In situ measurements and modeling of reactive trace gases in a small biomass burning plume. *Atmos. Chem. Phys.* **2016**, *16* (6), 3813−3824.
(33) Burling, I. R.; Yokelson, R. J.; Griffith, D. W. T.; Johnson, T. J.; Veres, P.; Roberts, J. M.; Warneke, C.; Urbanski, S. P.; Reardon, J.; Weise, D. R.; et al. Laboratory measurements of trace gas emissions from biomass burning of fuel types from the southeastern and southwestern United States. *Atmos. Chem. Phys.* **2010**, *10* (22), 11115−11130.

(34) Yokelson, R. J.; Burling, I. R.; Urbanski, S. P.; Atlas, E. L.; Adachi, K.; Buseck, P. R.; Wiedinmyer, C.; Akagi, S. K.; Toohey, D. W.; Wold, C. E. Trace gas and particle emissions from open biomass burning in Mexico. *Atmos. Chem. Phys.* **2011**, *11* (14), 6787−6808.
(35) Sekimoto, K.; Koss, A. R.; Gilman, J. B.; Selimovic, V.; Coggon, M. M.; Zarzana, K. J.; Yuan, B.; Lerner, B. M.; Brown, S. S.; Warneke, C.; et al. High- and low-temperature pyrolysis profiles describe volatile organic compound emissions from western US wildfire fuels. *Atmos. Chem. Phys.* **2018**, *18* (13), 9263−9281.
(36) Roberts, J. M.; Stockwell, C. E.; Yokelson, R. J.; de Gouw, J.; Liu, Y.; Selimovic, V.; Koss, A. R.; Sekimoto, K.; Coggon, M. M.; Yuan, B.; et al. The nitrogen budget of laboratory-simulated western US wildfires during the FIREX 2016 Fire Lab study. *Atmos. Chem. Phys.* **2020**, *20* (14), 8807−8826.
(37) Ohlemiller, T. J. Modeling of smoldering combustion propagation. *Prog. Energy Combust. Sci.* **1985**, *11* (4), 277−310.
(38) Rein, G. Smoldering combustion. In *SFPE Handbook of Fire Protection Engineering*, 5th ed.; Hurley, M. J., Gottuk, D., Hall, J. R., Harada, K., Kuligowski, E., Puchovsky, M., Torero, J., Watts, J. M., Wieczorek, C., Eds.; Springer: New York, 2016; pp 581−603. DOI: 10.1007/978-1-4939-2565-0_19.
(39) Mettler, M. S.; Mushrif, S. H.; Paulsen, A. D.; Javadekar, A. D.; Vlachos, D. G.; Dauenhauer, P. J. Revealing pyrolysis chemistry for biofuels production: Conversion of cellulose to furans and small oxygenates. *Energy Environ. Sci.* **2012**, *5* (1), 5414−5424.
(40) Lin, Y.-C.; Cho, J.; Tompsett, G. A.; Westmoreland, P. R.; Huber, G. W. Kinetics and mechanism of cellulose pyrolysis. *J. Phys. Chem. C* **2009**, *113* (46), 20097−20107.
(41) Yang, H.; Li, S.; Liu, B.; Chen, Y.; Xiao, J.; Dong, Z.; Gong, M.; Chen, H. Hemicellulose pyrolysis mechanism based on functional group evolutions by two-dimensional perturbation correlation infrared spectroscopy. *Fuel* **2020**, *267*, No. 117302.
(42) Yang, X.; Zhao, Y.; Li, W.; Li, R.; Wu, Y. Unveiling the pyrolysis mechanisms of hemicellulose: experimental and theoretical studies. *Energy Fuels* **2019**, *33* (5), 4352−4360.
(43) Zhou, X.; Li, W.; Mabon, R.; Broadbelt, L. J. A mechanistic model of fast pyrolysis of hemicellulose. *Energy Environ. Sci.* **2018**, *11* (5), 1240−1260.
(44) Ferdous, D.; Dalai, A. K.; Bej, S. K.; Thring, R. W. Pyrolysis of Lignins: experimental and kinetics studies. *Energy Fuels* **2002**, *16* (6), 1405−1412.
(45) Kawamoto, H. Lignin pyrolysis reactions. *J. Wood Sci.* **2017**, *63* (2), 117−132.
(46) Zhan, S.; Chenguang, W.; Kang, B.; Xinghua, Z.; Chiling, Y.; Renjie, D.; Longlong, M.; Changle, P. Py-GC/MS study of lignin pyrolysis and effect of catalysts on product distribution. *Int. J. Agric. Biol. Eng.* **2017**, *10* (5), 214−225.
(47) Jiang, G.; Nowakowski, D. J.; Bridgwater, A. V. Effect of the temperature on the composition of lignin pyrolysis products. *Energy Fuels* **2010**, *24* (8), 4470−4475.
(48) Leng, E.; Guo, Y.; Chen, J.; Liu, S.; E, J.; Xue, Y. A comprehensive review on lignin pyrolysis: Mechanism, modeling and the effects of inherent metals in biomass. *Fuel* **2022**, *309*, No. 122102.
(49) Mu, W.; Ben, H.; Ragauskas, A.; Deng, Y. Lignin pyrolysis components and upgrading—technology review. *Bioenergy Res.* **2013**, *6* (4), 1183−1204.
(50) Usino, D. O.; Ylitervo, P.; Moreno, A.; Sipponen, M. H.; Richards, T. Primary interactions of biomass components during fast pyrolysis. *J. Anal. Appl. Pyrolysis* **2021**, *159*, No. 105297.
(51) Couhert, C.; Commandre, J.-M.; Salvador, S. Is it possible to predict gas yields of any biomass after rapid pyrolysis at high temperature from its composition in cellulose, hemicellulose and lignin? *Fuel* **2009**, *88* (3), 408−417.
(52) Worasuwannarak, N.; Sonobe, T.; Tanthapanichakoon, W. Pyrolysis behaviors of rice straw, rice husk, and corncob by TG-MS technique. *J. Anal. Appl. Pyrolysis* **2007**, *78* (2), 265−271.
(53) Wang, S.; Guo, X.; Wang, K.; Luo, Z. Influence of the interaction of components on the pyrolysis behavior of biomass. *J. Anal. Appl. Pyrolysis* **2011**, *91* (1), 183−189.
(54) Carpenter, D.; Westover, T. L.; Czernik, S.; Jablonski, W. Biomass feedstocks for renewable fuel production: a review of the impacts of feedstock and pretreatment on the yield and product distribution of fast pyrolysis bio-oils and vapors. *Green Chem.* **2014**, *16* (2), 384−406.
(55) Lê Thành, K.; Commandré, J.-M.; Valette, J.; Volle, G.; Meyer, M. Detailed identification and quantification of the condensable species released during torrefaction of lignocellulosic biomasses. *Fuel Process. Technol.* **2015**, *139*, 226−235.
(56) Tran, L. S.; Herbinet, O.; Carstensen, H. H.; Battin-Leclerc, F. Chemical kinetics of cyclic ethers in combustion. *Prog. Energy Combust. Sci.* **2022**, *92*, 101019.
(57) Chen, B. J.; Liu, P.; Li, Z. P.; Hansen, N.; Roberts, W. L.; Pitsch, H. Furan formation pathways exploration in low temperature oxidation of 1,3-butadiene, trans-2-butene, and cis-2-butene. *Combust. Flame* **2021**, *232*, 111519.
(58) Suzuki, S.; Kiuchi, S.; Kinoshita, K.; Takeda, Y.; Sakaida, S.; Konno, M.; Tanaka, K.; Oguma, M. Formation of polycyclic aromatic hydrocarbons, benzofuran, and dibenzofuran in fuel-rich oxidation of toluene using a flow reactor. *Phys. Chem. Chem. Phys.* **2021**, *23* (11), 6509−6525.
(59) Dagaut, P.; Reuillon, M.; Cathonnet, M.; Presvots, D. Gas-Chromatography and Mass-Spectrometry Identification of Cyclic Ethers Formed from Reference Fuels Combustion. *Chromatographia* **1995**, *40* (3−4), 147−154.
(60) Dagaut, P.; Reuillon, M.; Cathonnet, M. High-pressure oxidation of liquid fuels from low to high-temperature. 2. mixtures of n-heptane and isooctane. *Combust. Sci. Technol.* **1994**, *103* (1−6), 315−336.
(61) Dagaut, P.; Reuillon, M.; Cathonnet, M. High-pressure oxidation of liquid fuels from low to high-temperature. 3. n-decane. *Combust. Sci. Technol.* **1994**, *103* (1−6), 349−359.
(62) Dagaut, P.; Cathonnet, M.; McGuinness, M.; Simmie, J. M. The ignition of oxetane in shock waves and oxidation in a jet-stirred reactor: An experimental and kinetic modeling study. *Combust. Flame* **1997**, *110* (4), 409−417.
(63) Dagaut, P.; McGuinness, M.; Simmie, J. M.; Cathonnet, M. The ignition and oxidation of tetrahydropyran: Experiments and kinetic modeling. *Combust. Sci. Technol.* **1997**, *129* (1−6), 1−16.
(64) Dagaut, P.; McGuinness, M.; Simmie, J. M.; Cathonnet, M. The ignition and oxidation of tetrahydrofuran. Experiments and kinetic modeling. *Combust. Sci. Technol.* **1998**, *135* (1−6), 3−29.
(65) Wurmel, J.; McGuinness, M.; Simmie, J. M. High-temperature oxidation of ethylene oxide in shock waves. *J. Chem. Soc. Faraday Trans.* **1996**, *92* (5), 715−721.
(66) Rotavera, B.; Taatjes, C. A. Influence of functional groups on low-temperature combustion chemistry of biofuels. *Prog. Energy Combust. Sci.* **2021**, *86*, No. 100925.
(67) Gschwend, D.; Soltic, P.; Wokaun, A.; Vogel, F. Review and performance evaluation of fifty alternative liquid fuels for spark-ignition engines. *Energy Fuels* **2019**, *33* (3), 2186−2196.
(68) Pinheiro Pires, A. P.; Arauzo, J.; Fonts, I.; Domine, M. E.; Fernández Arroyo, A.; Garcia-Perez, M. E.; Montoya, J.; Chejne, F.; Pfromm, P.; Garcia-Perez, M. Challenges and opportunities for bio-oil refining: A review. *Energy Fuels* **2019**, *33* (6), 4683−4720.
(69) Yokelson, R. J.; Susott, R.; Ward, D. E.; Reardon, J.; Griffith, D. W. T. Emissions from smoldering combustion of biomass measured by open-path Fourier transform infrared spectroscopy. *J. Geophys. Res. Atmos.* **1997**, *102* (D15), 18865−18877.
(70) Christian, T. J.; Kleiss, B.; Yokelson, R. J.; Holzinger, R.; Crutzen, P. J.; Hao, W. M.; Saharjo, B. H.; Ward, D. E. Comprehensive laboratory measurements of biomass-burning emissions: 1. Emissions from Indonesian, African, and other fuels. *J. Geophys. Res. Atmos.* **2003**, *108* (D23), 4719.
(71) Yokelson, R. J.; Burling, I. R.; Gilman, J. B.; Warneke, C.; Stockwell, C. E.; de Gouw, J.; Akagi, S. K.; Urbanski, S. P.; Veres, P.; Roberts, J. M.; et al. Coupling field and laboratory measurements to estimate the emission factors of identified and unidentified trace gases for prescribed fires. *Atmos. Chem. Phys.* **2013**, *13* (1), 89−116.

(72) Gkatzelis, G. I.; Coggon, M. M.; Stockwell, C. E.; Hornbrook, R. S.; Allen, H.; Apel, E. C.; Bela, M. M.; Blake, D. R.; Bourgeois, I.; Brown, S. S.; et al. Parameterizations of US wildfire and prescribed fire emission ratios and emission factors based on FIREX-AQ aircraft measurements. *Atmos. Chem. Phys.* **2024**, *24*, 929−956.
(73) Scharko, N. K.; Oeck, A. M.; Myers, T. L.; Tonkyn, R. G.; Banach, C. A.; Baker, S. P.; Lincoln, E. N.; Chong, J.; Corcoran, B. M.; Burke, G. M.; et al. Gas-phase pyrolysis products emitted by prescribed fires in pine forests with a shrub understory in the southeastern United States. *Atmos. Chem. Phys.* **2019**, *19* (15), 9681−9698.
(74) Hatch, L. E.; Rivas-Ubach, A.; Jen, C. N.; Lipton, M.; Goldstein, A. H.; Barsanti, K. C. Measurements of I/SVOCs in biomass-burning smoke using solid-phase extraction disks and two-dimensional gas chromatography. *Atmos. Chem. Phys.* **2018**, *18* (24), 17801−17817.
(75) Akagi, S. K.; Burling, I. R.; Mendoza, A.; Johnson, T. J.; Cameron, M.; Griffith, D. W. T.; Paton-Walsh, C.; Weise, D. R.; Reardon, J.; Yokelson, R. J. Field measurements of trace gases emitted by prescribed fires in southeastern US pine forests using an open-path FTIR system. *Atmos. Chem. Phys.* **2014**, *14* (1), 199−215.
(76) Akagi, S. K.; Yokelson, R. J.; Burling, I. R.; Meinardi, S.; Simpson, I.; Blake, D. R.; McMeeking, G. R.; Sullivan, A.; Lee, T.; Kreidenweis, S.; et al. Measurements of reactive trace gases and variable O_3 formation rates in some South Carolina biomass burning plumes. *Atmos. Chem. Phys.* **2013**, *13* (3), 1141−1165.
(77) Bertschi, I. T.; Yokelson, R. J.; Ward, D. E.; Christian, T. J.; Hao, W. M. Trace gas emissions from the production and use of domestic biofuels in Zambia measured by open-path Fourier transform infrared spectroscopy. *J. Geophys. Res.: Atmos.* **2003**, *108* (D13), 8469.
(78) Burling, I. R.; Yokelson, R. J.; Akagi, S. K.; Urbanski, S. P.; Wold, C. E.; Griffith, D. W. T.; Johnson, T. J.; Reardon, J.; Weise, D. R. Airborne and ground-based measurements of the trace gases and particles emitted by prescribed fires in the United States. *Atmos. Chem. Phys.* **2011**, *11* (23), 12197−12216.
(79) Christian, T. J.; Yokelson, R. J.; Carvalho, J. A.; Griffith, D. W. T.; Alvarado, E. C.; Santos, J. C.; Neto, T. G. S.; Veras, C. A. G.; Hao, W. M. The tropical forest and fire emissions experiment: Trace gases emitted by smoldering logs and dung from deforestation and pasture fires in Brazil. *J. Geophys. Res.: Atmos.* **2007**, *112* (D18), 308.
(80) Ciccioli, P.; Brancaleoni, E.; Frattoni, M.; Cecinato, A.; Pinciarelli, L. Determination of volatile organic compounds (VOC) emitted from biomass burning of mediterranean vegetation species by GC-MS. *Anal. Lett.* **2001**, *34* (6), 937−955.
(81) Friedli, H. R.; Atlas, E.; Stroud, V. R.; Giovanni, L.; Campos, T.; Radke, L. F. Volatile organic trace gases emitted from north American wildfires. *Global Biogeochem. Cycles* **2001**, *15* (2), 435−452.
(82) Greenberg, J. P.; Zimmerman, P. R.; Heidt, L.; Pollock, W. Hydrocarbon and carbon monoxide emissions from biomass burning in Brazil. *J. Geophys. Res. Atmos.* **1984**, *89* (D1), 1350−1354.
(83) Liu, X.; Huey, L. G.; Yokelson, R. J.; Selimovic, V.; Simpson, I. J.; Müller, M.; Jimenez, J. L.; Campuzano-Jost, P.; Beyersdorf, A. J.; Blake, D. R.; et al. Airborne measurements of western U.S. wildfire emissions: Comparison with prescribed burning and air quality implications. *J. Geophys. Res. Atmos.* **2017**, *122* (11), 6108−6129.
(84) Liu, X.; Zhang, Y.; Huey, L. G.; Yokelson, R. J.; Wang, Y.; Jimenez, J. L.; Campuzano-Jost, P.; Beyersdorf, A. J.; Blake, D. R.; Choi, Y.; et al. Agricultural fires in the southeastern U.S. during SEAC4RS: Emissions of trace gases and particles and evolution of ozone, reactive nitrogen, and organic aerosol. *J. Geophys. Res. Atmos.* **2016**, *121* (12), 7383−7414.
(85) McDonald, J. D.; Zielinska, B.; Fujita, E. M.; Sagebiel, J. C.; Chow, J. C.; Watson, J. G. Fine particle and gaseous emission rates from residential wood combustion. *Environ. Sci. Technol.* **2000**, *34* (11), 2080−2091.
(86) Permar, W.; Wang, Q.; Selimovic, V.; Wielgasz, C.; Yokelson, R. J.; Hornbrook, R. S.; Hills, A. J.; Apel, E. C.; Ku, I.-T.; Zhou, Y.; et al. Emissions of trace organic gases from western U.S. wildfires based on WE-CAN Aircraft measurements. *J. Geophys. Res. Atmos.* **2021**, *126* (11), No. e2020JD033838.
(87) Simpson, I. J.; Akagi, S. K.; Barletta, B.; Blake, N. J.; Choi, Y.; Diskin, G. S.; Fried, A.; Fuelberg, H. E.; Meinardi, S.; Rowland, F. S.; et al. Boreal forest fire emissions in fresh Canadian smoke plumes: C_1-C_{10} volatile organic compounds (VOCs), CO_2, CO, NO_2, NO, HCN and CH_3CN. *Atmos. Chem. Phys.* **2011**, *11* (13), 6445−6463.
(88) Stockwell, C. E.; Christian, T. J.; Goetz, J. D.; Jayarathne, T.; Bhave, P. V.; Praveen, P. S.; Adhikari, S.; Maharjan, R.; DeCarlo, P. F.; Stone, E. A.; et al. Nepal Ambient Monitoring and Source Testing Experiment (NAMaSTE): emissions of trace gases and light-absorbing carbon from wood and dung cooking fires, garbage and crop residue burning, brick kilns, and other sources. *Atmos. Chem. Phys.* **2016**, *16* (17), 11043−11081.
(89) Stockwell, C. E.; Jayarathne, T.; Cochrane, M. A.; Ryan, K. C.; Putra, E. I.; Saharjo, B. H.; Nurhayati, A. D.; Albar, I.; Blake, D. R.; Simpson, I. J.; et al. Field measurements of trace gases and aerosols emitted by peat fires in Central Kalimantan, Indonesia, during the 2015 El Niño. *Atmos. Chem. Phys.* **2016**, *16* (18), 11711−11732.
(90) Stockwell, C. E.; Veres, P. R.; Williams, J.; Yokelson, R. J. Characterization of biomass burning emissions from cooking fires, peat, crop residue, and other fuels with high-resolution proton-transfer-reaction time-of-flight mass spectrometry. *Atmos. Chem. Phys.* **2015**, *15* (2), 845−865.
(91) Wang, S.; Wei, W.; Du, L.; Li, G.; Hao, J. Characteristics of gaseous pollutants from biofuel-stoves in rural China. *Atmos. Environ.* **2009**, *43* (27), 4148−4154.
(92) Yokelson, R. J.; Christian, T. J.; Karl, T. G.; Guenther, A. The tropical forest and fire emissions experiment: laboratory fire measurements and synthesis of campaign data. *Atmos. Chem. Phys.* **2008**, *8* (13), 3509−3527.
(93) Yokelson, R. J.; Saharjo, B. H.; Stockwell, C. E.; Putra, E. I.; Jayarathne, T.; Akbar, A.; Albar, I.; Blake, D. R.; Graham, L. L. B.; Kurniawan, A.; et al. Tropical peat fire emissions: 2019 field measurements in Sumatra and Borneo and synthesis with previous studies. *Atmos. Chem. Phys.* **2022**, *22* (15), 10173−10194.
(94) Hayden, K. L.; Li, S. M.; Liggio, J.; Wheeler, M. J.; Wentzell, J. J. B.; Leithead, A.; Brickell, P.; Mittermeier, R. L.; Oldham, Z.; Mihele, C. M.; et al. Reconciling the total carbon budget for boreal forest wildfire emissions using airborne observations. *Atmos. Chem. Phys.* **2022**, *22* (18), 12493−12523.
(95) Travis, K. R.; Crawford, J. H.; Soja, A. J.; Gargulinski, E. M.; Moore, R. H.; Wiggins, E. B.; Diskin, G. S.; DiGangi, J. P.; Nowak, J. B.; Halliday, H.; et al. Emission Factors for Crop Residue and Prescribed Fires in the Eastern US During FIREX-AQ. *Journal of Geophysical Research: Atmospheres* **2023**, *128* (18), No. e2023JD039309.
(96) Koppmann, R.; Khedim, A.; Rudolph, J.; Poppe, D.; Andreae, M. O.; Helas, G.; Welling, M.; Zenker, T. Emissions of organic trace gases from savanna fires in southern Africa during the 1992 Southern African Fire Atmosphere Research Initiative and their impact on the formation of tropospheric ozone. *J. Geophys. Res. Atmos.* **1997**, *102* (D15), 18879−18888.
(97) Evtyugina, M.; Alves, C.; Calvo, A.; Nunes, T.; Tarelho, L.; Duarte, M.; Prozil, S. O.; Evtuguin, D. V.; Pio, C. VOC emissions from residential combustion of Southern and mid-European woods. *Atmos. Environ.* **2014**, *83*, 90−98.
(98) Evtyugina, M.; Calvo, A. I.; Nunes, T.; Alves, C.; Fernandes, A. P.; Tarelho, L.; Vicente, A.; Pio, C. VOC emissions of smouldering combustion from Mediterranean wildfires in central Portugal. *Atmos. Environ.* **2013**, *64*, 339−348.
(99) Selimovic, V.; Yokelson, R. J.; Warneke, C.; Roberts, J. M.; de Gouw, J.; Reardon, J.; Griffith, D. W. T. Aerosol optical properties and trace gas emissions by PAX and OP-FTIR for laboratory-simulated western US wildfires during FIREX. *Atmos. Chem. Phys.* **2018**, *18* (4), 2929−2948.
(100) Sekimoto, K.; Li, S.-M.; Yuan, B.; Koss, A.; Coggon, M.; Warneke, C.; de Gouw, J. Calculation of the sensitivity of proton-transfer-reaction mass spectrometry (PTR-MS) for organic trace gases using molecular properties. *Int. J. Mass Spectrom.* **2017**, *421*, 71−94.

(101) Seiler, W.; Crutzen, P. J. Estimates of gross and net fluxes of carbon between the biosphere and the atmosphere from biomass burning. *Clim. Change* **1980**, *2* (3), 207−247.
(102) van der Werf, G. R.; Randerson, J. T.; Giglio, L.; Collatz, G. J.; Mu, M.; Kasibhatla, P. S.; Morton, D. C.; DeFries, R. S.; Jin, Y.; van Leeuwen, T. T. Global fire emissions and the contribution of deforestation, savanna, forest, agricultural, and peat fires (1997−2009). *Atmos. Chem. Phys.* **2010**, *10* (23), 11707−11735.
(103) van der Werf, G. R.; Randerson, J. T.; Giglio, L.; van Leeuwen, T. T.; Chen, Y.; Rogers, B. M.; Mu, M.; van Marle, M. J. E.; Morton, D. C.; Collatz, G. J.; et al. Global fire emissions estimates during 1997−2016. *Earth Syst. Sci. Data* **2017**, *9* (2), 697−720.
(104) Pan, X.; Ichoku, C.; Chin, M.; Bian, H.; Darmenov, A.; Colarco, P.; Ellison, L.; Kucsera, T.; da Silva, A.; Wang, J.; et al. Six global biomass burning emission datasets: intercomparison and application in one global aerosol model. *Atmos. Chem. Phys.* **2020**, *20* (2), 969−994.
(105) Stockwell, C. E.; Bela, M. M.; Coggon, M. M.; Gkatzelis, G. I.; Wiggins, E.; Gargulinski, E. M.; Shingler, T.; Fenn, M.; Griffin, D.; Holmes, C. D.; et al. Airborne emission rate measurements validate remote sensing observations and emission inventories of western U.S. wildfires. *Environ. Sci. Technol.* **2022**, *56* (12), 7564−7577.
(106) Jin, L.; Permar, W.; Selimovic, V.; Ketcherside, D.; Yokelson, R. J.; Hornbrook, R. S.; Apel, E. C.; Ku, I. T.; Collett Jr, J. L.; Sullivan, A. P.; et al. Constraining emissions of volatile organic compounds from western US wildfires with WE-CAN and FIREX-AQ airborne observations. *Atmos. Chem. Phys.* **2023**, *23* (10), 5969−5991.
(107) Cabrera-Perez, D.; Taraborrelli, D.; Sander, R.; Pozzer, A. Global atmospheric budget of simple monocyclic aromatic compounds. *Atmos. Chem. Phys.* **2016**, *16* (11), 6931−6947.
(108) Porter, W. C.; Safieddine, S. A.; Heald, C. L. Impact of aromatics and monoterpenes on simulated tropospheric ozone and total OH reactivity. *Atmos. Environ.* **2017**, *169*, 250−257.
(109) van Wees, D.; van der Werf, G. R.; Randerson, J. T.; Rogers, B. M.; Chen, Y.; Veraverbeke, S.; Giglio, L.; Morton, D. C. Global biomass burning fuel consumption and emissions at 500 m spatial resolution based on the Global Fire Emissions Database (GFED). *Geosci. Model Dev.* **2022**, *15* (22), 8411−8437.
(110) Winer, A. M.; Lloyd, A. C.; Darnall, K. R.; Atkinson, R.; Pitts, J. N. Rate constants for the reaction of OH radicals with n-propyl acetate, sec-butyl acetate, tetrahydrofuran and peroxyacetyl nitrate. *Chem. Phys. Lett.* **1977**, *51* (2), 221−226.
(111) Ravishankara, A. R.; Davis, D. D. Kinetic rate constants for the reaction of OH with methanol, ethanol, and tetrahydrofuran at 298 K. *J. Phys. Chem.* **1978**, *82* (26), 2852−2853.
(112) Wallington, T. J.; Dagaut, P.; Liu, R.; Kurylo, M. J. The gas phase reactions of hydroxyl radicals with a series of esters over the temperature range 240−440 K. *Int. J. Chem. Kinet.* **1988**, *20* (2), 177−186.
(113) Moriarty, J.; Sidebottom, H.; Wenger, J.; Mellouki, A.; Le Bras, G. Kinetic studies on the reactions of hydroxyl radicals with cyclic ethers and aliphatic diethers. *J. Phys. Chem. A* **2003**, *107* (10), 1499−1505.
(114) Giri, B. R.; Khaled, F.; Szori, M.; Viskolcz, B.; Farooq, A. An experimental and theoretical kinetic study of the reaction of OH radicals with tetrahydrofuran. *Proc. Combust. Inst.* **2017**, *36* (1), 143−150.
(115) Illés, Á.; Rózsa, Z. B.; Thangaraj, R.; Décsiné Gombos, E.; Dóbé, S.; Giri, B. R.; Szőri, M. An experimental and theoretical kinetic study of the reactions of hydroxyl radicals with tetrahydrofuran and two deuterated tetrahydrofurans. *Chem. Phys. Lett.* **2021**, *776*, 138698.
(116) Lee, J. H.; Tang, I. N. Absolute rate constants for the hydroxyl radical reactions with ethane, furan, and thiophene at room temperature. *J. Chem. Phys.* **1982**, *77* (9), 4459−4463.
(117) Atkinson, R.; Aschmann, S. M.; Carter, W. P. L. Kinetics of the reactions of O_3 and OH radicals with furan and thiophene at 298 ± 2 K. *Int. J. Chem. Kinet.* **1983**, *15* (1), 51−61.
(118) Wine, P. H.; Thompson, R. J. Kinetics of OH reactions with furan, thiophene, and tetrahydrothiophene. *Int. J. Chem. Kinet.* **1984**, *16* (7), 867−878.
(119) Bierbach, A.; Barnes, I.; Becker, K. H. Rate coefficients for the gas-phase reactions of hydroxyl radicals with furan, 2-methylfuran, 2-ethylfuran and 2,5-dimethylfuran at 300 ± 2 K. *Atmos. Environ.* **1992**, *26* (5), 813−817.
(120) Elwardany, A.; Es-sebbar, E.; Khaled, F.; Farooq, A. A chemical kinetic study of the reaction of hydroxyl with furans. *Fuel* **2016**, *166*, 245−252.
(121) Whelan, C. A.; Eble, J.; Mir, Z. S.; Blitz, M. A.; Seakins, P. W.; Olzmann, M.; Stone, D. Kinetics of the reactions of hydroxyl radicals with furan and its alkylated derivatives 2-methyl furan and 2,5-dimethyl furan. *J. Phys. Chem. A* **2020**, *124* (37), 7416−7426.
(122) Angelaki, M. E.; Romanias, M. N.; Burkholder, J. B.; Papadimitriou, V. C. Rate coefficients for the gas-phase OH + furan (C_4H_4O) reaction between 273 and 353 K. *Int. J. Chem. Kinet.* **2024**, *56* (3), 119−130.
(123) Aschmann, S. M.; Nishino, N.; Arey, J.; Atkinson, R. Kinetics of the Reactions of OH Radicals with 2- and 3-Methylfuran, 2,3- and 2,5-Dimethylfuran, and E- and Z-3-Hexene-2,5-dione, and Products of OH + 2,5-Dimethylfuran. *Environ. Sci. Technol.* **2011**, *45*, 1859−1865.
(124) Eble, J.; Bänsch, C.; Olzmann, M. Kinetic Investigation of the Reactions of 2,5-Dimethylfuran and 2-Methylfuran with Hydroxyl Radicals. *Proceedings of the European Combustion Meeting*, Budapest, Hungary, March 30−April 2, 2015; The Combustion Institute, 2015; pp 2−5.
(125) Tapia, A.; Villanueva, F.; Salgado, M. S.; Cabañas, B.; Martínez, E.; Martín, P. Atmospheric degradation of 3-methylfuran: Kinetic and products study. *Atmos. Chem. Phys.* **2011**, *11* (7), 3227−3241.
(126) Liljegren, J. A.; Stevens, P. S. Measurements of the kinetics of the reaction of oh radicals with 3-methylfuran at low pressure. *Int. J. Chem. Kinet.* **2013**, *45* (12), 785−794.
(127) Bierbach, A.; Barnes, I.; Becker, K. H. Product and kinetic study of the OH-initiated gas-phase oxidation of furan, 2-methylfuran and furanaldehydes at ≈ 300 K. *Atmos. Environ.* **1995**, *29* (19), 2651−2660.
(128) Bierbach, A.; Barnes, I.; Becker, K. H.; Wiesen, E. Atmospherlc chemistry of unsaturated carbonyls: Butenedial, 4-oxo-2-pentena1, 3-hexene-2,5-dione, maleic anhydride, 3H-furan-2-one, and 5-methy1-3H-furan-2-one. *Environ. Sci. Technol.* **1994**, *28*, 715−729.
(129) Chattopadhyay, A.; Papadimitriou, V. C.; Marshall, P.; Burkholder, J. B. Temperature-dependent rate coefficients for the gas-phase OH + furan-2,5-dione ($C_4H_2O_3$, maleic anhydride) reaction. *Int. J. Chem. Kinet.* **2020**, *52* (10), 623−631.
(130) Atkinson, R.; Arey, J.; Tuazon, E. C.; Aschmann, S. M. Gas-phase reactions of 1,4-benzodioxan, 2,3-dihydrobenzofuran, and 2,3-benzofuran with OH radicals and O_3. *Int. J. Chem. Kinet.* **1992**, *24* (4), 345−358.
(131) Calogirou, A.; Jensen, N. R.; Nielsen, C. J.; Kotzias, D.; Hjorth, J. Gas-phase reactions of nopinone, 3-isopropenyl-6-oxo-heptanal, and 5-methyl-5-vinyltetrahydrofuran-2-ol with OH, NO_3, and ozone. *Environ. Sci. Technol.* **1999**, *33* (3), 453−460.
(132) Alwe, H. D.; Walavalkar, M. P.; Sharma, A.; Dhanya, S.; Naik, P. D. Tropospheric oxidation of cyclic unsaturated ethers in the day-time: Comparison of the reactions with Cl, OH and O_3 based on the determination of their rate coefficients at 298 K. *Atmos. Environ.* **2014**, *82*, 113−120.
(133) Atkinson, R. Kinetics of the gas-phase reactions of OH radicals with alkanes and cycloalkanes. *Atmos. Chem. Phys.* **2003**, *3* (6), 2233−2307.
(134) Burkholder, J. B.; Sander, S. P.; Abbatt, J.; Barker, J. R.; Cappa, C.; Crounse, J. D.; Dibble, T. S.; Huie, R. E.; Kolb, C. E.; Kurylo, M. J.; et al. *Chemical Kinetics and Photochemical Data for Use in Atmospheric Studies, Evaluation No. 19*, JPL Publication 19-5; Jet Propulsion Laboratory, Pasadena, CA, USA, 2020; http://jpldataeval.jpl.nasa.gov.
(135) Atkinson, R.; Arey, J. Atmospheric degradation of volatile organic compounds. *Chem. Rev.* **2003**, *103* (12), 4605−4638.
(136) Atkinson, R. Kinetics and mechanisms of the gas-phase reactions of the hydroxyl radical with organic compounds under atmospheric conditions. *Chem. Rev.* **1986**, *86* (1), 69−201.

https://doi.org/10.1021/acsearthspacechem.3c00226
ACS Earth Space Chem. XXXX, XXX, XXX−XXX

(137) Zhao, X.; Wang, L. Atmospheric oxidation mechanism of furfural initiated by hydroxyl radicals. *J. Phys. Chem. A* **2017**, *121* (17), 3247−3253.
(138) Atkinson, R.; Aschmann, S. M.; Pitts, J. N. Rate constants for the gas-phase reactions of the NO_3 radical with a series of organic compounds at 296 ± 2 K. *J. Phys. Chem.* **1988**, *92* (12), 3454−3457.
(139) Cabañas, B.; Baeza, M. T.; Salgado, S.; Martín, P.; Taccone, R.; Martínez, E. Oxidation of heterocycles in the atmosphere: Kinetic study of their reactions with NO_3 radical. *J. Phys. Chem. A* **2004**, *108* (49), 10818−10823.
(140) Atkinson, R.; Aschmann, S. M.; Winer, A. M.; Carter, W. P. L. Rate constants for the gas-phase reactions of NO_3 radicals with furan, thiophene, and pyrrole at 295 ± 1 k and atmospheric pressure. *Environ. Sci. Technol.* **1985**, *19* (1), 87−90.
(141) Kind, I.; Berndt, T.; Boge, O.; Rolle, W. Gas-phase rate constants for the reaction of NO_3 radicals with furan and methyl-substituted furans. *Chem. Phys. Lett.* **1996**, *256*, 679−683.
(142) Newland, M. J.; Ren, Y.; McGillen, M. R.; Michelat, L.; Daële, V.; Mellouki, A. NO_3 chemistry of wildfire emissions: a kinetic study of the gas-phase reactions of furans with the NO_3 radical. *Atmos. Chem. Phys.* **2022**, *22* (3), 1761−1772.
(143) Al Ali, F.; Coeur, C.; Houzel, N.; Bouya, H.; Tomas, A.; Romanias, M. N. Rate coefficients for the gas-phase reactions of nitrate radicals with a series of furan compounds. *J. Phys. Chem. A* **2022**, *126* (46), 8674−8681.
(144) Alvarado, A.; Atkinson, R.; Arey, J. Kinetics of the gas-phase reactions of NO_3 radicals and O_3 with 3-methylfuran and the OH radical yield from the O_3 reaction. *Int. J. Chem. Kinet.* **1996**, *28* (12), 905−909.
(145) Colmenar, I.; Cabañas, B.; Martínez, E.; Salgado, M. S.; Martín, P. Atmospheric fate of a series of furanaldehydes by their NO_3 reactions. *Atmos. Environ.* **2012**, *54* (3), 177−184.
(146) Andersen, C.; Nielsen, O. J.; Østerstrøm, F. F.; Ausmeel, S.; Nilsson, E. J. K.; Sulbaek Andersen, M. P. Atmospheric chemistry of tetrahydrofuran, 2-methyltetrahydrofuran, and 2,5-dimethyltetrahydrofuran: kinetics of reactions with chlorine atoms, OD radicals, and ozone. *J. Phys. Chem. A* **2016**, *120* (37), 7320−7326.
(147) Matsumoto, J. Kinetics of the Reactions of ozone with 2,5-dimethylfuran and its atmospheric implications. *Chem. Lett.* **2011**, *40* (6), 582−583.
(148) Li, M.; Liu, Y.; Wang, L. Gas-phase ozonolysis of furans, methylfurans, and dimethylfurans in the atmosphere. *Phys. Chem. Chem. Phys.* **2018**, *20* (38), 24735−24743.
(149) Alwe, H. D.; Walawalkar, M.; Sharma, A.; Pushpa, K. K.; Dhanya, S.; Naik, P. D. Rate coefficients for the gas-phase reactions of chlorine atoms with cyclic ethers at 298 k. *Int. J. Chem. Kinet.* **2013**, *45* (5), 295−305.
(150) Cabañas, B.; Villanueva, F.; Martín, P.; Baeza, M. T.; Salgado, S.; Jiménez, E. Study of reaction processes of furan and some furan derivatives initiated by Cl atoms. *Atmos. Environ.* **2005**, *39* (10), 1935−1944.
(151) Cabañas, B.; Tapia, A.; Villanueva, F.; Salgado, S.; Monedero, E.; Martín, P. Kinetic study of 2-furanaldehyde, 3-furanaldehyde, and 5-methyl-2-furanaldehyde reactions initiated by Cl atoms. *Int. J. Chem. Kinet.* **2008**, *40* (10), 670−678.
(152) Chattopadhyay, A.; Gierczak, T.; Marshall, P.; Papadimitriou, V. C.; Burkholder, J. B. Kinetic fall-off behavior for the Cl + furan-2,5-dione ($C_4H_2O_3$, maleic anhydride) reaction. *Phys. Chem. Chem. Phys.* **2021**, *23* (8), 4901−4911.
(153) Decker, Z. C. J.; Novak, G. A.; Aikin, K.; Veres, P. R.; Neuman, J. A.; Bourgeois, I.; Bui, T. P.; Campuzano-Jost, P.; Coggon, M. M.; Day, D. A.; et al. Airborne Observations Constrain Heterogeneous Nitrogen and Halogen Chemistry on Tropospheric and Stratospheric Biomass Burning Aerosol. *Geophys. Res. Lett.* **2024**, *51* (4), No. e2023GL107273.
(154) *Tropospheric Ultraviolet-Visible Model (TUV)*; National Center for Atmospheric Research, 2013, https://www2.acom.ucar.edu/modeling/tropospheric-ultraviolet-and-visible-tuv-radiation-model.
(155) Keller-Rudek, H.; Moortgat, G. K.; Sander, R.; Sörensen, R. The MPI-Mainz UV/VIS spectral atlas of gaseous molecules of atmospheric interest. *Earth Syst. Sci. Data* **2013**, *5*, 365−373.
(156) Pickett, L. W.; Hoeflich, N. J.; Liu, T.-C. The vacuum ultraviolet absorption spectra of cyclic ethers. II. Tetrahydrofuran, tetrahydropyran, 1,4-dioxane and furan. *J. Am. Chem. Soc.* **1951**, *73*, 4865−4869.
(157) Watanabe, K.; Nakayama, T. Absorption and photoionization coefficients of furan vapor. *J. Chem. Phys.* **1958**, *29*, 48−51.
(158) Rennie, E. E.; Johnson, C. A. F.; Parker, J. E.; Holland, D. M. P.; Shaw, D. A.; MacDonald, M. A.; Hayes, M. A.; Shpinkova, L. G. A study of the spectroscopic and thermodynamic properties of furan by means of photoabsorption, photoelectron and photoion spectroscopy. *Chem. Phys.* **1998**, *236*, 365−385.
(159) Holland, D. M. P.; Seddon, E. A.; Trofimov, A. B.; Gromov, E. V.; Wormit, M.; Dreuw, A.; Korona, T.; de Oliveira, N.; Archer, L. E.; Joyeux, D. A study of the excited electronic states of normal and fully deuterated furan by photoabsorption spectroscopy and high-level ab initio calculations. *J. Mol. Spectrosc.* **2015**, *315*, 184−195.
(160) Christianson, M. G.; Doner, A. C.; Koritzke, A. L.; Frandsen, K.; Rotavera, B. Vacuum-ultraviolet absorption cross-sections of functionalized cyclic hydrocarbons: Five-membered rings. *J. Quant. Spectrosc. Radiat. Transfer* **2021**, *258*, No. 107274.
(161) Colmenar, I.; González, S.; Jiménez, E.; Martín, P.; Salgado, S.; Cabañas, B.; Albaladejo, J. UV absorption cross sections between 290 and 380 nm of a series of furanaldehydes: Estimation of their photolysis lifetimes. *Atmos. Environ.* **2015**, *103*, 1−6.
(162) Ferreira da Silva, F.; Lange, E.; Limão-Vieira, P.; Jones, N. C.; Hoffmann, S. V.; Hubin-Franskin, M.-J.; Delwiche, J.; Brunger, M. J.; Neves, R. F. C.; Lopes, M. C. A.; et al. Electronic excitation of furfural as probed by high-resolution vacuum ultraviolet spectroscopy, electron energy loss spectroscopy, and *ab initio* calculations. *J. Chem. Phys.* **2015**, *143*, No. 144308.
(163) Back, R. A.; Parsons, J. M. The thermal and photochemical decomposition of maleic anhydride in the gas phase. *Can. J. Chem.* **1981**, *59*, 1342−1346.
(164) Marshall, P.; Papadimitriou, V. C.; Papanastasiou, D. K.; Roberts, J. M.; Burkholder, J. B. UV and infrared absorption spectra and 248 nm photolysis of maleic anhydride ($C_4H_2O_3$). *J. Photochem. and Photobio. A: Chem.* **2019**, *382*, No. 111953.
(165) Roberts, J. M.; Neuman, J. A.; Brown, S. S.; Veres, P. R.; Coggon, M. M.; Stockwell, C. E.; Warneke, C.; Peischl, J.; Robinson, M. A. Furoyl peroxynitrate (fur-PAN), a product of VOC−NO_x photochemistry from biomass burning emissions: photochemical synthesis, calibration, chemical characterization, and first atmospheric observations. *Environ. Sci. Atmos.* **2022**, *2*, 1087−1100.
(166) Stone, D.; Whalley, L. K.; Heard, D. E. Tropospheric OH and HO_2 radicals: field measurements and model comparisons. *Chem. Soc. Rev.* **2012**, *41* (19), 6348−6404.
(167) Brown, S. S.; Stutz, J. Nighttime radical observations and chemistry. *Chem. Soc. Rev.* **2012**, *41* (19), 6405−6447.
(168) Parrish, D. D.; Lamarque, J.-F.; Naik, V.; Horowitz, L.; Shindell, D. T.; Staehelin, J.; Derwent, R.; Cooper, O. R.; Tanimoto, H.; Volz-Thomas, A.; et al. Long-term changes in lower tropospheric baseline ozone concentrations: Comparing chemistry-climate models and observations at northern midlatitudes. *J. Geophys. Res. Atmos.* **2014**, *119* (9), 5719−5736.
(169) Wingenter, O. W.; Kubo, M. K.; Blake, N. J.; Smith, T. W., Jr.; Blake, D. R.; Rowland, F. S. Hydrocarbon and halocarbon measurements as photochemical and dynamical indicators of atmospheric hydroxyl, atomic chlorine, and vertical mixing obtained during Lagrangian flights. *J. Geophys. Res. Atmos.* **1996**, *101* (D2), 4331−4340.
(170) Wingenter, O. W.; Sive, B. C.; Blake, N. J.; Blake, D. R.; Rowland, F. S. Atomic chlorine concentrations derived from ethane and hydroxyl measurements over the equatorial Pacific Ocean: Implication for dimethyl sulfide and bromine monoxide. *J. Geophys. Res. Atmos.* **2005**, *110* (D20), 308.
(171) Riedel, T. P.; Wagner, N. L.; Dubé, W. P.; Middlebrook, A. M.; Young, C. J.; Öztürk, F.; Bahreini, R.; VandenBoer, T. C.; Wolfe, D. E.; Williams, E. J.; et al. Chlorine activation within urban or power plant

plumes: Vertically resolved $ClNO_2$ and Cl_2 measurements from a tall tower in a polluted continental setting. *J. Geophys. Res. Atmos.* **2013**, *118* (15), 8702−8715.
(172) Gómez Alvarez, E.; Borrás, E.; Viidanoja, J.; Hjorth, J. Unsaturated dicarbonyl products from the OH-initiated photooxidation of furan, 2-methylfuran and 3-methylfuran. *Atmos. Environ.* **2009**, *43* (9), 1603−1612.
(173) Aschmann, S. M.; Nishino, N.; Arey, J.; Atkinson, R. Products of the OH radical-initiated reactions of furan, 2- and 3 methylfuran, and 2,3- and 2,5-dimethylfuran in the presence of NO. *journal of Phyiscal Chemistry* **2014**, *118*, 457−466.
(174) Yuan, Y.; Zhao, X.; Wang, S.; Wang, L. Atmospheric oxidation of furan and methyl-substituted furans initiated by hydroxyl radicals. *J. Phys. Chem. A* **2017**, *121* (48), 9306−9319.
(175) Davis, A. C.; Sarathy, S. M. Computational study of the combustion and atmospheric decomposition of 2-methylfuran. *J. Phys. Chem. A* **2013**, *117* (33), 7670−7685.
(176) Jiang, J.; Carter, W. P. L.; Cocker, D. R.; Barsanti, K. C. Development and evaluation of a detailed mechanism for gas-phase atmospheric reactions of furans. *ACS Earth Space Chem.* **2020**, *4* (8), 1254−1268.
(177) Colmenar, I.; Martín, P.; Cabañas, B.; Salgado, S.; Villanueva, F.; Ballesteros, B. Evaluation of the SOA Formation in the Reaction of Furfural with Atmospheric Oxidants. *Atmosphere* **2020**, *11* (9), 927.
(178) Jenkin, M. E.; Saunders, S. M.; Wagner, V.; Pilling, M. J. Protocol for the development of the Master Chemical Mechanism, MCM v3 (Part B): tropospheric degradation of aromatic volatile organic compounds. *Atmos. Chem. Phys.* **2003**, *3* (1), 181−193.
(179) Bierbach, A.; Barnes, I.; Becker, K. H.; Wiesen, E. Atmospheric chemistry of unsaturated carbonyls: butenedial, 4-oxo-2-pentenal, 3-hexene-2,5-dione, maleic anhydride, 3h-furan-2-one, and 5-methyl-3h-furan-2-one. *Environ. Sci. Technol.* **1994**, *28* (4), 715−729.
(180) Rivett, A. C. D.; Sidgwick, N. V. CLVII.—The rate of hydration of acid anhydrides: succinic, methylsuccinic, itaconic, maleic, citraconic, and phthalic. *J. Chem. Soc. Trans.* **1910**, *97* (0), 1677−1686.
(181) Berndt, T.; Böge, O.; Rolle, W. Products of the Gas-Phase Reactions of NO_3 Radicals with Furan and Tetramethylfuran. *Environ. Sci. Technol.* **1997**, *31* (4), 1157−1162.
(182) Joo, T.; Rivera-Rios, J. C.; Takeuchi, M.; Alvarado, M. J.; Ng, N. L. Secondary organic aerosol formation from reaction of 3-methylfuran with nitrate radicals. *ACS Earth Space Chem.* **2019**, *3* (6), 922−934.
(183) Al Ali, F.; Coeur, C.; Houzel, N.; Genevray, P.; Cazier, F.; Cuisset, A.; Papadimitriou, V. C.; Tomas, A.; Romanias, M. N. Products and yields for the NO_3 radical initiated atmospheric degradation of 2-methylfuran (2-MF, $CH_3-C_4H_3O$). *Atmos. Environ.* **2024**, *319*, No. 120276.
(184) Colmenar, I.; Martín, P.; Cabañas, B.; Salgado, S.; Villanueva, F.; Ballesteros, B. Evaluation of the SOA Formation in the Reaction of Furfural with Atmospheric Oxidants. *Atmosphere* **2020**, *11*, 927.
(185) Huang, Z.; Zhao, N.; Ma, X.; Xu, F.; Zhang, Q.; Zhuang, T.; Wang, W. Theoretical study on the atmospheric oxidation reaction of 2-furanaldehyde initiated by NO_3 radicals. *Chem. Phys. Lett.* **2019**, *722*, 50−57.
(186) Villanueva, F.; Cabañas, B.; Monedero, E.; Salgado, S.; Bejan, I.; Martin, P. Atmospheric degradation of alkylfurans with chlorine atoms: Product and mechanistic study. *Atmos. Environ.* **2009**, *43* (17), 2804−2813.
(187) Villanueva, F.; Barnes, I.; Monedero, E.; Salgado, S.; Gómez, M. V.; Martin, P. Primary product distribution from the Cl-atom initiated atmospheric degradation of furan: Environmental implications. *Atmos. Environ.* **2007**, *41* (38), 8796−8810.
(188) Zhang, W.; Du, B. Products and mechanism of the Cl-initiated atmospheric oxidation of furan: A theoretical study. *Comput. Theor. Chem.* **2011**, *963* (2), 348−356.
(189) Tajuelo, M.; Rodríguez, D.; Rodríguez, A.; Escalona, A.; Viteri, G.; Aranda, A.; Diaz-de-Mera, Y. Secondary organic aerosol formation from the ozonolysis and OH-photooxidation of 2,5-dimethylfuran. *Atmos. Environ.* **2021**, *245*, No. 118041.
(190) Strollo, C. M.; Ziemann, P. J. Products and mechanism of secondary organic aerosol formation from the reaction of 3-methylfuran with OH radicals in the presence of NOx. *Atmos. Environ.* **2013**, *77*, 534−543.
(191) Jiang, X.; Tsona, N. T.; Jia, L.; Liu, S.; Zhang, H.; Xu, Y.; Du, L. Secondary organic aerosol formation from photooxidation of furan: effects of NOx and humidity. *Atmos. Chem. Phys.* **2019**, *19* (21), 13591−13609.
(192) Jiang, X.; Liu, D.; Xu, L.; Tsona, N. T.; Du, L. Assessing the influence of environmental conditions on secondary organic aerosol formation from a typical biomass burning compound. *J. Environ. Sci.* **2022**, *114*, 136−148.
(193) Jiang, H.; Frie, A. L.; Lavi, A.; Chen, J. Y.; Zhang, H.; Bahreini, R.; Lin, Y.-H. Brown carbon formation from nighttime chemistry of unsaturated heterocyclic volatile organic compounds. *Environ. Sci. Technol. Lett.* **2019**, *6* (3), 184−190.
(194) Chen, K.; Mayorga, R.; Raeofy, N.; Lum, M.; Woods, M.; Bahreini, R.; Zhang, H.; Lin, Y.-H. Effects of nitrate radical levels and pre-existing particles on secondary brown carbon formation from nighttime oxidation of furan. *ACS Earth Space Chem.* **2022**, *6* (11), 2709−2721.
(195) Odum, J. R.; Hoffmann, T.; Bowman, F.; Collins, D.; Flagan, R. C.; Seinfeld, J. H. Gas/Particle Partitioning and Secondary Organic Aerosol Yields. *Environ. Sci. Technol.* **1996**, *30* (8), 2580−2585.
(196) Bertschi, I.; Yokelson, R. J.; Ward, D. E.; Babbitt, R. E.; Susott, R. A.; Goode, J. G.; Hao, W. M. Trace gas and particle emissions from fires in large diameter and below ground biomass fuels. *J. Geophys. Res.: Atmos.* **2003**, *108* (D13), 8472.
(197) Hornbrook, R. S.; Blake, D. R.; Diskin, G. S.; Fried, A.; Fuelberg, H. E.; Meinardi, S.; Mikoviny, T.; Richter, D.; Sachse, G. W.; Vay, S. A.; et al. Observations of nonmethane organic compounds during ARCTAS-Part 1: Biomass burning emissions and plume enhancements. *Atmos. Chem. Phys.* **2011**, *11* (21), 11103−11130.
(198) Wolfe, G. M.; Hanisco, T. F.; Arkinson, H. L.; Blake, D. R.; Wisthaler, A.; Mikoviny, T.; Ryerson, T. B.; Pollack, I.; Peischl, J.; Wennberg, P. O.; et al. Photochemical evolution of the 2013 California Rim Fire: synergistic impacts of reactive hydrocarbons and enhanced oxidants. *Atmos. Chem. Phys.* **2022**, *22* (6), 4253−4275.
(199) Xu, L.; Crounse, J. D.; Vasquez, K. T.; Allen, H.; Wennberg, P. O.; Bourgeois, I.; Brown, S. S.; Campuzano-Jost, P.; Coggon, M. M.; Crawford, J. H.; et al. Ozone chemistry in western U.S. wildfire plumes. *Sci. Adv.* **2021**, *7* (50), No. eabl3648.
(200) Müller, M.; Mikoviny, T.; Feil, S.; Haidacher, S.; Hanel, G.; Hartungen, E.; Jordan, A.; Märk, L.; Mutschlechner, P.; Schottkowsky, R.; et al. A compact PTR-ToF-MS instrument for airborne measurements of volatile organic compounds at high spatiotemporal resolution. *Atmos. Meas. Technol.* **2014**, *7* (11), 3763−3772.
(201) Permar, W.; Jin, L.; Peng, Q.; O'Dell, K.; Lill, E.; Selimovic, V.; Yokelson, R. J.; Hornbrook, R. S.; Hills, A. J.; Apel, E. C.; et al. Atmospheric OH reactivity in the western United States determined from comprehensive gas-phase measurements during WE-CAN. *Environ. sci. Atmos.* **2023**, *3* (1), 97−114.
(202) Mouat, A. P.; Paton-Walsh, C.; Simmons, J. B.; Ramirez-Gamboa, J.; Griffith, D. W. T.; Kaiser, J. Measurement report: Observations of long-lived volatile organic compounds from the 2019−2020 Australian wildfires during the COALA campaign. *Atmos. Chem. Phys.* **2022**, *22* (17), 11033−11047.
(203) Decker, Z. C. J.; Zarzana, K. J.; Coggon, M.; Min, K.-E.; Pollack, I.; Ryerson, T. B.; Peischl, J.; Edwards, P.; Dubé, W. P.; Markovic, M. Z.; et al. Nighttime chemical transformation in biomass burning plumes: a box model analysis initialized with aircraft observations. *Environ. Sci. Technol.* **2019**, *53* (5), 2529−2538.
(204) Decker, Z. C. J.; Wang, S.; Bourgeois, I.; Campuzano Jost, P.; Coggon, M. M.; DiGangi, J. P.; Diskin, G. S.; Flocke, F. M.; Franchin, A.; Fredrickson, C. D.; et al. Novel analysis to quantify plume crosswind heterogeneity applied to biomass burning smoke. *Environ. Sci. Technol.* **2021**, *55* (23), 15646−15657.
(205) Wang, S.; Coggon, M. M.; Gkatzelis, G. I.; Warneke, C.; Bourgeois, I.; Ryerson, T.; Peischl, J.; Veres, P. R.; Neuman, J. A.; Hair,

J.; et al. Chemical tomography in a fresh wildland fire plume: A Large Eddy Simulation (LES) Study. *J. Geophys. Res. Atmos.* **2021**, *126* (18), No. e2021JD035203.
(206) Carter, W. P. L. Development of the SAPRC-07 chemical mechanism. *Atmos. Environ.* **2010**, *44* (40), 5324−5335.
(207) Pye, H. O. T.; Place, B. K.; Murphy, B. N.; Seltzer, K. M.; D'Ambro, E. L.; Allen, C.; Piletic, I. R.; Farrell, S.; Schwantes, R. H.; Coggon, M. M.; et al. Linking gas, particulate, and toxic endpoints to air emissions in the Community Regional Atmospheric Chemistry Multiphase Mechanism (CRACMM) version 1.0. *Atmos. Chem. Phys. Discuss.* **2023**, *23*, 5043−5099.
(208) Carter, T. S.; Heald, C. L.; Kroll, J. H.; Apel, E. C.; Blake, D.; Coggon, M.; Edtbauer, A.; Gkatzelis, G.; Hornbrook, R. S.; Peischl, J.; et al. An improved representation of fire non-methane organic gases (NMOGs) in models: emissions to reactivity. *Atmos. Chem. Phys.* **2022**, *22* (18), 12093−12111.

https://doi.org/10.1021/acsearthspacechem.3c00226
ACS Earth Space Chem. XXXX, XXX, XXX−XXX